Enhancement of Oral Bioavailability and Antiproliferative Potential of Betulinic Acid by PLGA Loaded Nanoparticle Approach

A

THESIS

SUBMITTED IN FULFILLMENT FOR THE AWARD OF THE DEGREE OF

Doctor of Philosophy

IN

PHARMACEUTICAL SCIENCES

Submitted By

PRANESH KUMAR

Enrollment No. 1351/16

Supervisor

DR. SUDIPTA SAHA

DEPARTMENT OF PHARMACEUTICAL SCIENCES

SCHOOL FOR BIOSCIENCES AND BIOTECHNOLOGY

BABASAHEB BHIMRAO AMBEDKAR UNIVERSITY

(A CENTRAL UNIVERSITY)

VIDYA VIHAR, RAIBARELI ROAD, LUCKNOW-226025 (U.P.), INDIA

(2020)

Dedicated

To

My Lovely

Parents and Family

DECLARATION

I hereby declare that the thesis titled **"Enhancement of Oral Bioavailability and Antiproliferative Potential of Betulinic Acid by PLGA Loaded Nanoparticle Approach"** has been prepared by me under the supervision of **Dr. Sudipta Saha** at Department of Pharmaceutical Sciences, School for Biosciences and Biotechnology, Babasaheb Bhimrao Ambedkar University, Lucknow (U.P.).

No part of this thesis has formed the basis for the award of any degree, diploma or fellowship previously. I further declare that the material embodied in the present work is based on original research work and indebtedness to others has been duly acknowledged at relevant places. I hereby also declare that the thesis is essentially free from all kinds of plagiarism.

Pranesh Kumar

Candidate

Supervisor

CERTIFICATE

This is to certify that the thesis titled **"Enhancement of Oral Bioavailability and Antiproliferative Potential of Betulinic Acid by PLGA Loaded Nanoparticle Approach"** submitted by **Mr. Pranesh Kumar** is an original research work and has not been previously submitted in part or full for the award of any other degree or diploma to this or any other university.

The thesis submitted to Babasaheb Bhimrao Ambedkar University Lucknow satisfies all the requirements as stipulated in the *Doctor of Philosophy (Ph.D.) regulations - 1999 as amended in 2008/2010/2013* and it is fit for submission and evaluation for the award of the degree of Doctor of Philosophy of the University.

Date: 21/12/2020

Supervisor

21/12/2020.

Head of the Department

ACKNOWLEDGEMENT

*All are meaningless without paying gratitude to **Almighty GOD**. At the end of my thesis, it is a pleasant task to express my thanks to all those who contributed in many ways to the success of this research work and made it an unforgettable experience for me and without them it is impossible to complete my work.*

*At this moment of accomplishment, first of all, I wish to express my deepest sense of gratitude and special thanks to my research advisor, mentor **Dr. Sudipta Saha,** Assistant Professor Department of Pharmaceutical Sciences, **Babasaheb Bhimrao Ambedkar University (A Central University), Lucknow,** Uttar Pradesh, India, under whose guidance, I have carried out my Ph.D. research work. It was his keen interest, **constant encouragement, valuable suggestions and guidelines**, which enable me to complete this work. His suggestions will remain with me as an in exhaustic source of scientific learning throughout my life. He has always given me a lot of encouragement, constant motivation, valuable ideas and timely support when ever needed.*

*With sincerity and immense pleasure, I express my deep sense of gratitude to **Prof Sanjay Singh, Honorable Vice Chancellor** of Babasaheb Bhimrao Ambedkar University, Lucknow, for providing infrastructure facilities for carrying the project advices throughout my academic career.*

*I warmly thank **Prof. (Dr.) Shubhini A. Saraf,** Professor and Dean, Department of Pharmaceutical sciences, Babasaheb Bhimrao Ambedkar University, Lucknow for her valuable advice, constructive criticism and her extensive discussions around my research work.*

*I warmly thank **Dr. G. Kaithwas,** Head, Department of Pharmaceutical sciences, Babasaheb Bhimrao Ambedkar University, Lucknow for her valuable advice, constructive criticism and her extensive discussions around my research work.*

It gives me great pleasure to acknowledge the support and cooperation rendered by ***Departmental Research Committee (DRC) members*** *of B.B.A.U, Lucknow.*

I am deeply grateful ***to Dr. PS Rajnikant, Dr. Vikash Mishra and Dr. Sapana Kuswaha*** *Department of Pharmaceutical sciences, Babasaheb Bhimrao Ambedkar University, Lucknow for her valuable advice, constructive criticism and her extensive discussions around my research work.*

I accord my thanks to the ***Prof. B. C. Yadav and Dr. Mukesh*** *BBAU, Lucknow for providing me* ***University Science Instrumentation Centre (USIC) facilities*** *to carry out my project.*

I express my sincere gratitude to ***Dr. B. Maity*** *and* ***Dr. Dinesh Kumar****, Centre of Biomedical Research (****CBMR****), Lucknow for providing the providing qRT-PCR, western blot and NMR facilities.*

I also express my sincere gratitude to ***Dr. Jyoti Kode,*** *the Advanced Centre for Treatment, Research and Education in Cancer (****ACTREC****), Tata Memorial Centre, Navi Mumbai, India for providing the in vitro SRB assay for anti-cancer screening of drugs.*

I also acknowledge the ***University Grant Commission,*** *Government of India for providing me with the necessary funding and fellowship to pursue my Doctoral research at B.B.A.U., Lucknow.*

I again acknowledge the ***DST and Government of India*** *for the award of DST INSPIRE Fellowship, Ref No* ***DST/INSPIRE Fellowship/2016/IF160364.***

I would like to express sincere thanks to ***Dr. Sunil Goria*** *(Librarian),* ***Mr. O.P. Saini*** *and* ***Mr. Nitesh Verma*** *(Asst. Librarian), B.B.A.U for their kind support.*

It gives me pleasure to acknowledge the support and co-operation rendered by office staff and non-teaching staff ***Mr.***

Bhandari, Mr. Amarjit and Mr. Anand during the research work.

I would like to thank my fellow labmates, Amit K Keshari, Amit Rai, Ashok K Singh and Vinit Raj for friendly and open-hearted support throughout my research period in this university.

All my colleagues Pawan kumar, Priyanka Maurya, Samipta, Raquibun Nisha and Umesh Kumar (CBMR) are always there for me who directly or indirectly have a big hand in success of our work.

I express my special gratitude to my junior Anurag k gautam, Vipul agrawal,Vimal maurya, Archana sonkar, Virendra for their help and moral support during the work.

My acknowledgement will be incomplete if I do not mention my Father Mr. Ram Nayan Prasad and mother Mrs. Mansha Devi with whom blessings I was able to achieve my goal successfully.

I wish to express my deepest sense of gratitude to my brothers Mr. Dravinesh Kumar and sister Arun Loachni.

Pranesh Kumar

Date: 21-12-20 *Pranesh Kumar*

TABLE OF CONTENTS

NMR based Metabolomics Studies.

List OF TABLES

between NDEA and NC, NDEA and PC, NDEA and B100, NDEA and BNP100 have also been presented.

LIST OF FIGURES

List of abbreviations

HCC	Hepatocellular carcinoma
B	Betulinic acid
BNP	Betulinic acid nanoparticle
PLGA	Poly(lactic-co-glycolic acid)
PVA	Polyvinyl alcohol
NDEA	N-nitrosodiethylamine
ALT	Alanine aminotransferase
AST	Aspartate aminotransferase
ALP	Alkaline phosphatase
CAT	Catalase
PC	Positive control
CC	Carcinogen control
CMC	Carboxymethyl cellulose
DNPH	2,4-dinitrophenylhydrazine
EDTA	Ethylene diamine tetra acetic acid
GI_{50}	Growth inhibition of 50%
ELISA	Enzyme-linked immunosorbent assay
FTIR	Fourier-transform infrared spectroscopy
GSH	Glutathione
HPLC	High pressure liquid chomatography
C^{13}NMR	carbon nuclear magnetic resonance
H^{1} NMR	Proton nuclear magnetic resonance
MS	Mass spectrometry
H_2O_2	Hydrogen peroxide

HDL	High-density lipoprotein
SRB	Sulforhodamine B
Hep-G2	Human hepatoma cells
IL-1β	Interleukin-1β
IL-2	Interleukin-2
IL-6	Interleukin-6
IL-10	Interleukin-10
LDH	Lactate dehydrogenase
NAA	N-acetyl aspartate
MDA	malonaldehyde
NAG	N-acetyl glutamate
NC	Normal control
NMR	Nuclear magnetic resonance
OPLS-DA	orthogonal partial least squares discriminant analysis
ProC	Protein carbonyl
PCA	Principal component analysis
QC	Quality control
ppm	Parts per million
qRT-PCR	Quantitative real-time reverse transcription-polymerase chain reaction
SEM	Scanning electron microscope
SOD	Superoxide dismutase
TBARS	Thiobarbituric acid reactive substances
TCA	Tricarboxylic acid
TGI	Total growth inhibition
TV	Tumor volume

VIP	Variable importance in projection

Abstract

The application of betulinic acid (B), a potent antineoplastic agent, is limited due to poor bioavailability, short plasma half-life and inappropriate tissue distribution. Thus, we aimed to prepare novel 50:50 poly(lactic-co-glycolic acid) (PLGA)-loaded B nanoparticles (BNP) and to compare its anti-hepatocellular carcinoma (anti-HCC) activity with parent B. BNP were synthesized and characterized using different methods such as scanning electron microscopy (SEM), fourier-transform infrared (FTIR) spectrometry and particle size analyses. Particle size of BNP was optimized through the application of the stabilizer, polyvinyl alcohol (PVA). The anti-HCC response was evaluated through *in vitro* cell line study using Hep-G2 cells, confocal microscopy, *in vivo* oral pharmacokinetics and animal studies. Further, for mechanistic and metabolic exploration the quantitative reverse transcription polymerase chain reaction (qRT-PCR), western blot, mathematical modelling and ^{1}H NMR based metabolomics analysis were conducted to observe the changes in the expression of specifc genes and proteins. Particle size of BNP was optimized through the application of the stabilizer, polyvinyl alcohol. Physicochemical characterization exhibited particle size of 257.1 nm with zeta potential -0.170 mV (optimized batch B, BNP). SEM and FTIR analyses of BNP showed that cylindrical particles of B converted to spherical particles in BNP and there were no interaction between B and used polymers. The release study of optimized BNP was highest (≥80%) than any other formulation. Later, *in vitro* cell culture analysis using Hep-G2 cells and confocal microscopy studies revealed that BNP had the highest inhibition and penetration properties than parent B. Oral pharmacokinetics studies using albino Wistar rats at single 100 mg dose again exhibited BNP had the higher 50% of plasma concentration ($t_{1/2}$), a higher maximum plasma concentration (Cmax) and took longer to reach the maximum plasma concentration (Tmax) than parent B. Next, our *in vivo* study using nitrosodiethyl amine (NDEA)-induced HCC model documented BNP decreased in number of nodules, restored body weight, oxidative stress parameters, liver marker enzymes and histological architecture than parent B. Again the quantitative real-time polymerase chain reaction and western blot analyses revealed that HCC was developed through lower expressions of e-NOS, BAX, BAD, Cyt C and higher expressions of i-NOS, Bclxl, Bcl-2. B and BNP normalised the expressions of these apoptogenic markers. Particularly, both activated i-NOS and e-NOS mediated Bcl-2 family proteins→CytC→Caspase 3 and 9 signalling cascades. Lastly the 1H-NMR-based metabolomics study also demonstrated that the perturbed metabolites in NDEA-induced rat serum restored to the normal level following

both treatments. Moreover, the prepared BNP showed a better therapeutic response against HCC and could be attributed as future candidate molecule for HCC treatment.

Keywords:

Betulinic acid, PLGA-loaded nanoparticles, Hep-G2 cells, Hepatocellular carcinoma, N-nitrosodiethylamine (NDEA), Bcl-2, BAD, BAX, Caspase-3 and -9, ^{1}H-NMR based metabolomics.

Chapter 1

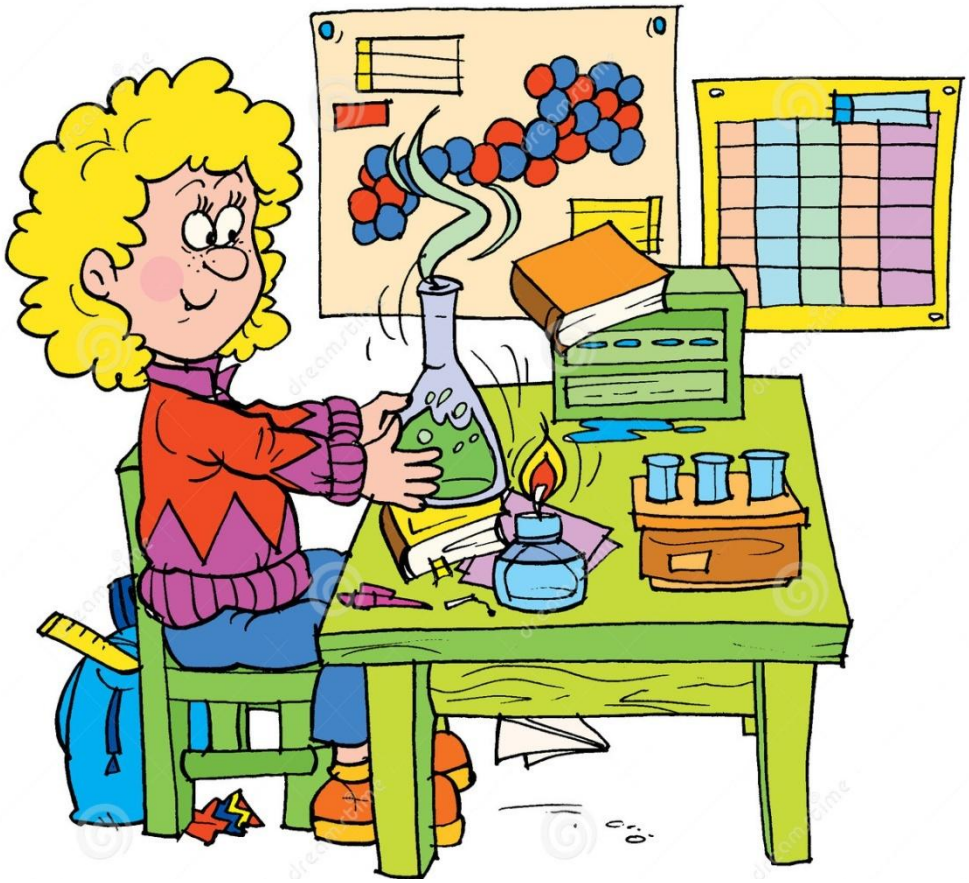

Introduction

1. Introduction

Hepatocellular carcinoma (HCC) is among the main widespread forms that represent more than 90% of the worldwide liver cancer cases. Although, breast cancer, lung cancer, and large intestine cancer have been recognized as the most severe forms, but, the highest death toll was identified for the liver cancer and lung cancer. The rate of mortality among HCC cases are extreme high with more than 750 thousands death annually. It is often designated as the 5^{th} most common cancer form and the 3^{rd} most prominent reason for death in human beings [1].

1.1 National Data

The national epidemiological data of HCC is presently unavailable. The lack of proper documentation and improper registry in national cancer registries represents a major challenge. Indian Council of Medical Research (ICMR)- National Cancer Registry Program (NCRP) have included data and is currently expanding to 21 population-based cancer registries as well as 6 hospital-based cancer registries. The data available in International Agency for Research on Cancer (IARC), World Health Organization (WHO) and ICMR stated that out of every million indigenous population of range 40 years to 70 years, 7 to 75 men and 2 to 22 women suffer from HCC in the age. The data highlighted that males are more prone to HCC in the ratio of 4:1 than females. The recent studies revealed that cirrhotics associated HCC is only 1.6% per year [2].

1.2 Present status

Various synthetic chemotherapeutic agents have showed promising effects on HCC, but, these could develop chemoresistance to patients following a longterm treatment [3]. Sorafenib, a leading drug molecule used for HCC treatment [4], often produces disease related metastasis and resistance [5]. In addition, it display significant adverse effects and its cost of treatment is extremely high [6]. To overcome these shortfalls, the natural products could be the alternative choice for hepatic cancer treatment [7]. The foremost negative aspect correlated with these natural products is the poor absorption profile through the oral route, which directed towards inferior usefulness [8]. Modern analysis discovered that the absorption and solubility via oral route might be improved in superiority via integration of the drug molecules into the poly(lactic-co-glycolic acid) (PLGA) [9,10]. Therefore, there is an insistent necessitate to discern newer plant-derived anticancer agents for effective treatment of HCC cancer.

1.3 Hepatocellular carcinoma

Hepatocellular carcinoma or hepatoma is considered the chief widespread malignant tumor of liver. Liver comprises of diverse cellular components like hepatocytes (80%, major cell form), blood cells, billiary cells, ito cells, Kupffer cells, perisinusoidal cells, etc. The mainstream of principal liver cancer (approximately >90%) occurs from the hepatocytes and is referred as hepatocellular carcinoma. During the process of hepatocarcinogenesis, preliminary carcinogen offences result in instigated cells from the normal liver parenchyma cells or hepatocytes by alteration in the genetic levels which is followed by an interaction generally with DNA. The chronic exposure of hepatocytes to tumor promoter or carcinogens like Phenobarbital leads to subsequent promotion of tumors and produces hepatic altered foci (clonally selected expansions of initiated cell populations). These carcinogenic contents cause further alterations at the genetic levels where under extreme accumulated levels produce hyperplastic nodules that eventually changes into hepatocellular carcinoma [11].

1.3.1 Stages of hepatocellular carcinoma

The conversion of hepatocytes (initiated) into the hepatocellular carcinoma (stages) is a complex multi-stage process. On the basis of morphology; *viz*. size, appearance, shape, growth, etc. and biochemical features like alteration of enzyme expression patterns or discrepancy in the staining patterns, the transformation of hepatocytes into the hepatocellular carcinoma is broadly classified into 3 stages such as initiation, promotion and progression. These three stages have different pathophysiological features and play dominant role in selective pharmacotherapeutics [11].

1.3.1.1 Initiation

Exposing hepatocytes to the chemical carcinogens (diethylnitrosamine, aflatoxins, 2-acetylaminofluorene, etc.) or ionizing radiation causes mutation as a result of alteration in DNA sequence. The conversion of a normal cell into a cancer cell occurs due to the mutations where activation of proto-oncogenes or inactivation of tumor suppressor genes results through specific mechanistic pathway(s). The “initiators” are referred to the chemicals that initiate the process by initially generating the electrophilic moieties that bind with DNA and disrupts the DNA repair mechanism. This step is irreversible for a limited cell population on brief exposure to the

initiators. The cells further develop focal lesions which act as origin sites for the successive development of malignant forms [12].

1.3.1.2 Promotion

Initiated hepatocytes are unable to grow autonomously [12] although they gain the potential to favor proliferation by possessing alterations in gene and protein expressions. Upon exposure to an environment where initiated cells are at greater risk, further genetic alterations begin, causing some reversible changes in the initiated cell populations. Repeated or long-term exposure to a promoting agent (phenobarbital, dietary fat, ethanol, estrogens, chronic exposure of carcinogens) or by some processes (e.g., partial hepatectomy), or by physiological condition (e.g., the neonatal liver) or diseased liver (virus infected or cirrhotic liver), the initiated cells induce focal proliferations. It begins with a selective, clonal amplification of the initiated cells into focal proliferations. [11]

1.3.1.3 Progression

One or more focal lesions from the promotion phase further proceed for more genetic and enzymatic alterations in the constituted hepatocytes, forming enzyme-altered foci. These lesions are initially presented as a small morphological feature formed from a single lesion or merger of multiple lesions and eventually transformed into hepatic nodule (macroscopic presentation) in the liver [11]. Due to the presence of biliary content, these macroscopic structures appear greyish or greenish. Without any extra intervention of external stimulus, slow alterations in the genetic levels and biochemical levels results in increased malignant features for hepatic nodules or hepatic altered foci and are permanently transformed into neoplasia [12].

1.3.2 Signs and symptoms

Patients with previous symptoms of chronic liver disease show occurrence of HCC. At the time of cancer detection, the histopathological investigations often show worsening of signs and symptoms. The most important clinically expressed features include inadvertent loss of weight, loss of appetite, abdominal swelling, weakness and fatigue, yellow discoloration of skin, nausea and vomiting, easy bruising from blood clotting abnormalities, abdominal pain, etc [13].

1.3.3 Risk factors associated to development of HCC

Cirrhosis and chronic liver disease continue to the most important jeopardy issue for the progression of the HCC. The gratuitous consumption of alcohol and viral hepatitis are the overriding aspects perceived worldwide [14].

Hepatitis-C and hepatitis-B linger the most important pervasive motive of the chronic hepatitis which can steadily directs towards cirrhosis and in due course to HCC. The transmission of Hepatitis B is carried out through grimy intravenous injections, infected blood transfusions, and via unprotected sexual contact [15]. Numerous epidemiological investigations have revealed incredible hepatocarcinogenicity with chronic infection from hepatitis B virus (HBV) [16]. However, only 10%–25% of them develop the symptoms. As well, HBV is exceptional in building up HCC devoiding any substantiation of the cirrhosis [17]. Treatment with HBV specific anti-virals or vaccination has the ability to minimize the HCC symptoms to the highest extent [18]. Additionally, hepatitis C virus (HCV) has been identified as the initiator of the HCC having traditional cirrhosis [19]. Antiviral pharmacotherapy lessens the HCC occurrence by 54% in case of HCV infection [20].

Aflatoxin produced by *Aspergillus* species found in grains and soybeans stored in warm humid conditions is considered as potent hepatocarcinogen. The risk of HCC with aflatoxin is greatly influenced by the dose and duration of exposure to it. Aflatoxin exerts a synergistic effect on HBV and HCV-induced HCC and thus, the risk becomes 30-fold greater with hepatitis B plus aflatoxin exposure when compared to that of the aflatoxin exposure alone [21]. After the removal of most potent aflatoxin, AFB1, from the environment, a considerable reduction in the incidence of HCC occurs [22].

In the HCC expansion, consumption of alcohol remains the prime reason where the amount of alcohol establishes the time-dependent relationship [23]. The key factors, obesity and diabetes mellitus (DM) amplifies the HCC condition to several-folds. DM affects the human liver unswervingly as the glucose metabolism process occurs imperatively. DM demonstrates cirrhosis, chronic hepatitis, liver failure, fatty liver, etc [24]. The association of DM with HCC has been reported by El-Serag *et al*. in a review where the researchers depicted several cohort-based studies and numerous case–control studies [25].

Hemochromatosis is a disorder concerning iron that is preliminary differentiated by an overfilling of concentration of body iron. Moreover, thalassemia (a prevalent iron overloading state) has been found to be closely associated in the progression of HCC. The relations of thalassemia and HCV have been found recently and researchers have stated that the above condition precipitates HCC conditions [26].

N-nitrosodiethylamine (NDEA), a carcinogen, produces hepatocellualar carcinoma via metabolic activation of hepatocyte through CYP 450 enzyme. NDEA is a class of DNA alkylating agent which leads to formation of mutagenic DNA adduct [27]. Aflatoxins have been reported carcinogenic properties in various studies and particularly AFB_1 have been characterized as carcinogen in various experiments [28]. NDEA is one of the most acceptable hepatotoxic chemicals which is processed liver fibrosis, chronic liver injury, liver cirrhosis and ultimately develops to hepatocellular carcinoma [29].

Glutamine generally acts as a fuel for the HCC growth because cancer consume large amount of the glutamine and is used as the energy source for the cancer. Glutaminolysis is considered a hallmark of tumor cell metabolism. In mitochondria, glutamine is oxidized into glutamate in presence of glutaminase enzyme and further it is converted to 2- oxoglutarate [30].

1.3.4 Pathophysiology of HCC

1.3.4.1 Diagnosis

The hepatic nodules can be spotted by Ultrasounds (US) techniques, comprising of contrast-enhanced ultrasound (CEUS) technique, and through miscellaneous non-invasive systems like multi-detector computed tomography (MDCT), magnetic resonance imaging (MRI), positron emission tomography (PET), etc. The typical vascular profile/hallmarks of HCC on dynamic imaging is discerned by the hypervascularity phenomenon in the arterial phase with a scrub down in the portal vein or late segments as judge alongside the neighboring liver parenchyma [31].

1.3.4.2 Treatment

Frequent pharmacotherapeutic penchants are reachable for HCC, depending on confined quantifiable proficiency, co-morbidities, stage of HCC, and liver function. A multidisciplinary

team, comprising of pathologists, hepatologists, surgeons, radiologists, and oncologists is elementary for the appropriate supervision.

1.3.4.3 Surgery

The estimation of liver functional reserve prior to surgical resection is elementary the utmost quantity of liver mass that can be securely eliminated while overestimation of liver functional may result in hepatic failure. Conversely, poor resection may notably augment the jeopardy of initial reappearance of HCC. The most important methods to evaluate liver function before hepatectomy are the indocyanine green (ICG) test, 99mTc-galactosyl human serum albumin liver scintigraphy and the galactose tolerance test.

1.3.4.4 Liver transplantation

Liver transplantation (replacing the diseased liver with a cadaveric or a living donor liver) has become a feasible alternative for several patients with HCC, given the advances in immunosuppression and surgical techniques.

1.3.4.5 Targeted Systemic Chemotherapy

- Sorafenib (Multi-kinase inhibitor targeting VEGFR, PDGFR and Raf-family kinase)
- Everolimus (mTOR inhibitor)
- Tivantinib (MET receptor tyrosine kinase inhibitor)
- Brivanib (Fibroblastic growth factor receptor and VEGFR inhibitor)
- Sorafenib and radio-embolization
- Linifanib (PDGFR and Multi-kinase inhibitor targeting VEGFR)
- Sorafenib and TACE combination

1.4 Literature review

Triterpenoids, originally a terpenoid (additionally known as isoprenoids), the biggest gathering of characteristic items to which the betulinic acid analogs additionally have a place. These chemical compounds comprise of six isoprene units and can be segregated from various plant sources [32]. Virtually all terpenes have same pharmacological activities in animals, including man and withal play a paramount role in human medicine. From this perspective, the most

consequential group of terpenes are triterpenes, triterpene glycosides, (withal known as saponines), and other triterpenoids, representing one of the numerous classes of natural compounds [33]. Betulinic acid, a product found in nature, was obtained from the *Dillenia indica* stem bark (family: Dilleniaceae), having a pentacyclic triterpene nucleus with the broad spectrum of biological and pharmacological activities like anti-cancer, anti-malarial, anti-HIV, anti-bacterial, anti-inflammatory, anthelmintic, anti-nociceptive activities, etc [34,35,36,37].

Several authors have been demonstrated their different views over the pharmacological action of betulinic acid. In view of the same, betulinic acid works through different targets for different biological activities which are following as.

- Dutta and colleagues (2015) synthesized novel compounds of betulinic acid derivatives and evaluated their structure active relationship by evaluating their *in vitro* cytotoxic potentials against four human cancer cell lines HT29, U937, MCF-7, HepG2, and non cancerous human PBMC. The study collectively indicated that one derivative namely BC-SM-05 induced apoptosis in HT29 cells via mitochondrial dependent pathway providing a promising therapeutic efficacy against colon cancer. [38]

- Yang *et al*. (2015) discovered that p^{53}–p^{66}/miR-21-Sod2 signaling is vital for BA-inhibited growth of tumors and cell proliferation particularly in case of hepatocellular carcinoma. [39]

- Fulda and Kroemer (2009) reviewed the anticancer activity of B towards various cancer related molecular targets and stated that the antiproliferative activity of B is manifested by downstream directive of the Bcl-2 family proteins like Bcl-XL and Bcl-2 where all the mitochondrial and cellular manifestations of apoptosis are induced in cancer cells. [40]

- Fulda and Debatin, (2000) identified B as a new cytotoxic agent active in treating neuroectodermal tumors including neuroblastoma *in vivo.* In this context, authors unveiled that B generally induced apoptosis by a direct effect on mitochondria independent of accumulation of wild type p53 protein and independent of death inducing ligand/receptor system such as CD95. [41]

- Tan Y *et al.* (2003), revealed that betulinic acid stimulated apoptosis in the human melanoma cells through the inhibition of pro-apoptotic SAP/JNK kinases and p38 MAPK (with no transmutation in the phosphorylation of ERK). [42]

- Aiken C, Chen CH (2005) stated that betulinic acid and their various derivatives induce anti-HIV activity through inhibition of protease dimerization, a prerequisite for protease activation. [43]

- Hashimoto *et al.* (1997) revealed that betulinic acid and dihydrobetulinic acid derivatives introduces anti HIV potential via inhibition of HIV-induced membrane fusion and also block PMA (phorbol 12-myristate 13-acetate) induced viral expression. [44]

- Subramanyam *et al*. (2009), explored that the binding attraction of human serum albumin (HSA) with various drugs is also increased after betulinic acid treatment, because betulinic acid increases the mass of HSA approximately 444 Da, mass raised from 65199 Dalton to 65643 Dalton (betulinic acid treated HSA) using micro TOF-Q mass spectrometry technique. [45]

- Chandramu *et al.* (2003), stated that the plant extract of betulinic possesses anti-feedant activity, the study was performed against the castor semilooper (*Achoea janata*) larvae (third instar) and antibacterial activity of betulinic acid was examined against *Escherichia coli* and *Bacillus subtilis* [46]

- Osunsanmi *et al.* (2015), investigated that anti-platelet aggregation perspectives of betulinic acid was concentration dependent and the study concluded that higher platelet aggregation inhibition was found at 10mg/mL concentration against the platelet agonists adenosine diphosphate (ADP), thrombin and epinephrine. [47]

- Tsai *et al.* (2011), explored that the anti-inflammatory activity of betulinic acid can reveal by down regulation of COX-2 and NO levels in λ-carrageenan induced edema paw tissues of mice on the basis of several studies. [48]

- Da Silva *et al.* (2013), revealed that novel semi-synthetic triterpene derivatives produces antimalarial activity through inhibition of potentially toxic β- haematin formation, as well

as ferriprotoporphyrin IX formation and the experiment was performed against *P. falciparum* 3D7. [49]

- Fulda S (2008) revealed that betulinic acid has anti-carcinogenic characteristics that in the main way generate the apoptosis signaling surge via the commencement of caspase-8 and caspase-3. [50]

- Xu *et al.* (2012), studied the absorption pharmacokinetics of the betulic acid in the intestines of rats and revealed that betulinic acid is a class of natural products that has poor oral absorption and bioavailability which may lead to lower effectiveness. [8]

- Wick *et al.* (1999), stated that the anticancer property of betulinic acid is mainly due to the activation of mitochondrial Bcl-2 pathways where caspase enzymes, various pro-apoptotic (BAX and BAD) and anti-apoptotic (Bcl-2 and Bcl-xl) proteins are involved. [51]

1.5 Research Envisaged

Betulinic acid (B) is a pentacyclic triterpenoid of natural origin with remarkable anticancer activity; however, its less oral bioavailability makes itself towards poor therapeutic efficacy. Recent investigations suggested that the bioavailability may be increased through the preparation of nanoparticles using PLGA, poly(lactic co-glycolic acid). Therefore, we aimed to prepare PLGA, loaded B nanoparticle (BNP) and characterization would be done with various analytical parameters. Later, pharmacokinetic studies of B and BNP would be find out using the Albino Wistar rats and data will be compared with standard B. Finally, antiproliferative potential against the hepatocellular carcinoma would be tested by *in vitro* human hepatoma cell lines (Hep-G2 cells).

Further, *in vivo* antiproliferative effects would be assessed using N-nitrosodiethylamine (NDEA)-induced hepatocellular carcinogenic rats. Various physiological, biochemical, morphological parameters in plasma and hepatic tissues would be performed to find out and compare the effects of B and BNP after oral administration.

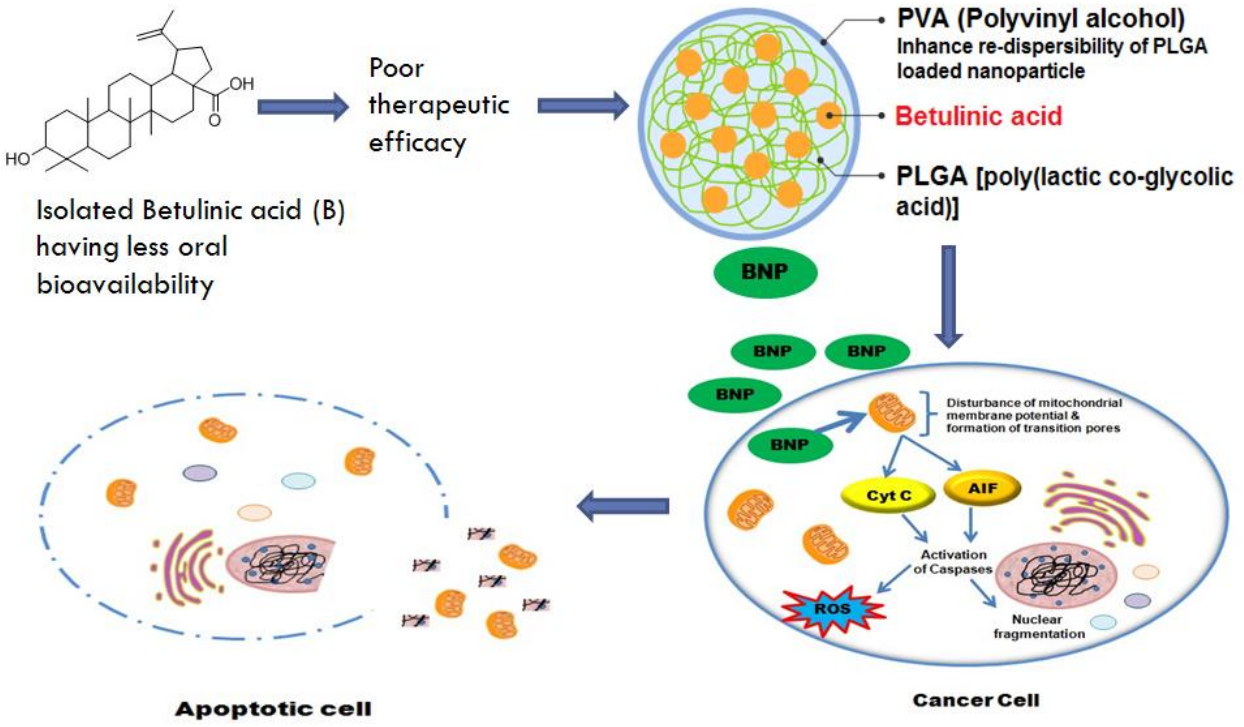

Figure 1 A brief rationale of the designed experiment

Again, various enzyme linked immunosorbent assay (ELISA), (Caspases, i-NOS, e-NOS and interleukins: IL-1ß, IL-2, IL-6, IL-10), qRT-PCR and western blot based gene expression study would be performed to determine the mechanism of action of B and BNP. Further qRT-PCR data based mathematical modelling would be performed to perform to determine the prospective of B and BNP to induce apoptosis to the cancer cells. Finally, metabolic perturbations in plasma would be carried out through NMR to evaluate metabolic changes during cancerous condition and after treatment. In conclusion, BNP may be a better alternative for hepatic carcinoma therapy for future drug design perspectives.

1.6 Objectives

1.6.1 Isolation of betulinic acid (B)from *Dillenia indica* and its characterization

1.6.2 Preparation of betulinic acid nanoparticle (BNP) and its characterization

1.6.3 *In vitro* ameliorative effect using human hepatoma cells (Hep-G2)

1.6.4 *In vivo* pharmacokinetic study using albino Wistar rats

1.6.5 *In vivo* antiproliferative action using N-nitrosodiethylanine (NEDA)-induced albino Wistar rats

1.6.6 NMR based metabolomic studies

1.7 Plan of work

1.7.1 Literature survey

1.7.2 Isolation of B from *Dillenia indica* and its characterization

1.7.3 Preparation of BNP and its characterization

1.7.4 Particle size, polydispersity index, zeta potential, entrapment efficiency, drug loading, *in vitro* release study, FTIR study and SEM.

1.7.5 *In vitro* ameliorative effect using human hepatoma cells (Hep-G2)

1.7.6 Cellular uptake study through confocal microscopy

1.7.7 Approval for animal study

1.7.8 Acquisition of animals (albino Wistar rats)

1.7.9 Acclimatization of animal

1.7.10 *In vivo* pharmacokinetic study

1.7.11 ***In vivo* Treatment study**

Animal study on albino Wistar rats (n= 8).

Table. 1 Treatment schedule

Group	Treatment	Dose	Route of Administration
NC	Carboxymethyl Cellulose	0.25% CMC (2 mL/kg)	Oral (p.o.)
CC	N-nitrosodiethylamine (NDEA)	100 mg/kg Weekly for 6 Weeks	Intra peritoneally (i.p.)
PC	NDEA+5-Flurourecil	100 mg/kg Weekly for 6 Weeks +10 mg/kg, 15 days	i.p.

NDEA+B 50	NDEA+B 50	100 mg/kg Weekly for 6 Weeks +50 mg/kg, 15 days	i.p.+ p.o.
NDEA+B100	NDEA+B100	100 mg/kg Weekly for 6 Weeks +100 mg/kg, 15 days	i.p.+ p.o.
NDEA+BNP 50	NDEA+BNP 50	100 mg/kg Weekly for 6 Weeks +50 mg/kg, 15 days	i.p.+ p.o.
NDEA+BNP 100	NDEA+BNP 100	100 mg/kg Weekly for 6 Weeks +100 mg/kg, 15 days	i.p.+ p.o.

1.7.12 Physiological parameter

1.7.12.1 Initial day body weight

1.7.12.2 Final day body weight

1.7.12.3 Weight variation

1.7.12.4 Liver weight

1.7.12.5 Tumor incident number

1.7.13 Enzymatic parameter analysis

The blood sample would be collected from retro-orbital pluxes after treatments rats will be sacrificed by decapitation and liver would be collected. The serum samples would be subjected to.

1.7.13.1 Aspartate aminotransferase (AST)

1.7.13.2 Alkaline phosphatase (ALP)

1.7.13.3 Alanine aminotransferase (ALT)

1.7.13.4 Lactate dehydrogenase (LDH)

1.7.14 Biochemical studies on hepatic tissues

1.7.14.1 Tissue glutathione reduced (GSH)

1.7.14.2 Thiobarbituric acid reactive substances (TBARS)

1.7.14.3 Tissue super oxide dismutase (SOD)

1.7.14.4 Tissue catalase (CAT)

1.7.14.5 Tissue protein carbonyl (ProC)

1.7.14.6 Bilirubin

1.7.14.7 Biliverdin

1.7.15 ELISA

1.7.15.1 Total nitrite/nitrate content

1.7.15.2 NOS

1.7.15.3 i-NOS and e-NOS

1.7.15.4 Caspase 3 and caspase 8

1.7.15.5 Interleukins: IL-1ß, IL-2, IL-6 and IL-10

1.7.16 qRT-PCR based gene expression study

i-NOS, e-NOS, BAD, BAX, Bcl-2, Bcl-xl, Cyt-c, caspase 3 and caspase 9

1.7.17 Western blot analyses

BAD, BAX, Bcl-2 and β- actin

1.7.18 qRT-PCR data based mathematical modelling

1.7.19 Lipid profile analysis

1.7.19.1 Total cholesterol (TC)

1.7.19.2 Triglyceride (TG)

1.7.19.3 High density lipoprotein (HDL)

1.7.19.4 Low density lipoprotein (LDL)

1.7.19.5 Very low density lipoprotein (VLDL)

1.7.20 Metabolic perturbations in plasma through NMR

1.7.20.1 Stock plot

1.7.20.2 Orthogonal projection to latent structure with discriminate analysis (OPLSDA)

1.7.20.3 VIP Score

1.7.20.4 Box-cum-whisker plots

1.7.20.5 Heat map

1.7.20.6 Pathway impact

1.7.20.7 Metabolic pathway

1.7.21 Morphological changes

1.7.21.1 Histopathology

1.7.21.2 SEM

1.7.22 Statistical analysis

Data would be analyzed as mean±SD (n=8). Statistically significant differences will be observed between CC and test groups [one way ANOVA followed by Bonferroni multiple comparison test (***$p<0.001$, **$p<0.01$ and *$p<0.05$)]

1.8 References

1. Cassier PA, Fumagalli E, Rutkowski P, Schöffski P, Van Glabbeke M, Debiec-Rychter M, Emile JF, Duffaud F, Martin-Broto J, Landi B, Adenis A. European Organisation for Research and Treatment of Cancer. EASL-EORTC clinical practice guidelines: management of hepatocellular carcinoma. Journal of Hepatology 2012;56:908-43.
2. Acharya SK. Epidemiology of hepatocellular carcinoma in India. Journal of clinical and experimental hepatology. 2014;4:S27-33.
3. Newman DJ, Cragg GM, Snader KM. Natural products as sources of new drugs over the period 1981− 2002. Journal of natural products. 2003 Jul 25;66(7):1022-37.
4. Bruix J, Sherman M. Management of hepatocellular carcinoma: an update. Hepatology. 2011;53(3):1020-2.
5. Wilhelm S, Carter C, Lynch M, Lowinger T, Dumas J, Smith RA, Schwartz B, Simantov R, Kelley S. Discovery and development of sorafenib: a multikinase inhibitor for treating cancer. Nature reviews Drug discovery. 2006;5(10):835-44.
6. Kondo M, Numata K, Hara K, Nozaki A, Fukuda H, Chuma M, Maeda S, Tanaka K. Treatment of advanced hepatocellular carcinoma after failure of sorafenib treatment: subsequent or additional treatment interventions contribute to prolonged survival postprogression. Gastroenterology research and practice. 2017;2017.
7. Cragg GM. Natural products in drug discovery and development. Journal of natural products. 1997;60, 52-60.
8. Xu H, Ren X, Du Y, Zhang L, Li T, Ge Y, Wang H. Study on absorption kinetics of betulic acid in rat's intestines. Zhongguo Zhong yao za zhi= Zhongguo zhongyao zazhi= China journal of Chinese materia medica. 2012;37(3):377-80.
9. Roy P, Das S, Bera T, Mondol S, Mukherjee A. Andrographolide nanoparticles in leishmaniasis: characterization and in vitro evaluations. International Journal of Nanomedicine. 2010;5:1113.
10. El-Say KM. Maximizing the encapsulation efficiency and the bioavailability of controlled-release cetirizine microspheres using Draper–Lin small composite design. Drug design, development and therapy. 2016;10:825.
11. Mukherjee B, Ghosh MK, Hossain CM. Chemically induced hepatocellular carcinoma and stages of development with biochemical and genetic modulation: a special reference

to insulin-like-growth factor II and Raf gene signaling. Hepatocellular Carcinoma-Basic Research. InTech. 2012;10:201-18.

12. Farber E, Sarma DR. Hepatocarcinogenesis: a dynamic cellular perspective. Laboratory investigation. 1987;56(1):4-22.
13. "Liver cancer overview". Mayo Clinic. Accessed March 19, 2020.
14. Balogh J, Victor III D, Asham EH, Burroughs SG, Boktour M, Saharia A, Li X, Ghobrial RM, Monsour Jr HP. Hepatocellular carcinoma: a review. Journal of hepatocellular carcinoma. 2016;3:41.
15. Ott JJ, Stevens GA, Groeger J, Wiersma ST. Global epidemiology of hepatitis B virus infection: new estimates of age-specific HBsAg seroprevalence and endemicity. Vaccine. 2012 Mar 9;30(12):2212-9.
16. International Agency for Research on Cancer (IARC). Monographs on the evaluation of carcinogenic risks to humans. Hepatitis Viruses. 1994; 59:182–221.
17. Crissien AM, Frenette C. Current management of hepatocellular carcinoma. Gastroenterology & hepatology. 2014;10(3):153.
18. Chiang CJ, Yang YW, You SL, Lai MS, Chen CJ. Thirty-year outcomes of the national hepatitis B immunization program in Taiwan. Jama. 2013;310(9):974-6.
19. Choo QL, Richman KH, Han JH, Berger K, Lee C, Dong C, Gallegos C, Coit D, Medina-Selby R, Barr PJ. Genetic organization and diversity of the hepatitis C virus. Proceedings of the national academy of sciences. 1991;88(6):2451-5.
20. Lok AS, Seeff LB, Morgan TR, Di Bisceglie AM, Sterling RK, Curto TM, Everson GT, Lindsay KL, Lee WM, Bonkovsky HL, Dienstag JL. Incidence of hepatocellular carcinoma and associated risk factors in hepatitis C-related advanced liver disease. Gastroenterology. 2009 Jan 1;136(1):138-48.
21. Liu Y, Wu F. Global burden of aflatoxin-induced hepatocellular carcinoma: a risk assessment. Environmental health perspectives. 2010;118(6):818-24.
22. Chen JG, Egner PA, Ng D, Jacobson LP, Muñoz A, Zhu YR, Qian GS, Wu F, Yuan JM, Groopman JD, Kensler TW. Reduced aflatoxin exposure presages decline in liver cancer mortality in an endemic region of China. Cancer prevention research. 2013;6(10):1038-45.

23. Batey RG, Burns T, Benson RJ, Byth K. Alcohol consumption and the risk of cirrhosis. Medical journal of Australia. 1992;156(6):413-6.
24. Wang C, Wang X, Gong G, Ben Q, Qiu W, Chen Y, Li G, Wang L. Increased risk of hepatocellular carcinoma in patients with diabetes mellitus: a systematic review and meta-analysis of cohort studies. International journal of cancer. 2012;130(7):1639-48.
25. El–Serag HB, Hampel H, Javadi F. The association between diabetes and hepatocellular carcinoma: a systematic review of epidemiologic evidence. Clinical Gastroenterology and Hepatology. 2006;4(3):369-80.
26. Balogh J, Victor III D, Asham EH, Burroughs SG, Boktour M, Saharia A, Li X, Ghobrial RM, Monsour Jr HP. Hepatocellular carcinoma: a review. Journal of hepatocellular carcinoma. 2016;3:41.
27. Leenders MW, Nijkamp MW, Rinkes IH. Mouse models in liver cancer research: a review of current literature. World journal of gastroenterology: WJG. 2008;14(45):6915.
28. Wogan GN. Impacts of chemicals on liver cancer risk. InSeminars in cancer biology 2000;10(3):201-10.
29. Song S, Yuan P, Li P, Wu H, Lu J, Wei W. Dynamic analysis of tumor-associated immune cells in DEN-induced rat hepatocellular carcinoma. International immunopharmacology. 2014;22(2):392-9.
30. Cabella C, Karlsson M, Canape C, Catanzaro G, Serra SC, Miragoli L, Poggi L, Uggeri F, Venturi L, Jensen PR, Lerche MH. In vivo and in vitro liver cancer metabolism observed with hyperpolarized [5-13C] glutamine. Journal of magnetic resonance. 2013;232:45-52.
31. Marrero JA, Hussain HK, Nghiem HV, Umar R, Fontana RJ, Lok AS. Improving the prediction of hepatocellular carcinoma in cirrhotic patients with an arterially-enhancing liver mass. Liver Transplantation. 2005;11(3):281-9.
32. Mullauer FB, Kessler JH, Medema JP. Betulinic acid, a natural compound with potent anticancer effects. Anti-cancer drugs. 2010;21(3):215-27.
33. Patocka J. Biologically active pentacyclic triterpenes and their current medicine signification. J Appl Biomed. 2003;1(1):7-12.
34. Moghaddam MG, Ahmad FB, Samzadeh-Kermani A. Biological activity of betulinic acid: a review.

35. Armstrong B, Doll R. Environmental factors and cancer incidence and mortality in different countries, with special reference to dietary practices. International journal of cancer. 1975;15(4):617-31.
36. Fujioka T, Kashiwada Y, Kilkuskie RE, Cosentino LM, Ballas LM, Jiang JB, Janzen WP, Chen IS, Lee KH. Anti-AIDS agents, 11. Betulinic acid and platanic acid as anti-HIV principles from Syzigium claviflorum, and the anti-HIV activity of structurally related triterpenoids. Journal of natural products. 1994;57(2):243-7.
37. Mayaux JF, Bousseau A, Pauwels R, Huet T, Henin Y, Dereu N, Evers M, Soler F, Poujade C, De Clercq E. Triterpene derivatives that block entry of human immunodeficiency virus type 1 into cells. Proceedings of the National Academy of Sciences. 1994;91(9):3564-8.
38. Dutta D, Sarkar A, Chakraborty B, Chowdhury C, Das P. Induction of apoptosis by a potent Betulinic acid derivative in Human colon carcinoma HT-29 cells. International Journal of Scientific and Research Publications. 2015;5(2):1-7.
39. Yang J, Qiu B, Li X, Zhang H, Liu W. p53-p66shc/miR-21-Sod2 signaling is critical for the inhibitory effect of betulinic acid on hepatocellular carcinoma. Toxicology letters. 2015;238(3):1-0.
40. Fulda S, Kroemer G. Targeting mitochondrial apoptosis by betulinic acid in human cancers. Drug discovery today. 2009;14(17-18):885-90.
41. Fulda S, Debatin KM. Betulinic acid induces apoptosis through a direct effect on mitochondria in neuroectodermal tumors. Medical and Pediatric Oncology: The Official Journal of SIOP—International Society of Pediatric Oncology (Societé Internationale d'Oncologie Pédiatrique. 2000;35(6):616-8.
42. Tan Y, Yu R, Pezzuto JM. Betulinic acid-induced programmed cell death in human melanoma cells involves mitogen-activated protein kinase activation. Clinical Cancer Research. 2003;9(7):2866-75.
43. Aiken C, Chen CH. Betulinic acid derivatives as HIV-1 antivirals. Trends in molecular medicine. 2005;11(1):31-6.
44. Hashimoto F, Kashiwada Y, Cosentino LM, Chen CH, Garrett PE, Lee KH. Anti-AIDS agents—XXVII. Synthesis and anti-HIV activity of betulinic acid and dihydrobetulinic acid derivatives. Bioorganic & medicinal chemistry. 1997;5(12):2133-43.

45. Subramanyam R, Gollapudi A, Bonigala P, Chinnaboina M, Amooru DG. Betulinic acid binding to human serum albumin: a study of protein conformation and binding affinity. Journal of Photochemistry and Photobiology B: Biology. 2009;94(1):8-12.
46. Chandramu C, Manohar RD, Krupadanam DG, Dashavantha RV. Isolation, characterization and biological activity of betulinic acid and ursolic acid from Vitex negundo L. Phytotherapy Research: An International Journal Devoted to Pharmacological and Toxicological Evaluation of Natural Product Derivatives. 2003;17(2):129-34.
47. Osunsanmi FO, Soyingbe OS, Ogunyinka IB, Ikhile RA, Ngila JC, Shode FO, Opoku AR. Antiplatelet aggregation and cytotoxic activity of betulinic acid and its acetyl derivative from Melaleuca bracteata. Journal of Medicinal Plants Research. 2015;9(22):647-54.
48. Tsai JC, Peng WH, Chiu TH, Lai SC, Lee CY. Anti-inflammatory effects of Scoparia dulcis L. and betulinic acid. The American Journal of Chinese Medicine. 2011;39(05):943-56.
49. Da Silva GN, Maria NR, Schuck DC, Cruz LN, De Moraes MS, Nakabashi M, Graebin C, Gosmann G, Garcia CR, Gnoatto SC. Two series of new semisynthetic triterpene derivatives: differences in anti-malarial activity, cytotoxicity and mechanism of action. Malaria journal. 2013;12(1):89.
50. Fulda S. Betulinic acid for cancer treatment and prevention. International journal of molecular sciences. 2008;9(6):1096-107.
51. Wick W, Grimmel C, Wagenknecht B, Dichgans J, Weller M. Betulinic acid-induced apoptosis in glioma cells: A sequential requirement for new protein synthesis, formation of reactive oxygen species, and caspase processing. Journal of Pharmacology and Experimental Therapeutics. 1999;289(3):1306-12.

Chapter 2

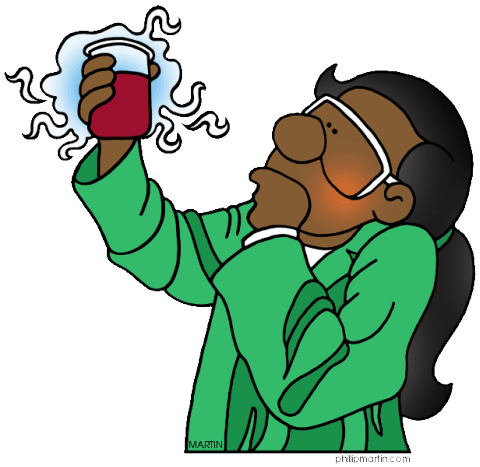

Isolation, Formulation and In vitro Anticancer Activity

2. Introduction

As per discussion in previous chapter, we aimed to isolate betulinic acid (B) from stem bark of Dillenia indica (family: Dilleniaceae) that contain pentacyclic triterpenoid unit which have remarkable anticancer activity [1]. Successive solvent extraction approach was adopted for isolation of B from air-dried, powdered and defatted plant material. However, its less oral bioavailability makes itself towards poor therapeutic efficacy, considering this shaft line we decided to formulate PLGA nonoparticle of B (BNP) [2].

Biodegradable nanoparticles are the most promising components in the modern pharmacotherapeutics for the extended release of several hydrophobic molecules (drugs). PLGA-based nanoparticles have been comprehensively studied and a number of products are currently available at present in the drug market [3,4]. In the road of progress, for surmounting the probable stern side effects of the drugs produced on systematic administration for long period, these biodegradable nanoparticles are boon for the approach of controlled drug delivery [5,6]. The submicron size of the nanoparticles, it offers additionally great advantages for site specific controlled delivery of the drugs [7]. PLGA copolymers, owing to its unique features are frequently applied for the controlled delivery of drug molecules and biological products (enzymes, cytokines, proteins, vaccines, etc.) [8-12]. The release of an ideal hydrophobic molecule in a controlled manner from the PLGA nanoparticles exclusively depends on size distribution, particle size, surface morphology, drug incorporation, and drug content [13]. The mechanism of drug release such as Higuchi's model, first-order, Korsemeyer-Peppas model, etc. plays critical function in estimating the influence of the above characteristics over the in-vitro drug release behavior.

An efficient emulsification and solvent evaporation technique was employed for PLGA nonoparticle development. Once the formulation and characterization have been completed, parent B and BNP were subjected to in vitro cell cytotoxicity on Hep-G2 cell line to investigate their anticancer potential against HCC cells. Further confocal lesser microscopy analysis of B and BNP were subjected to analyze their cellular uptake capacity against Hep-G2 cell line.

2.1 Materials and methods

2.1.1 Isolation and characterization of B

2 kg stem bark of Dillenia indica was procured exclusively during mid July from the coastal areas of West Bengal. The plant was authenticated at Shakti College of Pharmacy, Balrampur, Dist. Lucknow, Uttar Pradesh, India. The voucher specimen of reference number SCOP/2017/829 was obtained and deposited for future requirements.

The stem bark was kept under shade, dried in air, powdered coarsely, petroleum ether was used for defatting in a temperature range of 60°C–80°C. By employing the solvent extraction method, using the Soxhlet apparatus, the extraction process was conducted utilizing the methanol: water solvent system in the ratio of 98:2 v/v. The extracted samples were evaporated through rotary vacuum evaporator (IKA, Königswinter, Germany) to obtain the dry content. Further, methanol was employed to crystallize the content (Yield: 9.2% w/w).

Yield: 9.2%; melting point: 298°C; Fourier-transform infrared (FTIR; KBr) 3,630, 2,980, 2,934, 1,638, 1,480, 1,362, 1,195, 1,123, 784 cm-1; 1H NMR (DMSO-d6) 0.73, 0.85, 0.95, 1.01 and 1.73 (5 s, 15H, all tertiary -CH3), 1.39 (m, 2H, H-21), 1.40 (m, 2H, H-16), 1.44 (m, 2H, H-20), 1.51 (m, 4H, H-18, H-19 and H-15), 2.19 (m, 3H, H-1 and H-9), 2.30 (m, 2H, H-14), 3.04 (s, 2H, H-2), 4.37 (s, 2H, H-7), 4.64 (2, 2H, H-11), 4.77 (s, 2H, H-12), 12.16 (s, 1H, -COOH); 13C NMR (DMSO-d6) 14.85, 16.21, 16.42, 18.45, 19.40, 20.33, 25.54, 27.62, 28.57, 28.78, 29.33, 31.54, 36.79, 37.19, 38.97, 40.33, 40.71, 42.47, 44.65, 48.98, 50.38, 55.34, 55.88, 61.80, 77.23, 110.13, 118.13, 150.79, 177.12 and electrospray ionization mass spectrometry (+ve mode) (M+H)+ m/e 457.8.

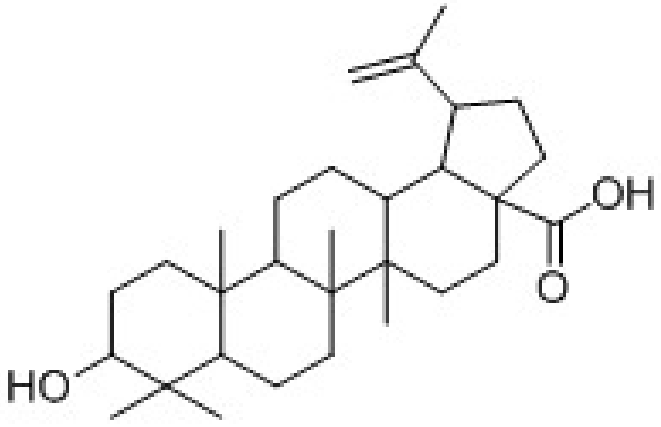

Figure 2 Structure of isolated betulinic acid (**B**)

2.1.2 Preparation of betulinic acid nonoparticle (BNP)

Emulsifcation and solvent evaporation techniques were adopted for the preparation of BNP. By employing the homogenization process and sonication process, smaller particle size was attained. In chloroform (3 mL), 2.5 mg of B and 50 mg of PLGA were dissolved. 12 mL of aqueous polyvinyl alcohol (PVA) was added in different concentrations (w/v) [Formulations A and B: 2% PVA; Formulations C and D: 4% PVA; and Formulations E and F: 6% PVA] and sonicated [360 W (at 30% amplitude)] for 15 to 30 min (Table 1). For 20 min, all the mixtures were homogenized in a refrigerated centrifuge having temperature of 4°C at 20,000 rpm. For completely removing the organic solvent, the mixture was overnight stirred using a mechanical stirrer. Further, ultracentrifuge was employed at a temperature of 4°C for 25 min duration at 30,000 rpm centrifugation to harvest BNP. The obtained content was thoroughly washed with distilled water, further recentrifuged, and stored at 4°C in vacuum desiccators for future applications. This procedure was supplementarily being employed for preparing large-scale (20 times more) [14].

2.1.3 Particle size, polydispersity index (PDI) and zeta potential

NanoPlus® Zeta (nano particle analyzer) was employed for determining the PDI and particle size of BNP batches by using the disposable zeta cells. The system comprised of evaluating the desired properties through 4 mW helium–neon laser beam that emit at 633 nm at 173° back scattering angle by photon correlation spectroscopy (PCS). The study was performed in a triplicate manner. In electrophoretic zeta cells, the prepared aliquots were introduced and the zeta potentials were suitably analyzed by the Smoluchowski equation [14].

2.1.4 BNP entrapment efficiency (%) and loading capacity (%)

Shimadzu LC-20AD (Kyoto, Japan) chromatographic system comprising of photodiode array detector was utilized for estimating the entrapment efficiency of BNP. The stationary phase comprised of Grace reversed phase (RP)-C_{18} column having dimension of 250 mm length, internal diameter of 4.6 mm, average particle size of 5.0 μm, and sustained at an ambient column temperature 25°C. The mobile phase comprised of acetonitrile: water in the ratio of 9:1 v/v. The flow rate was kept 1 mL/min at gradient elution mode for 15 min run-time duration. The content was analyzed using the chromatogram photodetector at 230 nm. By using the solvents;

acetonitrile: water in the ratio of 1:1 v/v, the column was thoroughly washed after each and every run. For determining the B concentration in each of the solution, the graph comprised of concentration (X-Axis) vs. peak area (Y-Axis) was initially prepared with equation y = 211.97x +3.99 and R^2 = 0.9987. RP-HPLC system was used to determine the mass in the supernatant (produced by centrifugation for 20 min at 20,000 rpm) before and after nanoparticulation. The actual loading capacity and the encapsulation efficiency were computed from the following formulae and expressed in percentage:

$$\%\ \text{B entrapment efficiency} = \left[\frac{\text{Mass of } \mathbf{B} \text{ originally taken} - \text{Mass of } \mathbf{B} \text{ in supernatant}}{\text{Mass of B originally taken}}\right] \text{X } 100 \quad [14]$$

$$\%\ \text{B loading capacity} = \left[\frac{\text{Weight of drug}}{\text{Weight of microsphere}}\right] \text{X } 100 \ [15]$$

2.1.5 *In vitro* release studies

The batches containing BNP equivalent to approx. 2 mg of B was subjected to evaluation for drug release under *in vitro* conditions. The batches were dissolved in phosphate buffer (100 μM, pH 7.4) of 1 mL volume and into the dialysis bags (Cut-off M.W. 10kDa) (Thermo Fisher Scientific, USA), the prepared dispersions were washed. The glass vials containing phosphate buffer of 10 mL volume at temperature of 37°C over a shaker bath served as the system on which the dialysis bags were carefully placed. 2 mL of the medium content was taken from the vials and sink condition was maintained by replacing with the fresh buffer medium of same volume. The amount of drug release per unit time was spectrophotometrically determined at 230 nm. The experiment was performed in a triplicate manner and the cumulative drug release was plotted against time [14,15]. The drug release was applied to Korsmeyer–Peppas model and K-value and n-value were determined using the GraphPad Prism 5.0 software.

2.1.6 FTIR and scanning electron microscopy (SEM) studies

For determining the plausible interaction between the drug (B) and polymers (PLGA, PVA), the FTIR studies (Thermo Fischer Scientific Nicolet™ 6700) were performed in the range of 4,000 cm^{-1}-400 cm^{-1}. The spectra for B, PLGA, PVA, and BNP were recorded after mixing the compounds (5 mg) with KBr (200 mg) and pelletized at 1,000 psi.

The samples for SEM (JEOL JSM-6490LV, Tokyo, Japan) were prepared by slightly sprinkling powder on a double adhesive tape stuck to an aluminium stub. Afterwards, the stub containing the coated samples was placed in the scanning electron microscope (SEM) chamber. The samples were then randomly scanned and photomicrographs were taken at the acceleration voltage of 15 kV and the result of SEM was reported.

2.1.7 Cell culture and sulforhodamine B (SRB) assay

National Cell Repository (NCCS, Pune, India) provided the HepG2 cell line which was cultured later for *in vitro* testing in our laboratory. The liver cells were cultured successfully in a T-75 flask with Roswell Park Memorial Institute (RPMI)-1640 medium containing L-glutamine (2 μM) and fetal bovine serum (10%) in 95% air, 5% CO_2, relative humidity of 100% and temperature of 37°C for the duration of 24 hr. After successful culturing of the cells, 100 μL concentrations of the cells were inoculated at a concentration of 5×10^3 cells/well into 96 well plates. At 100 μg/mL concentration, the solutions of compounds of interest were prepared in dimethyl sulfoxide (DMSO). Further, the content was diluted with distilled water to produce 1 mg/mL concentration and stored under frozen state before the commencement of study. To each of the well, varied concentrations; 10 μg/mL, 20 μg/mL, 40 μg/mL, and 80 μg/mL of compound containing medium were added and further incubated for 48 hrs duration at standard conditions. Trichloroacetic acid (30%) of 50 μL concentration was added to the above content and incubated at a temperature of 4°C for 1 hr duration for terminating the reaction. The plates were washed with tap water for five times and dried under air. Moreover, in 1% acetic acid, SRB solution of 50 μL concentration was added to achieve the desired content of 0.4% w/v and further incubated at room temperature for 20 min time duration. After successful staining, five times washing was done with acetic acid (1%) to remove the residual dye and the plates were dried in air. The elution of the bound stain was done subsequently with the help of 10 μM Trizma base and at wavelength of 540 nm, the absorbance was recorded from the plate reader. The reference wavelength was kept at 690 nm. The experiment was performed in a triplicate manner and the average value was estimated. By employing the absorbance measurements, control growth referred to (C), time zero presented by [Tz], five concentration levels represented by [Ti] and test growth in the presence of drug, the % growth was estimated at each concentration levels of the drug molecule. The % inhibition of the growth was computed from:

$$\left(\frac{\mathrm{Ti}-\mathrm{Tz}}{\mathrm{C}-\mathrm{Tz}}\right) \mathrm{x}\ 100 \text{ for conventrations fot which } \mathrm{Ti} \geq \mathrm{Tz}$$

$$\left(\frac{\mathrm{Ti}-\mathrm{Tz}}{\mathrm{Tz}}\right) \mathrm{x}\ 100 \text{ for conventrations fot which } \mathrm{Ti} < Tz$$

GI_{50} was calculated from $[(Ti - Tz)/(C - Tz)] \times 100 = 50$, which is the concentration of drug that leads to 50% reduction in the protein net content enhancement (as measured by SRB staining) in the control cells during the incubation of the drug [16].

2.1.8 Confocal laser scanning microscopy

On a Lab-Tek chambered cover glasses (Nalge Nunc International, Naperville, IL, USA), HepG2 cells were seeded. The content was incubated in 95% air, 5% CO_2 environment at 37°C temperature, until majority of the cells confluent (~70%). Hank's buffered salt solution (HBSS; pH 7.4) was used to replace the above growth medium on the day of study. The content was equilibrated with HBSS for 30 min at temperature of 37°C and fluorescein isothiocyanate (FITC)-loaded BNP suspension was added to replace the buffer. Further, the monolayers were incubated for 1 hr or 2 hr. The prepared monolayers were washed 3-times (to remove non-complex nanoparticles) at the termination of the study with fresh transport buffer (pre-warmed). 70% ethanol was utilized for fixing the cells and in the fluorescent mounting medium, the samples were mounted for confocal laser scanning microscopic analysis. The confocal system comprised of FluoView FV300 (Olympus corporation, Tokyo, Japan), the imaging software [17].

2.2 Results

B suffers from poor oral bioavailability and limited solubility which results in low pharmacological responses and therefore affects the therapeutic index [18-24]. The enhancement in the solubility of poorly soluble drugs results in overcoming these problems and ultimately leads to augmentation of oral bioavailability. By forming the nanoparticles of B, the solubility was enhanced drastically. The drug has a very limited solubility in the polar solvents whereas fair solubility was demonstrated in chloroform, a medium polar solvent owing to lipophilicity. The nanoparticles (BNP) were fabricated with different PVA concentrations with homogenization and 30 min sonication (Table 2). A stable, clear BNP dispersion in water was found for all batches, with batch-B presenting the smallest particle size.

Table 2 Characterization of **BNP** preparations. Data presented as mean±SD (n=3). Optimized batch was Batch B (30 min sonication time with 2% PVA, **BNP**: Betulinic acid nanoparticles).

BNP prepara-tions	Sonication time and % of PVA (Poly venyl alcohol)	Particle size (nm)	Zeta potential (mV)	Polydispersity index (PDI)	Entrapment efficiency (%)	Loading capacity (%)
Batch A	Sonication time: 15 min and 2% PVA	353.9	-0.198	0.234±0.011	67.23±5.47	7.25±0.53
Batch B	**Sonication time: 30 min and 2% PVA**	**257.1**	**-0.170**	**0.356±0.002**	**84.56±3.96**	**11.13±0.60**
Batch C	Sonication time: 15 min and 4% PVA	568.4	-0.243	0.081±0.011	57.11±3.98	6.67±0.48
Batch D	Sonication time: 30 min and 4% PVA	509.4	-0.215	0.060±0.015	60.67±2.89	6.91±0.39
Batch E	Sonication time: 15 min and 6% PVA	679.3	-0.275	0.057±0.016	61.33±4.55	7.05±0.43
Batch F	Sonication time: 30 min and 6% PVA	657.7	-0.269	0.129±0.012	56.22±2.75	6.38±0.27

2.2.1 Nanoparticle size, zeta potential and PDI

The developed BNP batches were characterized further by zeta potential, PDI, and particle size (Table 2). 2% PVA played an imperative role in exhibiting smaller morphology (257.1 nm) of the nanomaterial as evidenced from the batch-B. An ideal Gaussian particle distribution (symmetry = asymmetry = 1) with an impressive zeta potential of −0.170 mV. On enhancing the concentration of PVA to 6%, it was perceived that high levels have an oscillating effect on the

particle size where no further reduction of nanomaterial resulted. PDI represents the molecular mass distribution in the polymeric samples. The PDI was recorded within the 0 to 1 range.

2.2.2 Nanoparticle entrapment efficiency and loading capacity

The drug delivery efficacy (payload efficiency) is influenced by the entrapment efficiency and plays dominant role in optimization process of nanoparticle batches. The most optimized batch; batch-B presented the highest entrapment efficiency of 84.56% ±3.96% with loading capacity of 11.13% ±0.60%.

2.2.3 *In vitro* drug release and reaction kinetics

The cumulative percentage drug release of all the fabricated BNPs were shown in Figure 3A. The release characteristics of all the nanoformulations were found to be biphasic with higher initial drug release (upto 300 min / 5 hr) that indicated surface adsorption of the nanoparticles. Although, every batches illustrated faster release upto 1,440 min. The particle size has critical role on the drug release characteristics of all the batches. Both the batches A (~70%) and B (~80%, highest) demonstrated higher drug release profile as compared to the other prepared batches. The activities such as sonication, homogenization, and use of low concentration PVA effectively resulted in the lower particle size formation. The optimized batch-B expressed the best Gaussian particle distribution, sustained release profile, and smallest particle size. The drug release from all the batches followed the zero-order kinetics model that was regular with the prolonged-release of the drug from the system. The Korsmeyer–Peppas model ($Mt/M\alpha = Ktn$) was pertained to demonstrate the release kinetics, where **Mt** is the mass released at time point "t"; **M*α*** the total mass load; **n** is the release exponent, and **K** is the constant accommodating the structural and geometric features. The value of release exponent (n) was found to be 0.9493.

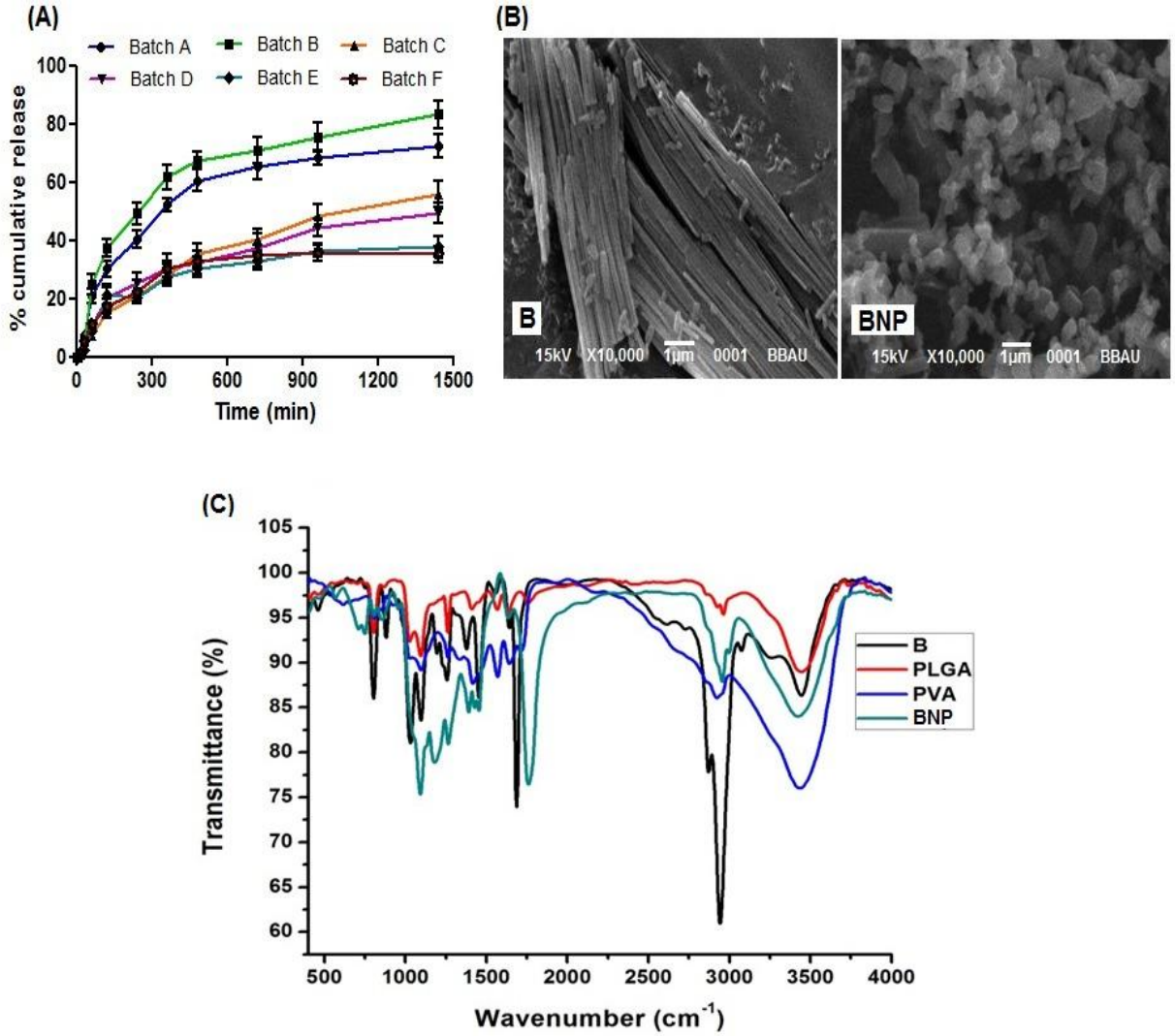

Figure 3 (A) *In vitro* release profile of **BNP** preparations. Results expressed as mean ± SD (n = 3), **(B)** SEM images of **B** and **BNP** (Optimized batch B), **(C)** FTIR spectrum of (A) PVA, (B) PLGA, (C) **B**, (D) **BNP**.

2.2.3 SEM and FTIR studies

The morphological exploration of fabricated BNP batch-B was performed through SEM analysis. The parent compound illustrated cylindrical shaped morphology which was transformed into nanomaterial of uniformly spherical morphology (Figure 3B). The FTIR spectra of the parent compound and its nanoparticle form presented analogous peaks. Both had hydroxyl (O−H) stretching vibrations at 2,900 cm^{-1} as well as carbonyl (C−O) stretching vibrations between 1,625 cm^{-1} and 1,650 cm^{-1} which concluded that there was no such interactions among the drug

molecule and the employed polymers (PVA and PVA). The polymers did not showed any such interaction as evidenced from the characteristic peaks (Figure 3C).

2.2.4 *In vitro* cytotoxicity of B and BNP on the HepG2 cell line and confocal microscopy

Against the liver cancer cell line (HepG2), the drug (B), its nanoparticle (BNP), and polymers (PVA and PLGA) were screened for *in vitro* cytotoxicity and compared with Adriamycin (ADR), the reference drug (Figure 4A). The results revealed that both the polymers (PVA and PLGA) do not produced any substantial cytotoxic effect against the hepatoma cell line. The PLGA–PVA-loaded nanoparticle (BNP) expressed higher cytotoxic activity (GI_{50} = <10 μg/mL) as compared to the parent molecule (GI_{50} = 10 μg/mL) against the HepG2 cell line. The nanomaterial was found to exhibit superior anti-proliferative activity than plain B. The FITC-loaded nanoparticles presented a significant macrophage uptake against Hep-G2 cell line in a different experiment set. The fluorescence microscopy displayed peak uptake of BNP within 2 hrs of incubation. The confocal micropictograms displayed the penetration of nanoparticles inside the cancerous hepatoma cells (Figure 4B). Because of lower particle size of BNP, they entered into the cancerous cells as compared to B. The anti-HCC activity was mediated by high content of B in the localization of macrophage.

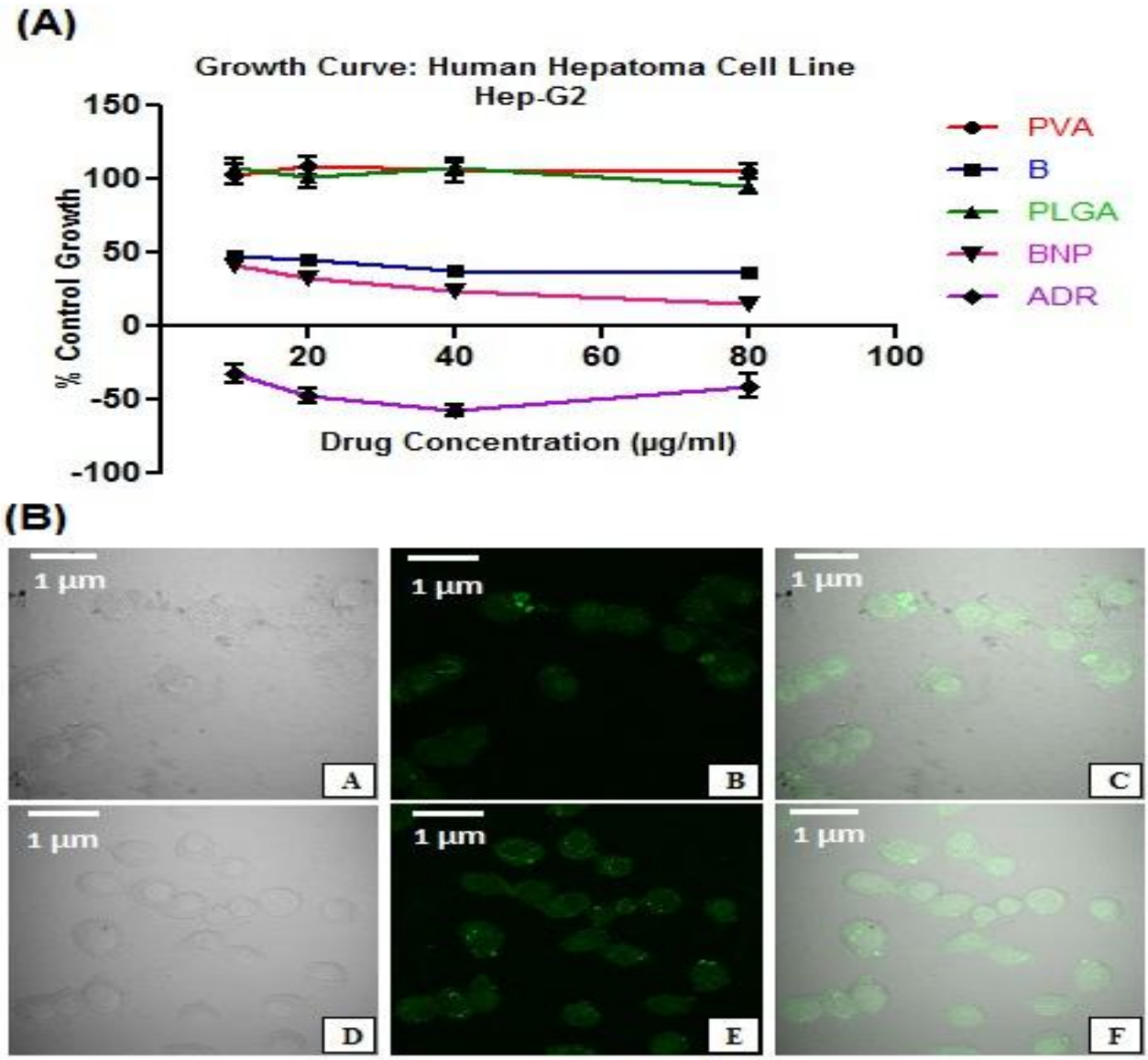

Figure. 4 (A) Growth curve of **B**, PVA, **BNP**, PLGA, and ADR on HepG2 cells, **(B)** Confocal microphotographs of FITC-labeled **B** (A–C) and FITC-labeled **BNP** (D–F) representing the PLGA-loaded nanoparticles uptake in the cancer HepG2 cells. Bright field is shown in A and D, green fluorescent channel displayed in B and E, and the overlay of channels are presented in C and F.

2.3 Discussion

B has been identified as the prominent anti-cancer candidate in the modern day due to their dominant anti-proliferative activity against a number of cell lines and normal cell sparing

attributes. Therefore, broadens the therapeutic window successfully [20,21]. In several tumor selectivity studies related to B, it has been identified that normal cells are more resistant as compared to the cancerous cells, thereby indicating a high tumor selectivity of the compound [25]. B incites a number of cascades that are direct involved in cellular death and also able to overcome the associated drug resistance involved during the therapeutic regimens.

However, when it comes for *in vivo* therapeutics, rarely the drug impresses any researcher owing to low aqueous solubility characteristics which leads to poor dissolution profile and ultimately results in a poor bioavailability [26,27]. This situation necessitates the requirement for a reliable delivery system that can plausibly augment the solubility characteristics.

The compliance with the evergreen statement of "necessity is the mother of invention" was justified by our group where we fabricated nanomaterials of compound B, termed as BNP using the polymers PVA and PLGA, thereby producing PLGA-PVA-BNP that demonstrated enhanced solubility and translated boost in anticancer effects. Biopolymers such as PVA and PLGA were employed as they are the safest among all for human use and also we had previously used these biopolymers for andrographolide nanomaterial biosynthesis [14]. PLGA played a key role in reducing the interfacial tension and stabilizing the nanomaterials [14,15] whereas PVA has stabilization effect [28,29].

The sonication time (30 min duration) and PVA concentration (2%) of batch-B offered a great reduction in the particle size of the nanomaterial. The release profile (~80%), entrapment efficiency (~84%), and loading capacity (~11%) of BNP signifies its best overall performance. The high viscosity of the dispersed phase results in maintenance of particle size, allowing swift solidification, and reduces the leaching effect of the drug in the continuous phase. The FTIR spectrum concluded no such interactions of the drug with the polymer. The process was performed in commercial scale and a huge quantity of BNP was fabricated, characterized, and *in vivo* studies.

When the nanoparticles (BNP) were screened against HepG2 hepatoma cell line, excellent cytotoxic potential as well as selectivity (GI_{50} = <10 μg/mL) were perceived which was higher than the parent compound (GI_{50} = 10 μg/mL). Although, PLGA–PVA nanoparticles imparted remarkable anti-proliferative effect but the polymers were devoid of considerable *in vitro*

potentials against cancer. Captivatingly, the *in vitro* study data reflected that the growth curve of BNP at 10 μg/mL concentration demonstrates the controlled growth rates of 50% or <50%, nevertheless, they do not emerge in the % control growth rate plot's negative region. Therefore, it is awfully anticipated that BNP has the effective capability to exterminate the cancerous cells while diminishing the effect on normal cell death. This activity was additional authenticated through the confocal images where it was observed that BNP presented good penetration ability and penetrate into the Hep-G2 cell to a better degree than the parent B. Both the experiments concluded that BNP presented higher anti-cancer potential than parent B.

2.4 References

1. Jalil J, Sabandar CW, Ahmat N, Jamal JA, Jantan I, Aladdin NA, Muhammad K, Buang F, Mohamad HF, Sahidin I. Inhibitory effect of triterpenoids from Dillenia serrata (Dilleniaceae) on prostaglandin E2 production and quantitative HPLC analysis of its koetjapic acid and betulinic acid contents. Molecules. 2015;20(2):3206-20.
2. Xu H, Ren X, Du Y, Zhang L, Li T, Ge Y, Wang H. Study on absorption kinetics of betulic acid in rat's intestines. Zhongguo Zhong yao za zhi= Zhongguo zhongyao zazhi= China journal of Chinese materia medica. 2012;37(3):377-80.
3. Woo BH, Jiang G, Jo YW, DeLuca PP. Preparation and characterization of a composite PLGA and poly (acryloyl hydroxyethyl starch) microsphere system for protein delivery. Pharmaceutical research. 2001;18(11):1600-6.
4. Budhian A, Siegel SJ, Winey KI. Controlling the in vitro release profiles for a system of haloperidol-loaded PLGA nanoparticles. International Journal of Pharmaceutics. 2008;346(1-2):151-9.
5. Mu L, Feng SS. A novel controlled release formulation for the anticancer drug paclitaxel (Taxol®): PLGA nanoparticles containing vitamin E TPGS. Journal of controlled release. 2003;86(1):33-48.
6. Bibby DC, Davies NM, Tucker IG. Mechanisms by which cyclodextrins modify drug release from polymeric drug delivery systems. International journal of pharmaceutics. 2000;197(1-2):1-1.
7. Barratt G. Colloidal drug carriers: achievements and perspectives. Cellular and Molecular Life Sciences CMLS. 2003;60(1):21-37.
8. Lam XM, Duenas ET, Daugherty AL, Levin N, Cleland JL. Sustained release of recombinant human insulin-like growth factor-I for treatment of diabetes. Journal of Controlled Release. 2000;67(2-3):281-92.
9. Cohen S, Yoshioka T, Lucarelli M, Hwang LH, Langer R. Controlled delivery systems for proteins based on poly (lactic/glycolic acid) microspheres. Pharmaceutical research. 1991;8(6):713-20.
10. Whittlesey KJ, Shea LD. Delivery systems for small molecule drugs, proteins, and DNA: the neuroscience/biomaterial interface. Experimental Neurology. 2004;190(1):1-6.

11. Lagarce F, Faisant N, Desfontis JC, Marescaux L, Gautier F, Richard J, Menei P, Benoit JP. Baclofen-loaded microspheres in gel suspensions for intrathecal drug delivery: in vitro and in vivo evaluation. European journal of pharmaceutics and biopharmaceutics. 2005;61(3):171-80.
12. Anderson JM, Shive MS. Biodegradation and biocompatibility of PLA and PLGA microspheres. Advanced drug delivery reviews. 2012;64:72-82.
13. Gabor F. Ketoprofen-poly (D, L-lactic-co-glycolic acid) microspheres: influence of manufacturing parameters and type of polymer on the release characteristics. Journal of microencapsulation. 1999;16(1):1-2.
14. Roy P, Das S, Bera T, Mondol S, Mukherjee A. Andrographolide nanoparticles in leishmaniasis: characterization and in vitro evaluations. International Journal of Nanomedicine. 2010;5:1113.
15. El-Say KM. Maximizing the encapsulation efficiency and the bioavailability of controlled-release cetirizine microspheres using Draper–Lin small composite design. Drug Design Development and Therapy. 2016;10:825–839.
16. Keshari AK, Singh AK, Raj V, Rai A, Trivedi P, Ghosh B, Kumar U, Rawat A, Kumar D, Saha S. p-TSA-promoted syntheses of 5H-benzo [h] thiazolo [2, 3-b] quinazoline and indeno [1, 2-d] thiazolo [3, 2-a] pyrimidine analogs: molecular modeling and in vitro antitumor activity against hepatocellular carcinoma. Drug Design, Development and Therapy. 2017;11:1623.
17. Roy P, Das S, Mondal A, Chatterji U, Mukherjee A. Nanoparticle engineering enhances anticancer efficacy of andrographolide in MCF-7 cells and mice bearing EAC. Current pharmaceutical biotechnology. 2012 Dec 1;13(15):2669-81.
18. Fulda S. Betulinic acid for cancer treatment and prevention. International journal of molecular sciences. 2008;9(6):1096-107.
19. Wick W, Grimmel C, Wagenknecht B, Dichgans J, Weller M. Betulinic acid-induced apoptosis in glioma cells: A sequential requirement for new protein synthesis, formation of reactive oxygen species, and caspase processing. Journal of Pharmacology and Experimental Therapeutics. 1999;289(3):1306-12.

20. Fulda S, Jeremias I, Steiner HH, Pietsch T, Debatin KM. Betulinic acid: A new cytotoxic agent against malignant brain-tumor cells. International journal of cancer. 1999;82(3):435-41.
21. Zuco V, Supino R, Righetti SC, Cleris L, Marchesi E, Gambacorti-Passerini C, Formelli F. Selective cytotoxicity of betulinic acid on tumor cell lines, but not on normal cells. Cancer letters. 2002;175(1):17-25.
22. Thurnher D, Turhani D, Pelzmann M, Wannemacher B, Knerer B, Formanek M, Wacheck V, Selzer E. Betulinic acid: a new cytotoxic compound against malignant head and neck cancer cells. Head & Neck: Journal for the Sciences and Specialties of the Head and Neck. 2003;25(9):732-40.
23. Noda Y, Kaiya T, Kohda K, KAWAZOE Y. Enhanced cytotoxicity of some triterpenes toward leukemia L1210 cells cultured in low pH media: possibility of a new mode of cell killing. Chemical and pharmaceutical bulletin. 1997;45(10):1665-70.
24. Ehrhardt H, Fulda S, Führer M, Debatin KM, Jeremias I. Betulinic acid-induced apoptosis in leukemia cells. Leukemia. 2004;18(8):1406-12.
25. Selzer E, Pimentel E, Wacheck V, Schlegel W, Pehamberger H, Jansen B, Kodym R. Effects of betulinic acid alone and in combination with irradiation in human melanoma cells. Journal of investigative dermatology. 2000;114(5):935-40.
26. Jäger S, Laszczyk MN, Scheffler A. A preliminary pharmacokinetic study of betulin, the main pentacyclic triterpene from extract of outer bark of birch (Betulae alba cortex). Molecules. 2008;13(12):3224-35.
27. Drag-Zalesinska M, Kulbacka J, Saczko J, Wysocka T, Zabel M, Surowiak P, Drag M. Esters of betulin and betulinic acid with amino acids have improved water solubility and are selectively cytotoxic toward cancer cells. Bioorganic & medicinal chemistry letters. 2009;19(16):4814-7.
28. Vandervoort J, Ludwig A. Biocompatible stabilizers in the preparation of PLGA nanoparticles: a factorial design study. International journal of pharmaceutics. 2002;238(1-2):77-92.
29. Murakami H, Kawashima Y, Niwa T, Hino T, Takeuchi H, Kobayashi M. Influence of the degrees of hydrolyzation and polymerization of poly (vinylalcohol) on the preparation

and properties of poly (DL-lactide-co-glycolide) nanoparticle. International journal of pharmaceutics. 1997;149(1):43-9.

Chapter 3

In vivo Pharmacokinetic and Pharmacodynamic

3. Introduction

In consequence with the previous chapter, we have selected pure betulinic acid (B) and PLGA noanoparticle of betulinic acid (BNP) for further *in vivo* pharmacodynamic and *in vivo* pharmacokinetic analysis. In view of this, we firstly performed the *in vivo* pharmacokinetic investigation of B and BNP in the plasma of rat at 100 mg/kg dose of oral administration [1]. This study was performed using reverse phase high performance liquid chromatography (RP-HPLC) attached with photodiode array (PDA) detector. The intra-day and inter-day variations were analyzed to find out the precision of the developed method. Additionally, to evaluate the accuracy of the method, a recovery test was performed by spiking analytes into rat plasma using different standard solvents. The optimized method is simple and robust for detection of B and BNP in rat plasma and utilized in the pharmacokinetic study to determine absorption, distribution and clearance rate of B and BNP.

Hepatocellular carcinoma (HCC) is one of the most lethal cancers with limited treatment options [2]. This is probably due to the lack of clear and precise mechanisms causing HCC pathogenicity [3]. As per reports, chemotherapy with standard cytotoxic agents such as doxorubicin, cisplatin or 5-fluorouracil, shows below 10% response rate without a clear benefit in overall survival [4,5]. In addition, these are poorly tolerated in patients as a result of systemic toxicities and their associated adverse effects [6]. Although FDA approved drug sorafenib is known for its established efficacy for HCC therapy, the response rate is very limited due to local metastasis and chemotherapeutic resistance [7,8]. To overcome these shortfalls, the natural products could be the alternative choice for hepatic cancer treatment [9]. Betulinic acid is a naturally occurring product obtained from the stem bark of *Dillenia indica*, having a pentacyclic triterpene nucleus with the broad spectrum of biological and pharmacological activities like anticancer, antimalarial, anti-HIV, antibacterial, anti-inflammatory, anthelmintic, antinociceptive activities [10,11,12,13]. In an extension to our attempts to produce effective new therapeutic approaches for treating HCC, we explored the *in vivo* antiproliferative perspectives of B and BNP involving the function of oxidative stress parameters and inflammatory mediators in NDEA-induced HCC model in the male albino Wistar rats.

Chronic exposure to chemical carcinogens leads to several biochemical and genetic variations in the cells. N-nitrosodiethylamine (NDEA), a known environmental hepatic carcinogen and one of

the most toxic compounds has been employed as the inducer of tumor in diverse hepatic cancer models. In addition to it, the genotoxic and the mutagenic properties have been identified so far [14]. The cytochrome P_{450} enzyme-dependent metabolism of the NDEA results in reactive oxygen species (ROS) generation along with production of several free radicals, which ultimately results in the tumorigenic activity [15,16]. Presently, NDEA-induced HCC in rat models is comprehensively employed as an archetypal experimental model to examine the diverse hepatocarcinoma stages [17].

3.1 Materials and methods

3.1.1 Chemicals and reagents

HPLC grade acetonitrile (ACN), and water (H_2O) were procured from the Himedia Laboratories Ltd., Mumbai, India. Other required chemicals, like N-nitrosodiethyl amine (NDEA), 2,4-dinitrophenylhydrazine (DNPH), and GSH, were purchased exclusively from Sigma-Aldrich USA. AST kits, ALT kits, LDH kits, and ALP kits were obtained from Transasia Biomedicals Pvt. Ltd., Baddi, India. Interleukin-2 kits and Interleukin-6 kits were purchased exclusively from Sigma-Aldrich, USA while interleukin IL-1β and interleukin-10 were attained exclusively from Genetex Biotech Asia Pvt. Ltd., India. Caspase-8 and caspase-3 were acquired from Invitrogen Bioservices (Thermo Fisher) India Pvt. Ltd., India. Analytical grade reagents, chemicals (99% purity), and pure solvents were utilized for the research. In-house Borosil® distilled water system was used for obtaining double-distilled water.

3.1.2 Experimental animals

Wistar albino healthy rats of single sex (male), having 80 g to 120 g weight were procured from the Central Animal House Facility (CAHF), SD College of Pharmacy and Vocational Studies (SDCPVS), Muzaffarnagar, India with association of Babasaheb Bhimrao Ambedkar University (A Central University), Lucknow, India. After obtaining permission from the Institutional Animal Ethical Committee (IAEC), SDCPVS (Ref No SDCOP&VS/AH/CPCSEA/01/0027), the experiments and protocols were conducted with compliance to CPCSEA guidelines of Ethics, Department of Animal Welfare, Government of India. All the methods were performed with accord to the pertinent IAEC rules and directives. The experimental animals were kept under controlled conditions (25°C±5°C temperature; 44%–56% relative humidity; and 12 hr light: 12

hr dark cycle) in CAHF. The animals were kept inside the polypropylene cages, bedded with rice husks. They were allowed to have free access to water and were fed with standard rat pellets. Before, the commencement of experiment, the subjects were kept for 7 days and were suitably acclimatized.

3.1.3 *In vivo* pharmacokinetic studies

3.1.3.1 Determination of BNP and B in rat plasma

In a separate experiment, BNP and B were orally administered at 100 mg/kg body weight to the albino Wistar rats and blood was collected from retro-orbital plexus at 0.083 hr, 0.25 hr, 0.5 hr, 1 hr, 2 hr, 4 hr, 8 hr, 12 hr, 16 hr, 24 hr, and 48 hr time points from retro-orbital plexus (n=3). After collection, blood samples were collected into 2 mL eppendorf tube containing EDTA (Ethylenediaminetetraacetic acid) and centrifuged at 10,000 rpm for 10 min to separate the plasma and stored at –20°C until analysis. HPLC analysis was conducted within 20 days of plasma samples collection [18,19].

3.1.3.2 Preparation of plasma standards and test samples

In all, 1 mg/mL stock solution of B was prepared in ACN. A total of 0.02, 0.1, 0.2, 0.5, 1, 2, 5, 10, 50, 100 μg/mL of working solutions were prepared from this stock solution in ACN. In all, 100 μL of blank plasma and 100 μL of working solutions were taken in separate tubes and vortexed for 30 min. Subsequently, the centrifugation process was performed at 13,000 rpm for the duration of 5 min where the supernatant was separated and carefully taken into the other centrifuge tubes and were dried further at 40°C temperature for the whole night. Afterward, the centrifuge tubes were reconstituted with ACN (50 μL), vortexed for the duration of 10 min, and 20 μL volume was injected to the HPLC system for the chromatographic analysis. The final concentrations of the working solutions were found to be 0.01 μg/mL, 0.05 μg/mL, 0.1 μg/mL, 0.25 μg/mL, 0.5 μg/mL, 1 μg/mL, 2.5 μg/mL, 5.0 μg/mL, 25 μg/mL, and 50 μg/mL, respectively. Quality control (QC) samples were also prepared at concentrations of 0.005 μg/mL, 0.5 μg/mL, and 40 μg/mL, representing high quality control (LQC), medium quality control (MQC) and low quality control (HQC) samples, respectively. Triplicate calibrants and QC samples were prepared at each concentration. For test samples, 100 μL of test plasma and 100 μL of ACN were taken in

a test tube and vortexed for 30 min. The procedure was similar to the previously described method.

3.1.3.3 HPLC conditions

For the plasma determination of B sample and BNP sample, separations were conducted through a Waters® chromatographic system (LC-20AD) endowed with a photodiode array detector system. The elution was performed on a gradient mode employing the mobile phase ACN:H_2O at a ratio of 9:1. The flow rate was kept at 1 mL/min with 15 min runtime. The separation was performed using RP-C18 column (5.0 µ particle size, 4.6 mm internal diameter and 250 mm length) with λmax of 230 nm, and the temperature was maintained at 40°C throughout the experiment. The washing of the column was performed after each and every run by employing ACN:H_2O as the elution solvent in ratio of 1:1 along with blank ACN injection. The final data were analyzed by utilizing the software WinNonlin v.1.5.3.

3.1.4 *In vivo* pharmacodynamic studies

3.1.4.1 Experimental design

Wistar albino rats of 6-weeks age were employed. The experimental animal was allocated randomly to the 7-groups, each having 8 candidates [20-22]. The following groups were designed:

- **Group 1:** Normal control group; 0.25% carboxymethyl cellulose (2 mL/kg)
- **Group 2:** Carcinogen control group; 100 mg/kg of N-nitrosodiethylamine (NDEA) through intraperitoneal (i.p.) route. It was administered once a week for the total 6 weeks duration.
- **Group 3:** Positive control group; NDEA + 10 mg/kg of 5-fluorouracil (5-FU) through intraperitoneal (i.p.) route. It was administered after the induction of HCC for 15 days.
- **Group 4:** NDEA + 50 mg/kg of B. It was administered orally after the induction of HCC for 15 days.
- **Group 5:** NDEA + 100 mg/kg of B. It was administered orally after the induction of HCC for 15 days.

- **Group 6:** NDEA + 50 mg/kg of BNP. It was administered orally after the induction of HCC for 15 days.
- **Group 7:** NDEA + 100 mg/kg of BNP. It was administered orally after the induction of HCC for 15 days.

Recent reports [21,22] stated that in Wistar albino rats, HCC gets induced by injecting 100 mg/kg b.w. NDEA, once a week for six weeks duration. The adopted protocol involved administration of NDEA to the experimental animals belonging to the Group-2 to Group-6 after adapting and initial acclimatizing for 7 days. After administration of NDEA for the 6 weeks, curative agents such as B, BNP, and 5-FU were administration against hepatic injury for the duration of 15 days. After the termination of the study, the experimental animals were sacrificed by the application of cervical decapitation method. The animal livers were immediately excised, rinsed in ice-cold 0.9% saline, and further stored at -80°C temperature for further oxidative parameter analysis, morphological investigations, and determining the apoptotic parameters.

3.1.4.2 Calculation of various physiological parameters

The alterations in the body weight were determined at the initial day and the final day of the study, and the % weight gains were estimated. The carcinogenic nodules amounts and their percentage occurrence were also estimated to scrutinize the cytotoxic outcomes between the treated groups and untreated groups.

3.1.4.3 Estimation of various enzymes and antioxidant markers

The enzyme levels in the serum, including lactate dehydrogenase (LDH), aspartate aminotransferase (AST), alkaline phosphatase (ALP) and alanine aminotransferase (ALT), were determined by utilizing the available commercial kits. The oxidative stress parameters, including catalase (CAT), protein carbonyl (ProC), superoxide dismutase (SOD), glutathione (GSH) and thiobarbituric acid reactive substances (TBARS) were estimated in liver tissue.

3.1.4.3.1 Serum aspartate aminotransferase (AST) and alanine aminotransferase (ALT) Working solutions were formed by initially dissolving 4 mL of reagent 1 (mixture of Lalanine and α-ketoglutarate for ALT and mixture of L-aspartate and α-ketoglutarate for AST) and 1 mL

of reagent 2 (mixture of nicotinamide adenine dineucleotide phosphate, NADP and lactate dehydrogenase, LDH) and kept at 2 to 8°C for future use. The whole assay was performed in a cuvette and each cuvette contained 1.0 mL of working solution and 0.1 mL of serum. This was incubated for 1 min at 37°C and the change in optical density (ΔA340/min) was measured per minute for the next 3 min using a UV/VIS Spectrophotometer (Labtronics, Australia). Data were calculated by the following equations [23]:

$$\Delta A340/min = [A340 (time\ 2) - A340 (time\ 1)]/[time\ 2 (min) - time\ 1 (min)]$$

$$ALT \text{ or } AST \text{ Activity } (U\ L^{-1}) = \Delta A340/min \times 1746$$

3.1.4.3.2 Plasma alkaline phosphatase (ALP)

All groups contained 1 mL buffer substrate and 3 mL distilled water. Later, 0.1 mL distilled water, 0.1 mL phenol and 0.1 mL serum were added to the blank, standard and test groups, respectively. All the groups, including the normal control, were incubated for 15 min at 37°C. Then, plasma (0.1 mL) was added to the control group after incubation. All the tubes were mixed properly and absorbance was measured at 510 nm of wavelength. Plasma ALP was calculated as follows [24]:

$$ALP \text{ activity } (U\ L^{-1}) = [A (test) - A (control)/A (standard) - A (blank)] \times 7.1$$

3.1.4.3.3 Lactate dehydrogenase (LDH)

According to the manufacturer's protocol, serum samples (0.1 mL) were added in working reagent (1 mL) and at 340 nm, the absorbance was measured on regular intervals for 3 min at 1 min interval. Serum LDH was calculated as follows [24]:

$$\Delta A340/min = [A340 (time\ 2) - A340 (time\ 1)]/[time\ 2 (min) - time\ 1 (min)]$$

$$LDH \text{ Activity } (U\ L^{-1}) = \Delta A340/min \times 16030$$

3.1.4.3.4 Tissue thiobarbituric acid reactive substances (TBARS)

TBARS assay was performed as per the method prescribed in the previous literature with slight modifications [25]. 1.0 mL of 10% (w/v) tissue homogenate, 0.5 mL of 30% trichloroacetic acid and 0.5 mL of 0.8% thiobarbituric acid were taken together in a falcon tube and covered with

aluminium foil. Then, for 30 min time duration, at 80°C temperature, the tubes were kept in a shaking water bath. Later, it was cooled for 15 min and centrifuged at 3000 rpm for 15 min. Absorbance was recorded spectrophotometrically at 540 nM against blank in which tissue sample is absent. The amount of MDA present in a sample was calculated according to the following equation:

nM of MDA/mg of protein = (V × OD at 540 nM) / (0.56 × protein concentration)
where, V is final volume of the test solution.

3.1.4.3.5 Tissue protein carbonyl (ProC)

PC assay was performed as per the method prescribed in the previous literature with slight modifications [24]. 10% tissue homogenate was formed in the distilled water. From this, 150 µL of the tissue homogenate was taken into the eppendorf tube and precipitated by adding 500 µL of 10% trichloracetic acid. Then the tubes were centrifuges at 13,000 rpm for 2 min and supernatant was discarded. Later, the cell pellets were incubated with 500µL of 0.2% 2,4-dinitrophenylhydrazine with constant vortexing at every 5 min interval for 1 h. After that, supernatant was removed and cell pellets were washed with 500µL ethanol:ethyl acetate (1:1) solution three times. At last, pellets were dissolved in 600µL Guanidine Hydrochloride (6M) and absorbance was measured at 360 nM. Blanks solution was prepared in the similar procedure where cells were absent. The PC content was calculated as follows:

ProC (µM/µg of protein) = (A360 sample – A360 sample blank)/ µg of protein

3.1.4.3.6 Tissue glutathione (GSH)

GSH assay was performed as per the method prescribed in the previous literature with slight modifications [24]. 10% w/v tissue homogenate (0.2 mL) was taken in an eppendorf tube and 1.8 mL distilled water added to it. Simultaneously, we prepared precipitating solution by mixing ethylenediaminetetraacetic acid disodium salt (0.2 g), sodium chloride (30 g), and glacial metaphosphoric acid (1.67 g) in 100 mL distilled water. This precipitating solution was added to the above mixture. The mixture was afterward permitted to stand for 5 min and filtered. To 2 ml of filtrate, 1.0 mL of 0.4% w/v 5,5'-dithio-bis-2-nitrobenzoic acid and 8.0 mL of phosphate solution (0.3 M) were added and centrifuged at 13000 rpm for the duration of 1 min. A blank

was prepared in an alike way where the tissue section was absent. Afterward, the spectrophotometric absorbance was determined at 412 nM. The Bradford reagent was employed to estimate the total protein content and compared with the standard bovine serum albumin. The tissue GSH content was calculated as follows:

GSH (mM/mg of protein) = (310.4 × Ei × OD at 412 nm)/mg of protein, where Ei is the correction factor (0.542).

3.1.4.3.7 Tissue superoxide dismutase (SOD)

Determination of SOD in the test samples were performed as per the method prescribed in the previous literature with slight modifications [26]. 100 µL of 10% cytosolic supernatant was prepared with tris–hydrochloric acid buffer (pH=8.5) and final volume was adjusted up to 3.0 mL with the same buffer. Finally, 25µL of pyrogallol was added and change in absorbance was recorded at 420 nM at one minute interval for 3 minutes. Blank was prepared in which tissue sample was absent. One unit of SOD is described as the amount of enzyme required causing 50%inhibition of pyrogallol autooxidation per 3 mL of assay mixture and is given by the formula:

Unit of SOD/µg or protein = [100 × [(A-B)/(A×50)]]/µg of protein.

where A = Change in absorbance per minute in control and B = Change in absorbance per minute in test sample.

3.1.4.3.8 Tissue catalase (CAT)

CAT enzyme estimation was performed as per procedure which was described previously [24]. 10% (w/v) tissue homogenate was prepared in 50mM phosphate buffer and centrifuged at 10000 rpm for 20 minutes. 50 µL of supernatant was added to a tube containing 2.95 mL of 19 mM solution of hydrogen peroxide (H2O2) prepared in potassium phosphate buffer. Disappearance of H2O2 was monitored at 1 min interval for 3 mins at 240 nM. CAT activity was calculated as follows:

nM of H2O2/min/µg of protein = (ΔA/min × volume of assay)/(0.0719 × volume of sample × µg of protein)

3.1.4.4 Estimation of catabolic by-products

The levels of catabolic by-products (bilirubin and biliverdin) were estimated in liver tissue.

3.1.4.4.1 Tissue bilirubin

Bilirubin in liver was measured as per the following procedure published earlier in the literature with slight modifications [24,27]. All the tissue samples were thawed and homogenized in phosphate buffer saline (8.0 g sodium chloride, 0.2 g potassium chloride, 0.2 g potassium dihydrogen phosphate, 1.15 g disodium hydrogen phosphate, 0.372 g ethylenediaminetetraacetic acid disodium salt, pH 7.4). 500 µL of tissue homogenate (10%) was added to 2.0 mL of 1.5% butylatedhydroxy toluene in acetone:ethanol (1:1) in a eppendorf tube. Simultaneously, fresh diazo reagent was prepared by mixing 300µL of 10% sodium nitriteand 8.0 mL of 2M p-toluene sulfonic acid, then combining 4.0 mL of this mixture with 2.0 mL of 2.1% p-iodoaniline in glacial acetic acid, kept at room temperature for 2.0 min. Then this solution was diluted with distilled water (10 mL) and 200µL of 1.5M ammonium sulfamate. This working diazo reagent was kept on ice for 5min and 500µL was added to each sample homogenates. Diazo blank reagent was freshly prepared by combining 2 mL of p-toluene sulfonic acid and 5.0 mL of 10% ascorbic acid, followed by addition of 2.1% p-iodoaniline in glacial acetic acid and 2.0 mL of n-butyl acetate, mixed and used immediately. Finally, all the tubes were incubated for 1 hour on ice in dark. After incubation freshly prepared 3.0 mL of 1% ascorbic acid in 0.1 M sodium chloride was added to each vial. All the vials were shaken vigorously, kept for 1.0 min and centrifuged at 2400 rpm for 10 min. The absorbance of the upper organic phase was taken at 530 nM wavelength. The content of bilirubin was calculated as follows:

A530 sample – A530 sample blank = ΔA530Test

3.1.4.4.2 Tissue biliverdin

Estimation of biliverdin was performed as per the method prescribed in the previous literature with slight modifications [24,27]. Tissue samples were homogenized in phosphate buffer saline as per described in the previous section. 500 µL of tissue homogenate (10%) was combined with 500µL of 10 M glacial acetic acid, 400µL of 40 mM ascorbic acid, 500µL of double distilled water and 100µL of 200 mM barbituric acid. Samples were incubated in a water bath at 95°C in

dark and then samples were extracted with butanol, vortexed and centrifuged. The upper organic layer was carefully removed and extracted with 2.5 mL 2M sodium hydroxide. The absorbance of upper layer was taken at 535 nM wavelength. The content of biliverdin was calculated as follows:

A535sample – A535 sample blank = ΔA535Test

3.1.4.5 Estimation of cytokines by ELISA

Elevated levels of pro-inflammatory cytokines such as IL-2, IL-6, IL-10 and IL-1β in hepatic tissue were examined by ELISA as per manufacturer's instructions. Furthermore, the levels of caspase-3 and -8 were also examined by ELISA as per manufacturer's protocol [28].

3.1.4.6 Histopathological and Scanning Electron Microscopic (SEM) analysis of liver tissue

The histopathology and SEM analysis of liver tissue of various groups were performed.

3.1.4.6.1 Histopathology

Histopathological studies were also performed to find out the morphological changes of liver cells after B and BNP administration. The hepatic tissues from each group were evaluated for their morphological modification using eosin and hematoxylin staining. The hepatic tissues were overnight conserved in 10% formalin overnight. Next day, the cells again were superseded by 70% isopropanol overnight. Presently, the tissues were made in contact with isopropanol at various concentrations (70%, 90%, and 100%) and dehydrated by using 100% xylene. The tissue samples were then embedded in bees wax and 5 µM sections were prepared by using microtome. Then, the tissues were succeeded by hematoxylin and eosin staining and observed under microscope (magnification 40X) [24].

3.1.4.6.2 SEM analysis

The hepatic tissue samples of 2–4 mm were taken carefully and primary fixation was performed using the 2.5% glutaraldehyde for at 4°C temperature for the duration of 2–6 hr. Subsequently, 0.1 M phosphate buffer was employed for washing for 15 min duration at a temperature of 4°C. Afterward, a postfixation agent, osmium tetroxide (1%) was employed for the duration of 2 hr at 4°C. Again, the samples were washed in 0.1 M phosphate buffer for three times at 15-min

interval and kept at 4°C. Later, these samples were dehydrated with acetone at a variety of concentrations (30%, 50%, 70%, 90%, 95%, and 100%). Later, all the samples were air dried at critical point drying (31.5°C at 1100 psi) and room temperature. At last, samples were mounted over the aluminum stubs with adhesive tape and scrutinized for the morphological modification employing the SEM (JEOL JSM-6490LV) [24].

3.1.5 Statistical data analysis

Statistical data analysis was performed using GraphPad Prism 5.0. All results were expressed as mean ± standard deviation (SD). The data were examined by one-way analysis of variance (ANOVA) followed by the Bonferroni multiple comparison test. Statistical significant differences were considered with respect to the carcinogen control group (***$p<0.001$, **$p<0.01$ and *$p<0.05$).

3.2 Results

3.2.1 Determination of plasma concentration of B and BNP using HPLC

A linear regression performed over a range of 0.01–50 μg/mL yielded a correlation coefficient (r2) of >0.9987 for B. The accuracy of the assay was found to be within 83%–94%, and recovery of the samples was 75–81%. The compound B's retention time (Rt) was observed to be 8.87 min (Figure 5A). The time required to reach the maximum plasma concentration (Tmax), plasma concentration reached 50% (t1/2), total area under the curve (AUC), and the maximum plasma concentration (Cmax) as described in Figure 4B as well as Table 3 were found to be 8h, 11.11 h, 838.43 μg·h/mL, and 47.43 μg/mL for BNP and 4h, 10.73 hr, 133.81 μg·h/mL, and 10.34 μg/mL for B, respectively. Higher Tmax from nanoparticles was observed because of nanoparticles are present in blood circulation for longer time which improved the anti-HCC response in this study.

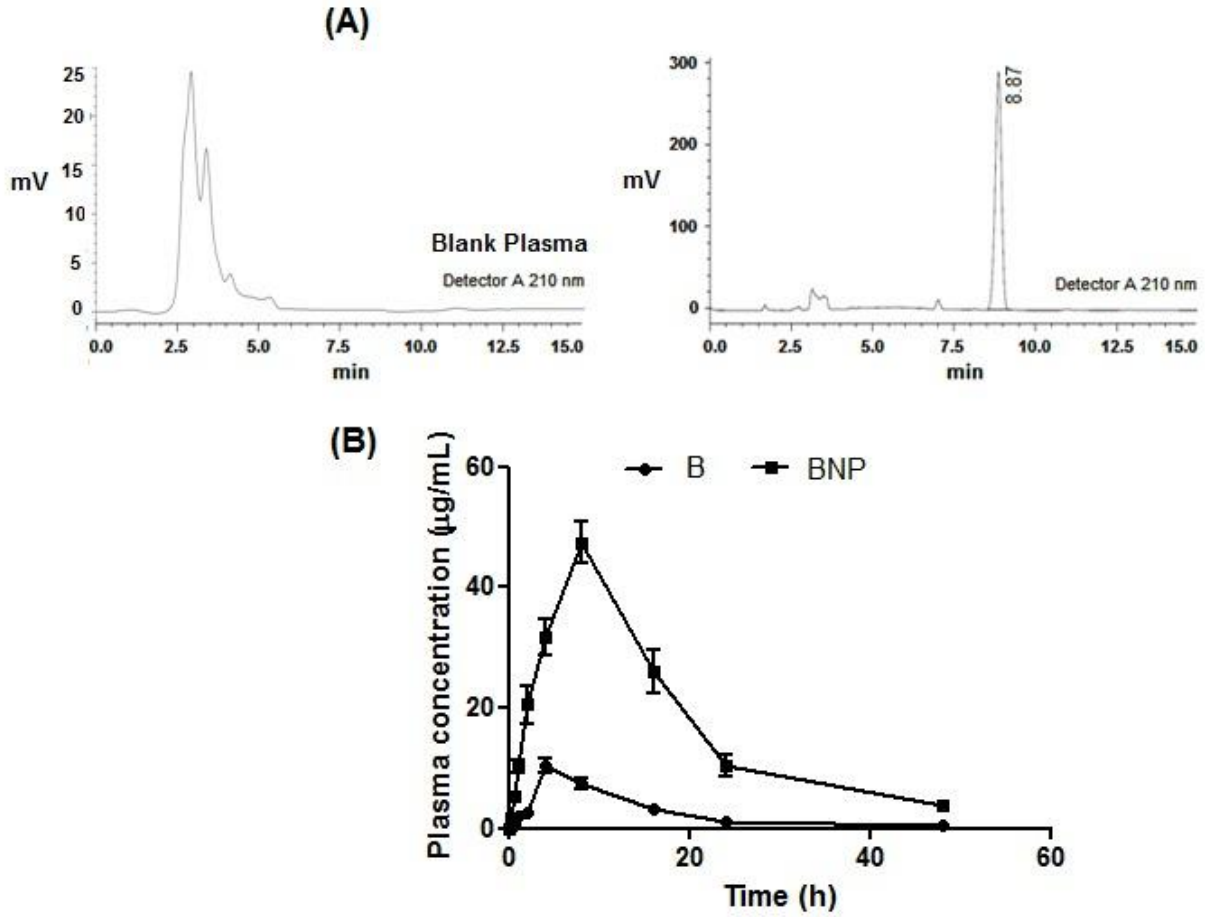

Figure 5 Plasma-concentration studies (A) High Performance Liquid chromatogram of B. (B) Plasma drug concentrations in albino Wistar rats of BNP and B after oral administration at diverse time points.

Table 3 Pharmacokinetic parameters of **B** and **BNP**

Parameter	**B**	**BNP**
$t_{1/2}$	10.73	11.11
T_{max} (h)	4.00	8.00
C_{max} (µg/ mL)	10.34±0.45	47.43±0.75
AUMC (µg.h^2/ mL)	1724.12	12182.35
MRT (h)	12.88±1.35	14.53±1.56
CL (h)	0.007	0.0011
$AUC_{0-\infty}$ (µg.h/mL)	133.81±35.71	838.43±41.32

3.2.2 Calculation of physiological and biochemical parameters in liver

The protective effects of B and BNP were estimated through various physiological parameters, including liver weight, body weight, and tumor incidence number in the rat liver. The body weight variation in the carcinogen control group was more prominent than that in the normal control group. The treatment with BNP, B, and 5-FU effectively regularized the body weight disparity as perceived in the carcinogen control group. An augmentation in the tumor incidence number and liver weight were perceived in the carcinogen control group. The treatment with BNP, B, and 5-FU caused a lessening in the tumor incidence number and liver weight when contrasted with the carcinogen control group. The general consequences of 100 mg/kg dose of BNP was superior to 5-FU, the most popular chemotherapeutic agent (Table 4).

Table 4 Role of **BNP** and **B** treatment on the rat liver factors in NDEA-exposed carcinogenesis. (CC: Carcinogen Control, NC: Normal Control, **B**: Betulinic acid (50mg/kg), PC: Positive Control, **B**: Betulinic acid (100 mg/kg), **BNP**: Betulinic acid nanoparticles (50mg/kg) and **BNP**: Betulinic acid nanoparticles (100 mg/kg).

Sr. No.	Groups	Initial day body weight (g)	Final day body weight (g)	Weight variation (g)	Liver weight (g)	Tumor incidence no.
1	NC	120.00±3.34	146.00±4.27	26.00±2.12	8.26±0.93	0.00±0.00
2	CC	121.00±2.23	102.00±1.46	-19.00±2.16	13.97±1.62	32.00±1.31
3	PC	115.00±4.68	125.00±3.15***	10.00±1.26***	10.43±1.71***	6.00±0.83***
4	**B**(50)	121.00±1.89	132.00±4.25***	11.00±1.82***	12.78±0.73	19.00±0.97***
5	**B**(100)	118.00±2.15	130.00±2.12***	12.00±2.93***	12.03±1.25*	14.00±1.01***
6	**BNP**(50)	114.00±2.12	130.00±2.19***	16.00±3.75***	11.61±0.63**	12.00±0.84***
7	**BNP**(100)	120.00±1.89	142.00±4.78***	22.00±1.98***	9.36±0.39***	4.00±0.31***

Note: Data represented here as mean±SD (n=8). Statistically important disparity were detected between test group with CC groups [one way ANOVA followed by Bonferroni multiple comparison test (***$p<0.001$, **$p<0.01$ and *$p<0.05$)]

In addition to it, we stated that the carcinogen control group expressed a noticeable augmentation in the hepatic damage marker enzyme stages of ALT, AST, LDH, and ALP in the rat serum when evaluated against the normal control group (Figure 6A). The treatment with BNP, 5-FU, and B, displayed their ability to significantly restore ($p<0.001$) these markers to the standard stage. The consequence demonstrated by BNP at 100 mg/kg was correspondent to the 5-FU and further asserted than B.

(A)

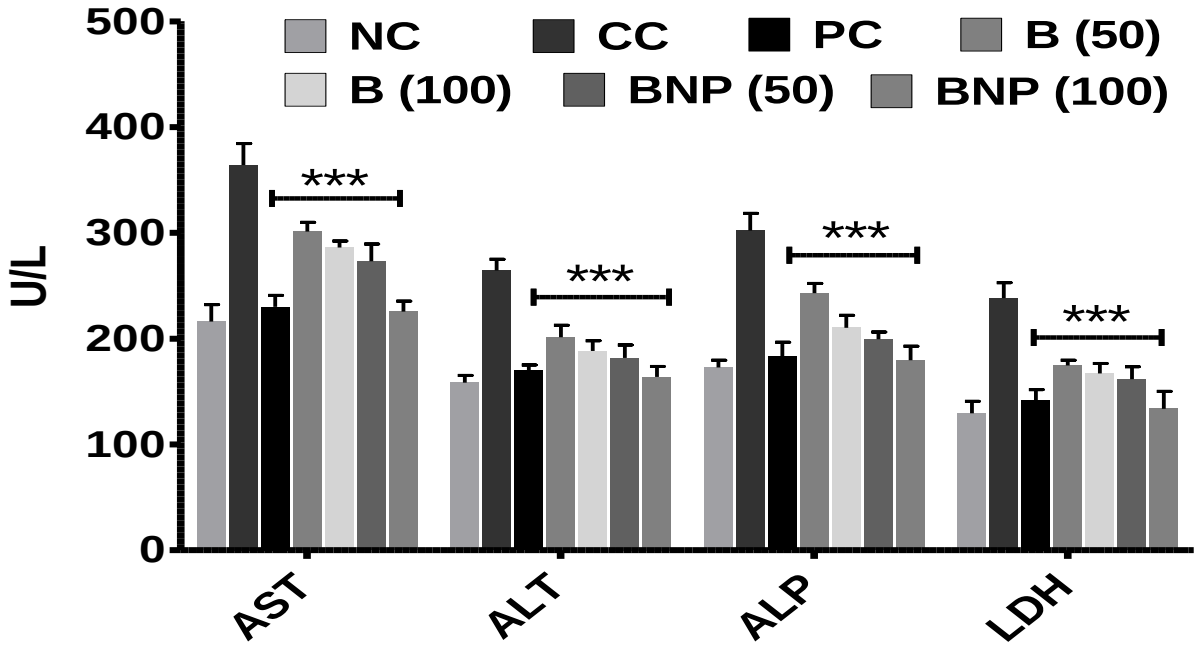

(B)

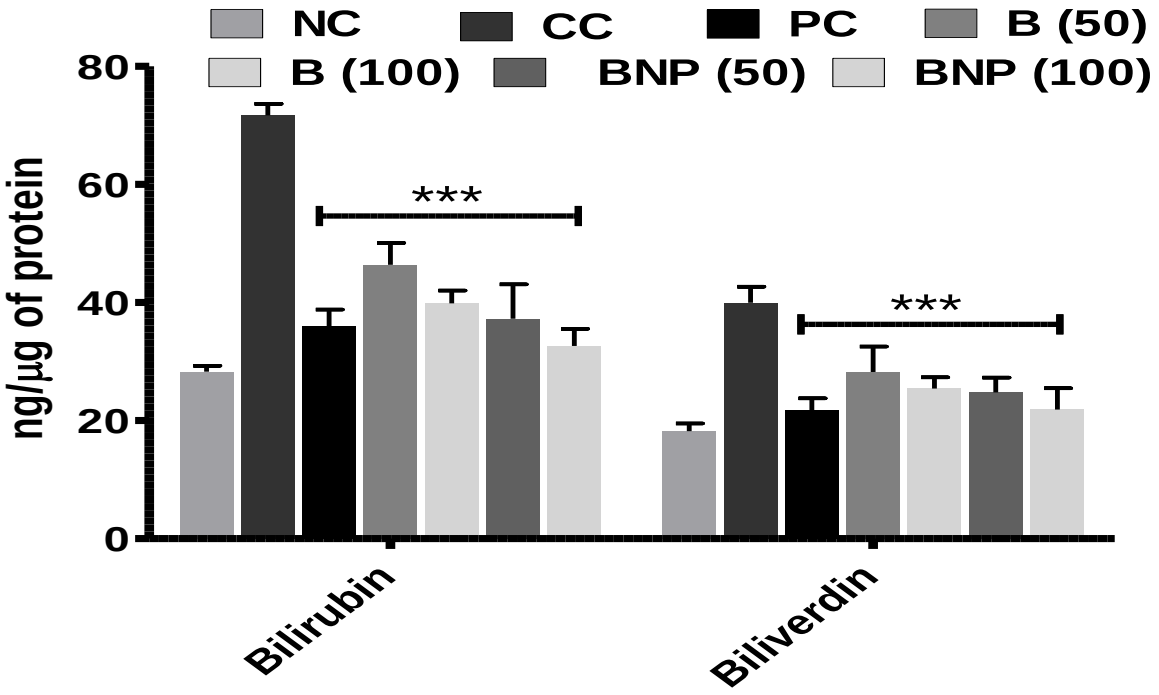

Figure 6 The potentials of orally administered **BNP** and **B** at 100 mg/kg and 50 mg/kg for 15 days in the carcinogen control rats, **(A)** The enzyme levels of ALT, AST, LDH, and ALP in serum, **(B)** Catabolic by-products (biliverdin and bilirubin).

Note: Data are represented as mean±SD (n=8). Statistically significant differences were observed between carcinogen control and test groups [one way-ANOVA followed by Bonferroni multiple comparison test (***p<0.001, **p<0.01, *p<0.05)].

Additionally, the consequences of BNP and B on catabolic pigments such as biliverdin and bilirubin in the hepatic tissues were also investigated (Figure 6B). The administrations of BNP and B revealed a considerable (p<0.001) normalization in the stages of biliverdin and bilirubin that were raised higher than 2-folds in the carcinogen control group. The outcomes of BNP were nearly analogous to5-FU, the standard chemotherapeutic agent.

3.2.3 Calculation of oxidative stress parameters in liver tissue

The antioxidant potential of the liver was evaluated due to the purposeful participation of the oxidative stress in the pathogenesis of the cancer. Table 5 described the consequences of treatment over the oxidative stress markers (SOD, malondialdehyde, CAT, GSH, and ProC). It was perceived that CAT enzyme and SOD enzyme were significantly diminished in the carcinogen control group as evaluated to the normal control group, whereas only an inconsequential lessening was observed in the BNP-, 5-FU-, B-treated groups. The GSH concentration was reduced up to 5-folds to 6-folds in the carcinogen control rats, and was considerably (p<0.001) reinstated after treatment with 5-FU and BNP, but not with B. To the converse, the stage of ProC was enhanced up to 2-folds in the carcinogen control group, which productively reinstated after treating with BNP, 5-FU, and B. Likewise, the stage of MDA was enhanced up to 2-folds in the carcinogen control group, which considerably (p<0.001) reinstated after the treatment with 100 mg/kg BNP and 5-FU.

Table 5 Study of anti-oxidative parameters in NDEA-exposed carcinogenesis in rats. (NC: Normal Control, CC: Carcinogen Control, PC: Positive Control, **B**: Betulinic acid (50mg/kg), **B**: Betulinic acid (100 mg/kg), **BNP**: Betulinic acid nanoparticles (50mg/kg) and **BNP**: Betulinic acid nanoparticles (100 mg/kg).

Sr. No.	Parameters	NC	CC	PC	B(50)	B(100)	BNP(50)	BNP(100)
1.	SOD (U/µg of protein)	0.26±0.02	0.06±0.01	0.24±0.09***	0.19±0.07***	0.21±0.05***	0.22±0.04***	0.25±0.04***
2.	CAT (nM of H_2O_2/min/µg	10.06±0.65	4.88±0.23	8.41±0.68***	5.75±0.27	6.81±0.73***	7.02±0.77***	8.32±0.51***

	of protein)							
3.	ProC (μM/μg of protein)	0.58±0.02	1.35±0.01	0.69±0.03***	0.91±0.02***	0.76±0.02***	0.74±0.01***	0.61±0.03***
4.	TBARS (nM of MDA/mg of protein)	0.07±0.01	0.16±0.03	0.09±0.01***	0.13±0.05	0.11±0.04*	0.10±0.01**	0.08±0.02***
5.	GSH (mM/mg of Protein)	6.46±0.56	1.12±0.57	5.04±0.61***	3.25±0.65*	3.50±0.32*	4.63±0.33***	5.00±0.21***

Note: Data represented here as mean±SD (n=8). Statistically considerable disparities were detected among the test groups and CC groups [one way ANOVA followed by Bonferroni multiple comparison test (***$p<0.001$, **$p<0.01$ and *$p<0.05$)]

3.2.4 Effects of B and BNP on proinflammatory (IL-2, IL-6, IL-10 and IL-1β) and apoptotic mediators (caspase-3 and -8)

In order to explore the effects of B and BNP on cancer-associated inflammatory and apoptotic events, we conducted ELISA and predicted the concentration of proinflammatory cytokines (IL-2, IL-6, IL-10 and IL-1β; Figure 7A) and apoptotic mediators (caspase-3 and -8) in rat liver (Figure 7B). The liver inflammatory markers concentrations were lifted up in the carcinogen control group. To the converse, the apoptotic markers were strikingly decreased up to 2-folds in the carcinogen control group. The reduction in caspase-8 levels and caspase-3 levels was further distinct than the elevations in all the cytokines. Both B and BNP restored the caspase-8 levels and caspase-3 levels more efficiently than those of the tested cytokines. Although both compounds, BNP and B, demonstrated their capacity to rise the decreased levels of caspase-8 and caspase-3, the restoring capability of BNP was more prominent than that of B and 5-FU.

(A)

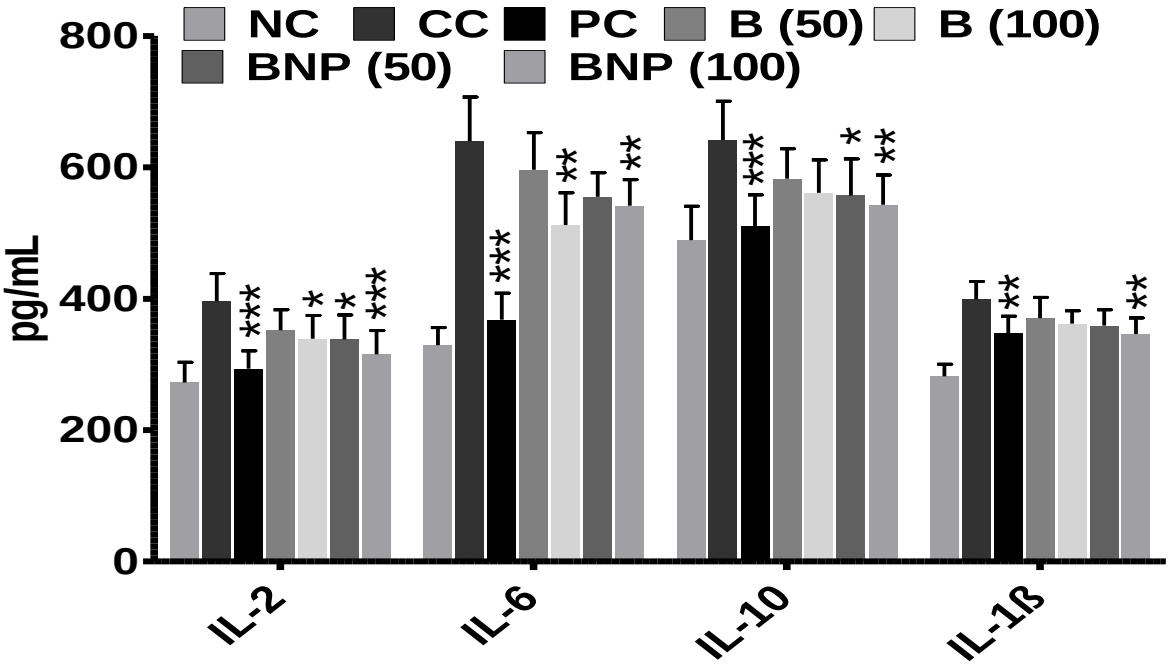

(B)

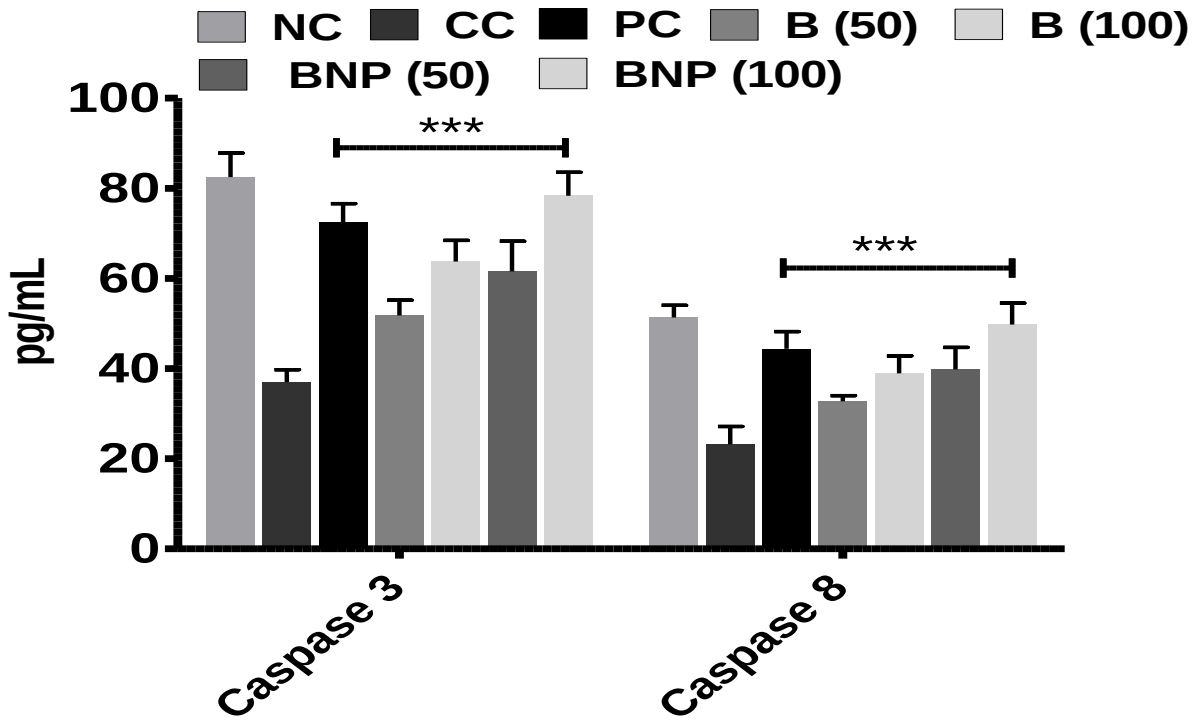

Figure 7 Therapeutic potentials of **BNP** and **B** after oral administration at doses 100 mg/kg and 50 mg/kg for 15 days in carcinogen control rats. **(A)** Anti-proliferative biomarkers IL-6, IL-2, IL-1β, IL-10 **(B)** Caspase-8 and Caspase-3.

Note: The data are represented as mean±SD where n=8. Statistically significant disparities were detected between test groups and carcinogen control [one way-ANOVA followed by Bonferroni multiple comparison test **p<0.01, (***p<0.001, *p<0.05)].

3.2.5 Morphology, histopathology and SEM analysis

Morphological changes were observed using intact liver of the various groups. There was an obvious image disparity in the carcinogenic nodules quantity among the BNP, B, and carcinogen control groups (Figure 8A). Furthermore, histological changes in the liver tissue were observed in normal and various treated groups using hematoxylin and eosin (H&E) staining. In the normal control group, the section showed normal architecture of cells with the presence of nuclei within the cells.

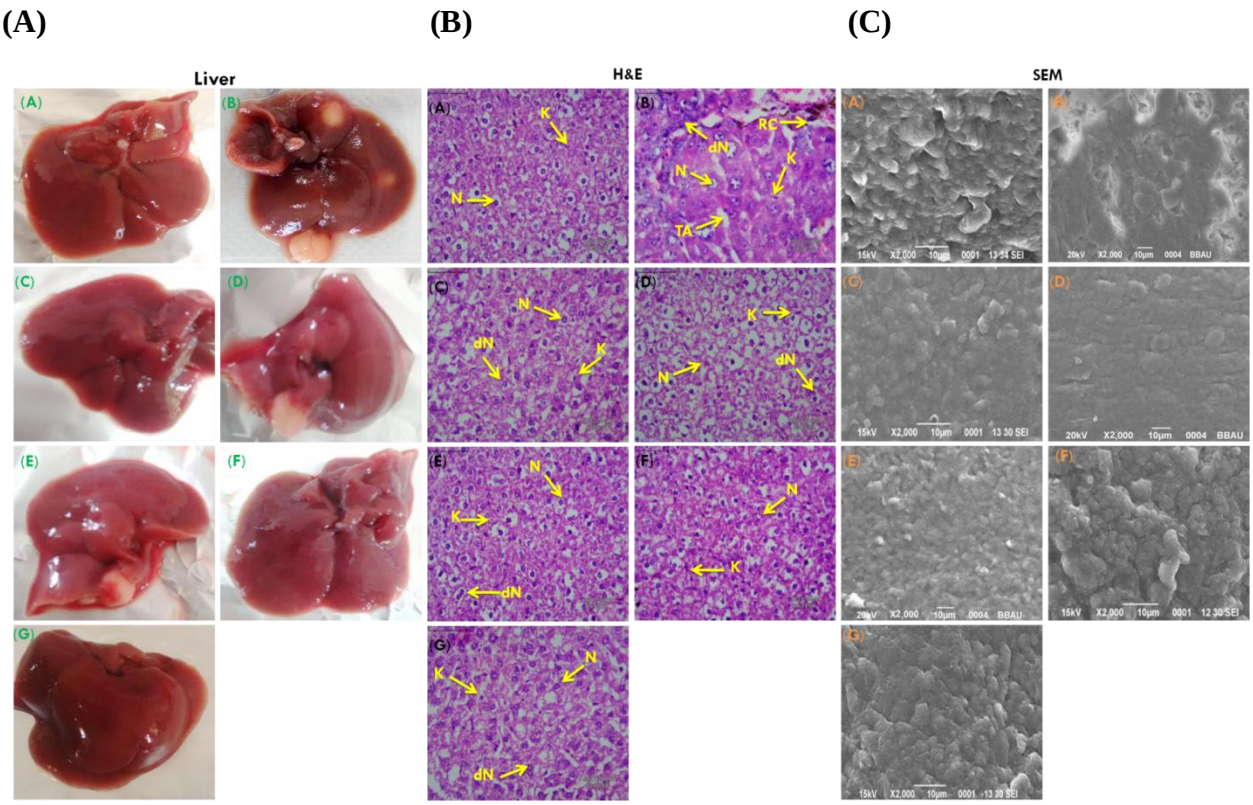

Figure 8 Highlights of the plausible alterations in the hepatopathology of NDEA-induced rats.

Notes: (A) Integral liver depicting the abundant carcinogenic nodules in the carcinogen control group that were reduced extensively or deficient after treating with B (50), 5-FU, BNP (50), B (100), and BNP (100). (B) Histopathological changes (40×, scale bar 50 µm). (C) SEM

photomicrographs of the liver tissues (2,000×). Again, histopathology and SEM analysis show that BNP has greater potential to restore liver cell architecture than B. The studied groups are as follows: (1) NC, (2) CC (NDEA), (3) PC (NDEA + 5-FU), (4) NDEA + B (50), (5) NDEA + B (100), (6) NDEA + BNP (50) and (7) NDEA + BNP (100). N, normal nucleus; dN, degenerated nucleus; RC, ruptured hepatic cells; TA, tumor anaplastic cells and K, Kupffer cells.

However, the carcinogen control group of the liver demonstrated the existence of binucleate, pasting of architecture, and enlarged polygonal hepatocytes. Particularly, carcinogenic animals' liver section presented degenerated nucleus (dN), irregular sinusoids, ruptured hepatic cells (RC) of Kupffer cells (K), tumor anaplastic cells (TA), and tumoral vacuoles. A noticeable enhancement in the disgusting microscopic manifestation of the hepatic tissue was monitored after treating with BNP and B at 100 mg/kg and 50 mg/kg (Figure 8B). Furthermore, SEM analysis also pursued by an analogous prototype where degenerated tumor cells and loss of architecture were less important in BNP, B, and 5-FU treated rats as compared to the carcinogenic control group (Figure 8C).

3.3 Discussion

Through in vitro human cancer cell line study we have already noted that BNP hold a promise to be a potential drug candidate for HCC treatment. However for deep pharmacological understanding, BNP need to go through in vivo pharmacological screening. Prior to this, it was also essential to explore *in vivo* oral pharmacokinetics of the prepared BNP [29, 30]. *In vivo* pharmacokinetic studies expressed that the nano-form of B (BNP) exhibited a superior volume of distribution in the rat plasma as compared to the parent compound B. The lower the particle size of the BNP, the higher the extent of the oral administration of the B. The acquired data from the pharmacokinetic studies (through AUC results) revealed that BNP had roughly 7-folds higher distribution in the rat plasma as compared to B. This amazing examination persuaded us to assess the anti-HCC perspectives of BNP in the experimental rat model bearing hepatocarcinoma features.

After discovering distinguished acceptable pharmacokinetic properties and *in vitro* efficacy, these compounds were investigated for *in vivo* study. The prime exploration of this research advocated that treating with 100 mg/kg dose of BNP appreciably reinstate the liver weight,

tumor incidence number, and body weight in the rat liver. The purposeful function of the oxidative stress in the tumor succession has extensively been a vehemently contested subject matter. It has beforehand stated that an augmentation in the oxidative stress results owing to the reactive oxygen species (ROS) generation and faults in the redox defense mechanisms [31]. This study divulged the biochemical variations correlated with NDEA-induced oxidative stress that were substantiated through decreased CAT, GSH, and SOD levels, on the contrary, enhancement in the formation of ProC and MDA. Modification in these biochemical factors corroborated the commencement of the liver oxidative stress under HCC conditions. The production of surfeit ROS during the oxidative stress condition significantly entails HCC pathogenesis through upregulation of intracellular signaling pathways, overexpression of oncogenes, and biochemical perturbation [32]. Treating BNP and B augments the anti-oxidative physiological progression by recovering the modified levels of SOD, GSH, MDA, CAT, and ProC. Besides, biliverdin and bilirubin are the catabolic derivatives of red blood corpuscles and disparity in the stages of biomarkers will designate the diseased hepatic state [33]. It was detected that NDEA exposure raises the stages of biliverdin and bilirubin, and they were considerably regularizes after the BNP and B treatments. In addition, enhanced levels of AST and ALT are a symptom of cirrhosis and hepatic liver damage [34]. Among the profile of liver function tests, ALP is an self-governing aspect for the survival of the HCC patient, and its preoperative stage can be employed to observe the reappearance in the high-risk HCC patients [35]. Therefore, the elevated intensity detected in the enzymes related with the liver function (ALT, ALP, and AST) replicated the progression of carcinogenesis during the condition of HCC. BNP treatment considerably lessens these enzymes levels to the normal that point towards the lessening in the hepatic injury [36]. Likewise, a significant augmentation in serum LDH level demonstrated non-specific modification in the integrity of the cell membrane and HCC liver metastases [37]. An elevated stages of serum LDH was detected in the NDEA-exposed group, which could be accountable for the damage of the liver cells and incidence of pre-neoplastic lesions. BNP treatment results in the reduction of the hepatic injury and improvement of preneoplastic lesions, almost certainly by its capability to get better the LDH enzyme stages and thereby potentiate its anti-HCC activities.

The cytokines present in the serum are the key managers engaged in the cancer progression inflammation pathogenesis [38]. B usually brings to bear anticancer activity moreover by activating the apoptotic mitochondrial pathway or by inducing cellular stress, such as DNA

damage and cytokine withdrawal [39-50]. Therefore, we examined the modified stages of caspases and cytokines between diverse faction through the ELISA and investigated the consequences of BNP and B treatments over the carcinogen control group. In NDEA-exposed rats, the inflammatory cytokines were raised and were declined to a definite degree after BNP and B administrations. On the contrary, caspase-8 and caspase-3 were rapidly decreased in the carcinogen control group and were notably raised again to the normal levels after BNP and B administrations. It was perceived that distinct to the tested cytokines, the stages of caspase-8 and caspase-3 in the NDEA-exposed group were quickly restored to normal after administration of B and BNP, and this effect was more pronounced in the BNP-treated group than the B-treated group. This surveillance yet again corroborated that the expression of the caspases participate and play crucial function in the HCC condition development and our lately developed BNP formulation can act primarily through the overexpression of the caspase-8 and caspase-3 at the precise cancer milieu of the liver. There was an obvious image disparity in the quantity of the carcinogenic nodules between the BNP and the carcinogen control groups. The manner of liver tissue in NDEA-exposed rats was extremely changed as verified through the expression of RC, multiple degenerated tumor cells, loss of architecture, TA, and tumoral vacuoles in H&E staining. Yet, the treatment with BNP and B decreases the occurrence of these modifications through the reinstatement of renewal of the liver parenchymal cells. Almost unaltered morphology and normal appearance were perceived predominantly for the BNP-treated group, which supplementary substantiated well with formerly conversed biochemical features and divulged the superior anti-tumor efficacy of the BNP. Afterward, the SEM analysis also followed an analogous prototype where trouncing of the architecture and degenerated tumor cells were slightest dominant in the BNP-treated group.

3.4 References

1. Yang J, Qiu B, Li X, Zhang H, Liu W. p53-p66shc/miR-21-Sod2 signaling is critical for the inhibitory effect of betulinic acid on hepatocellular carcinoma. Toxicology letters. 2015;238(3):1-0.
2. Lin J, Wu L, Bai X, Xie Y, Wang A, Zhang H, Yang X, Wan X, Lu X, Sang X, Zhao H. Combination treatment including targeted therapy for advanced hepatocellular carcinoma. Oncotarget. 2016;7(43):71036.
3. Sun L, Sun G, Yu Y, H Coy D. Is notch signaling a specific target in hepatocellular carcinoma?. Anti-Cancer Agents in Medicinal Chemistry (Formerly Current Medicinal Chemistry-Anti-Cancer Agents). 2015;15(7):809-15.
4. Marin JJ, Castaño B, Martinez-Becerra P, Rosales R, Monte MJ. Chemotherapy in the treatment of primary liver tumours. Cancer therapy. 2008;6(2).
5. Park SH, Lee Y, Han SH, Kwon SY, Kwon OS, Kim SS, Kim JH, Park YH, Lee JN, Bang SM, Cho EK. Systemic chemotherapy with doxorubicin, cisplatin and capecitabine for metastatic hepatocellular carcinoma. BMC cancer. 2006;6(1):3.
6. Okada S. Cancer chemoprevention as adjuvant therapy for hepatocellular carcinoma. 2001;31:357–358.
7. Park JG. Long-term outcomes of patients with advanced hepatocellular carcinoma who achieved complete remission after sorafenib therapy. Clinical and molecular hepatology. 2015;21(3):287.
8. Wilhelm S, Carter C, Lynch M, Lowinger T, Dumas J, Smith RA, Schwartz B, Simantov R, Kelley S. Discovery and development of sorafenib: a multikinase inhibitor for treating cancer. Nature reviews Drug discovery. 2006;5(10):835-44.
9. Cragg GM, Boyd MR, Khanna R, Newman DJ, Sausville EA. Natural product drug discovery and development. InPhytochemicals in Human Health Protection, Nutrition, and Plant Defense. 1999;1-29.
10. Moghaddam MG, Ahmad FB, Samzadeh-Kermani A. Biological activity of betulinic acid: a review. Pharmacology & Pharmacy 2012;03 (02):119-23
11. Armstrong B, Doll R. Environmental factors and cancer incidence and mortality in different countries, with special reference to dietary practices. International journal of cancer. 1975;15(4):617-31.

12. Fujioka T, Kashiwada Y, Kilkuskie RE, Cosentino LM, Ballas LM, Jiang JB, Janzen WP, Chen IS, Lee KH. Anti-AIDS agents, 11. Betulinic acid and platanic acid as anti-HIV principles from Syzigium claviflorum, and the anti-HIV activity of structurally related triterpenoids. Journal of natural products. 1994;57(2):243-7.
13. Mayaux JF, Bousseau A, Pauwels R, Huet T, Henin Y, Dereu N, Evers M, Soler F, Poujade C, De Clercq E. Triterpene derivatives that block entry of human immunodeficiency virus type 1 into cells. Proceedings of the National Academy of Sciences. 1994;91(9):3564-8.
14. Velu P, Vijayalakshmi A, Iyappan P, Indumathi D. Evaluation of antioxidant and stabilizing lipid peroxidation nature of Solanum xanthocarpum leaves in experimentally diethylnitrosamine induced hepatocellular carcinogenesis. Biomedicine & Pharmacotherapy. 2016;84:430-7.
15. Heindryckx F, Colle I, Van Vlierberghe H. Experimental mouse models for hepatocellular carcinoma research. International journal of experimental pathology. 2009;90(4):367-86.
16. Raghunandhakumar S, Paramasivam A, Senthilraja S, Naveenkumar C, Asokkumar S, Binuclara J, Jagan S, Anandakumar P, Devaki T. Thymoquinone inhibits cell proliferation through regulation of G1/S phase cell cycle transition in N-nitrosodiethylamine-induced experimental rat hepatocellular carcinoma. Toxicology letters. 2013;223(1):60-72.
17. Kumar M, Verma V, Nagpal R, Kumar A, Gautam SK, Behare PV, Grover CR, Aggarwal PK. Effect of probiotic fermented milk and chlorophyllin on gene expressions and genotoxicity during AFB1-induced hepatocellular carcinoma. Gene. 2011;490(1-2):54-9.
18. Bhandari R, Kaur IP. A sensitive HPLC method for determination of isoniazid in rat plasma, brain, liver and kidney. Journal of Chromatography Separation Technique. 2012;3(2) 1-5.
19. Conte JE, Lin E, Zurlinden E. High-performance liquid chromatographic determination of pyrazinamide in human plasma, bronchoalveolar lavage fluid, and alveolar cells. Journal of chromatographic science. 2000;38(1):33-7.

20. Matsuzaki T, Murase N, Yagihashi A, Shinozuka H, Shimizu Y, Furuya T, Burrell N, Iwatsuki S, Starzl TE. Liver transplantation for diethylnitrosamine-induced hepatocellular carcinoma in rats. InTransplantation proceedings 1992;24(2):748.
21. Shiota G, Harada KI, Ishida M, Tomie Y, Okubo M, Katayama S, Ito H, Kawasaki H. Inhibition of hepatocellular carcinoma by glycyrrhizin in diethylnitrosamine-treated mice. Carcinogenesis. 1999;20(1):59-63.
22. Furuta K, Sato S, Miyake T, Okamoto E, Ishine J, Ishihara S, Amano Y, Adachi K, Kinoshita Y. Anti-tumor effects of cimetidine on hepatocellular carcinomas in diethylnitrosamine-treated rats. Oncology reports. 2008;19(2):361-8.
23. Keshari AK, Kumar G, Kushwaha PS, Bhardwaj M, Kumar P, Rawat A, Kumar D, Prakash A, Ghosh B, Saha S. Isolated flavonoids from Ficus racemosa stem bark possess antidiabetic, hypolipidemic and protective effects in albino Wistar rats. Journal of ethnopharmacology. 2016;181:252-62.
24. Kushwaha PS, Raj V, Singh AK, Keshari AK, Saraf SA, Mandal SC, Yadav RK, Saha S. Antidiabetic effects of isolated sterols from Ficus racemosa leaves. RSC advances. 2015;5(44):35230-7.
25. Lodhi RL, Maity S, Kumar P, Saraf SA, Kaithwas G, Saha S. Evaluation of mechanism of heaptotoxicity of leflunomide using abino wistar rats. Afr J Pharm Pharmacol. 2013;7(24):1625-31.
26. Saha S, Chan DS, Lee CY, Wong W, New LS, Chui WK, Yap CW, Chan EC, Ho HK. Pyrrolidinediones reduce the toxicity of thiazolidinediones and modify their anti-diabetic and anti-cancer properties. European journal of pharmacology. 2012;697(1-3):13-23.
27. Kumar P, Singh AK, Raj V, Rai A, Maity S, Rawat A, Kumar U, Kumar D, Prakash A, Guleria A, Saha S. 6, 7-dimethoxy-1, 2, 3, 4-tetrahydro-isoquinoline-3-carboxylic acid attenuates heptatocellular carcinoma in rats with NMR-based metabolic perturbations. Future science OA. 2017;3(3):FSO202.
28. Keshari AK, Singh AK, Kumar U, Raj V, Rai A, Kumar P, Kumar D, Maity B, Nath S, Prakash A, Saha S. 5H-benzo [h] thiazolo [2, 3-b] quinazolines ameliorate NDEA-induced hepatocellular carcinogenesis in rats through IL-6 downregulation along with oxidative and metabolic stress reduction. Drug design, development and therapy. 2017;11:2981.

29. Poulin P, Theil FP. Prediction of pharmacokinetics prior to *in vivo* studies. 1. Mechanism-based prediction of volume of distribution. Journal of pharmaceutical sciences. 2002;91(1):129-56.
30. Poulin P, Theil FP. Prediction of pharmacokinetics prior to *in vivo* studies. II. Generic physiologically based pharmacokinetic models of drug disposition. Journal of pharmaceutical sciences. 2002;91(5):1358-70.
31. Liu HT, Huang YC, Cheng SB, Huang YT, Lin PT. Effects of coenzyme Q10 supplementation on antioxidant capacity and inflammation in hepatocellular carcinoma patients after surgery: a randomized, placebo-controlled trial. Nutrition journal. 2015;15(1):85.
32. Newman DJ. Natural products as leads to potential drugs: an old process or the new hope for drug discovery?. Journal of medicinal chemistry. 2008;51(9):2589-99.
33. Makos BK, Youson JH. Tissue levels of bilirubin and biliverdin in the sea lamprey, Petromyzon marinus L., before and after biliary atresia. Comparative Biochemistry and Physiology Part A: Physiology. 1988;91(4):701-10.
34. Green RM, Flamm S. AGA technical review on the evaluation of liver chemistry tests. Gastroenterology. 2002;123(4):1367-84.
35. Yu MC, Chan KM, Lee CF, Lee YS, Eldeen FZ, Chou HS, Lee WC, Chen MF. Alkaline phosphatase: does it have a role in predicting hepatocellular carcinoma recurrence?. Journal of Gastrointestinal Surgery. 2011;15(8):1440-9.
36. Ilamathi M, Prabu PC, Ayyappa KA, Sivaramakrishnan V. Artesunate obliterates experimental hepatocellular carcinoma in rats through suppression of IL-6-JAK-STAT signalling. Biomedicine & Pharmacotherapy. 2016;82:72-9.
37. Xu HN, Kadlececk S, Profka H, Glickson JD, Rizi R, Li LZ. Is higher lactate an indicator of tumor metastatic risk? A pilot MRS study using hyperpolarized 13C-pyruvate. Academic radiology. 2014;21(2):223-31.
38. Wu H, Li N, Jin R, Meng Q, Chen P, Zhao G, Wang R, Li L, Li W. Cytokine levels contribute to the pathogenesis of minimal hepatic encephalopathy in patients with hepatocellular carcinoma via STAT3 activation. Scientific reports. 2016;6:18528.
39. Adamson CS, Waki K, Ablan SD, Salzwedel K, Freed EO. Impact of human immunodeficiency virus type 1 resistance to protease inhibitors on evolution of resistance

to the maturation inhibitor bevirimat (PA-457). Journal of virology. 2009;83(10):4884-94.

40. Fulda S. Betulinic acid for cancer treatment and prevention. International journal of molecular sciences. 2008;9(6):1096-107.
41. Wick W, Grimmel C, Wagenknecht B, Dichgans J, Weller M. Betulinic acid-induced apoptosis in glioma cells: A sequential requirement for new protein synthesis, formation of reactive oxygen species, and caspase processing. Journal of Pharmacology and Experimental Therapeutics. 1999;289(3):1306-12.
42. Fulda S, Jeremias I, Steiner HH, Pietsch T, Debatin KM. Betulinic acid: A new cytotoxic agent against malignant brain-tumor cells. International journal of cancer. 1999;82(3):435-41.
43. Zuco V, Supino R, Righetti SC, Cleris L, Marchesi E, Gambacorti-Passerini C, Formelli F. Selective cytotoxicity of betulinic acid on tumor cell lines, but not on normal cells. Cancer letters. 2002;175(1):17-25.
44. Thurnher D, Turhani D, Pelzmann M, Wannemacher B, Knerer B, Formanek M, Wacheck V, Selzer E. Betulinic acid: a new cytotoxic compound against malignant head and neck cancer cells. Head & Neck: Journal for the Sciences and Specialties of the Head and Neck. 2003;25(9):732-40.
45. Noda Y, Kaiya T, Kohda K, KAWAZOE Y. Enhanced cytotoxicity of some triterpenes toward leukemia L1210 cells cultured in low pH media: possibility of a new mode of cell killing. Chemical and pharmaceutical bulletin. 1997;45(10):1665-70.
46. Ehrhardt H, Fulda S, Führer M, Debatin KM, Jeremias I. Betulinic acid-induced apoptosis in leukemia cells. Leukemia. 2004;18(8):1406-12.
47. Gopal DR, Narkar AA, Badrinath Y, Mishra KP, Joshi DS. Betulinic acid induces apoptosis in human chronic myelogenous leukemia (CML) cell line K-562 without altering the levels of Bcr-Abl. Toxicology letters. 2005;155(3):343-51.
48. Selzer E, Pimentel E, Wacheck V, Schlegel W, Pehamberger H, Jansen B, Kodym R. Effects of betulinic acid alone and in combination with irradiation in human melanoma cells. Journal of investigative dermatology. 2000;114(5):935-40.
49. Fulda S. Betulinic acid: a natural product with anticancer activity. Molecular nutrition & food research. 2009;53(1):140-6.

50. Rieber M, Strasberg RM. Induction of p53 without increase in p21WAF1 in betulinic acid-mediated cell death is preferential for human metastatic melanoma. DNA and cell biology. 1998;17(5):399-406.

Chapter 4

Mechanistic Exploration and ^{1}H NMR based Metabolomics Studies

4. Introduction

As per discussion in previous chapter, the effectiveness of betulinic acid (B) and PLGA loaded nanoparticles of B (BNP) against hepatocellular carcinoma (HCC) was established. However, the molecular mechanism and metabolic perturbation of both BNP and B against HCC had not been elucidated yet at both molecular and cellular levels. So that in extension of our earlier report, the current research described the molecular mechanisms and metabolic exploration of their anti-neoplastic responses.

To achieve this aim we selected higher dose of both BNP and B at 100 mg/kg dose for further experimental analysis because higher dose of BNP and B produces maximum response against the HCC in previous chapter.

Various literatures suggested that chronic liver injury through apoptosis plays an essential function in the progress of HCC and NDEA could effectively produce HCC [1]. Thus, to evaluate the anti-HCC potentials of B and BNP, and related molecular and cellular mechanisms, we performed *in vivo* experiments in NDEA induced HCC rat model. The tissue concentrations of various nitrite/nitrate contents, nitric oxide synthase (NOS), inflammatory mediators (e-NOS and i-NOS) and apoptotic markers were initially measured. The consequences of BNP and B on the apoptotic pathways (i-NOS and e-NOS mediated Bcl-2 family proteins→CytC→Caspase-3 and Caspase-9 signaling cascades) were subsequently examined at molecular level through western blot analyses and qRT-PCR analyses. The ^{1}H-NMR-based serum metabolomic studies was also conducted to elucidate the alterations of metabolic perturbations related with HCC condition following BNP and B treatments.

4.1. Materials and methods

4.1.1 Chemicals and reagents

Thermo-Fischer® Scientific Ltd., Bangalore, India and Genetix® Biotech Asia Private Limited, New Delhi, India supplied the chemicals and solvents required for the qRT-PCR analyses and western blot studies. All other analytical grades chemicals and solvents (99% purity) were acquired from HiMedia® Limited, Mumbai, India. The distilled water (double distillate) (Borosil®, India) was utilized during the complete research.

4.1.2 Experimental design

Six-week-old male albino Wistar rats (100- 120 g) were become accustomed to the necessary laboratory circumstances (temperature, 25±1˚C, light/dark cycle of 12 h, provided a free access to the diet (commercial pellets) and water *ad libitium*) for a week prior to the commencement of the research. The animals were separate out into five groups bearing eight rats in every group (n=8), and the groups were organized in the desired manner:

- Group 1 (normal control group) containing 0.25% carboxy methyl cellulose (2 mL/kg) orally (p.o.) administration
- Group 2 (carcinogen control group): Intraperitoneal (i.p.) administration of N-nitrosodiethylamine (NDEA; 100 mg/kg) for 6 weeks with frequency of once a week, [2,3,4]
- Group 3 (positive control group): Intraperitoneal (i.p.) administration of NDEA (dose of 100 mg/kg) + 5-fluorouracil (5-FU at dose of 10 mg/kg) (i.p.) for 15 days after HCC induction
- Group 4: NDEA (i.p.) + B (100 mg/kg) (p.o.) for 15 days after the HCC induction
- Group 5: NDEA (i.p.) + BNP (100 mg/kg) (p.o.) for 15 days after the HCC induction

4.1.3 Measurement of total nitrite/nitrate content and nitric oxide synthase (NOS)

Based on the method given by Motawi and Miranda, the total nitrite/nitrate content in the hepatic tissue homogenates was estimated. The NOS (Abcam, Cambridge, United Kingdom) activity in the hepatic tissue homogenates was determined by ELISA according to the suggested protocol by the manufacturer [5,6].

4.1.4 Analysis of e-NOS and i-NOS by ELISA

The Wuhan EIAab Science Company Limited, Wuhan, China provided e-NOS and i-NOS kits. The hepatic tissues were investigated through ELISA following manufacturer's instructions [7].

4.1.5 Quantitative Real-time polymerase chain reaction (qRT-PCR) analysis

A 10 mg of hepatic tissue sample from each group were used to isolate total mRNA employing TriaZol reagent. The mRNA was then completely purified by RNeasy mini kit and the amount

was estimated by Nano Drop instrument at 260nm/280nm. Based on the manufacturer's practice, the corresponding deoxyribose nucleic acid (cDNA) was determined employing the GeneSure first strand cDNA synthesis kit (Genetix Biotech Asia Private Limited, New Delhi, India). The qRT-PCR (forty times repetition) was achieved using the Agilent Stratagene Mx3000P series (Applied Biosystems, Foster City, USA) by utilizing the Sybr® green PCR master mix. The cDNA was initially denatured at 94 ºC for 5 min, and the annealing was further performed at 58 ºC for 30 sec. These were ultimately elongated at 72 ºC for 35 sec. The mRNA was normalized with control β-actin. The ΔCt values were normalized with the untreated control samples according to the following equation [8,9]: $\Delta Ct = Ct_{\text{gene of interest}} - Ct_{\text{housekeeping gene}}$. The relative changes in the expression level of one specific gene were calculated based on following expression: $2^{-\Delta\Delta Ct}$ $\Delta\Delta Ct = \Delta Ct_{test} - \Delta Ct_{control}$. The forward and backward primers were tabulated in Table 6 [10,11,12,13,14,15] and various genes such as e-NOS, Cyt-C, Bcl-2, Bcl-xl, BAX, BAD, i-NOS, caspase-3, caspase-9 were evaluated for this mechanistic studies.

Table 6 Primer Sequences used for mRNA expression analysis by qRT-PCR

Sr. No.	Gene	Primer sequence	References
1	β-actin	5′-AAGTCCCTCACCCTCCCAAAAG-3′ (forward)	10
		5′- AAGCAATGCTGTCACCTTCCC-3′ (reverse)	
2	e-NOS	5′-CGGCATCACCAGGAAGAAGA-3′ (forward)	11
		5′-CATGAGCG AGGCGGAGAT-3′ (reverse)	
3	Cyt-C	5′-TTTGGATCCAATGGGTGATGTTGAG-3′ (forward)	12
		5′-TTTGAATTCCTCATTAGTAGCTTTTTTGAG-3′ (reverse)	
4	Bcl-2	5′-CTGGTGGACAACATCGCTCTG-3′ (forward)	13
		5′-GGTCTGCTGACCTCACTTGTG-3′ (reverse)	
5	Bcl-xl	5′-AGGCTGGCGATGAGTTTGAA-3′ (forward)	13
		5′-TGAAACGCTCCTGGCCTTTC-3′ (reverse)	
6	BAX	5'-TTCATCCAGGATCGAGCAGA-3' (forward)	13
		5'-GCAAAGTAGAAGGCAACG-3' (reverse)	
7	BAD	5'-CTCCGAAGAATGAGCGATGAA-3' (forward)	10
		5'-ATCCCACCAGGACTGGATAA-3' (reverse)	

8	i-NOS	5′-GTGCTAATGCGGAAGGTCATG-3′ (forward) 5′ -GCTTCCGACTTTCCTGTCTC AGTA-3′ (reverse)	11
9	Caspase -3	5′-GGTATTGAGACAGACAGTGG-3′ (forward) 5′-CATGGGATCTGTTTCTTTGC-3′ (reverse)	14
10	Caspase -9	5′-AGTTCCCGGGTGCTGTCTAT-3′ (forward) 5′-GCCATGGTCTTTCTGCTCAC-3′ (reverse)	15

4.1.6 Western blot analysis

The degree of protein expressions of Bcl-xl, Bcl-2, and BAD were assessed by immunoblotting technique. The lysis of cells were performed by radioimmunoprecipitation assay (RIPA) buffer, centrifuged for the duration of 15 min at 10,000 rpm at a temperature of 4ºC and the protein content was estimated using Bradford reagent. The proteins (50 µg) were electrophoresed on 12% sodium dodecyl sulfate (SDS)-polyacrylamide gel and immediately transferred to polyvinylidene fluoride membrane. The formed membranes were wedged with skimmed milk (5%) in phosphate buffered saline containing tween-20 (PBS-T, 0.1%) for 3 hr duration at a temperature of 4°C and probed with primary antibodies (Cell Signaling Technology, USA) diluted in PBS-T (in the ratio of 1:500 dilution for every individual component) containing Bcl-xl (54H6), Bcl-2 (D17C4), β-actin (13E5) mouse monoclonal antibody, and BAD (D24A9) overnight at a temperature of 4°C. The membranes were then washed with the tris-buffered saline containing the tween-20 (TBS-T) three times and incubated with anti-rabbit secondary antibodies linked to horse-radish peroxidase at 1:3000 dilutions at the room temperature for 3 h. Subsequently, the prepared film was thoroughly washed with TBST for 3 times, developed with improved chemiluminescence ECL (Pierce™ ECL Western Blotting Substrate) and the images were captured using the Chemidoc® system (Clinx Scientific Instruments, China) [9,10,11].

4.1.7 Mathematical modeling

The ODE-based model was utilized and standardized by means of the MATLAB software. The dynamical constraints were taken from the earlier literature [17,18]. The behavioral concentration of BAX+BAD, Bcl-2+Bcl-xl, Caspase-3, and Caspase-9, cancer cells over time

was presented by scheming the concentrations vs. time graph, considering the diverse values of e-NOS and i-NOS obtained in qRT-PCR analyses for different experimental groups.

4.1.8 Measurement of serum lipid profile

Serum lipid concentrations were ascertained spectrophotometrically by using a lipid profile kit (Agape Diagnostic Ltd., Kerala, India). As per manufacturer instruction, 10 mL of plasma or standard was added with 1.0 mL of working solution. The mixture was incubated for the duration of 5 min at a temperature of 37°C and was evaluated spectrophotometrically at 505 nm. The cholesterol concentration in plasma was estimated by the following procedure:

$$\text{Cholesterol concentration (mg /dL)} = \frac{\text{Absorbance of serum}}{\text{Absorbance of standard}} \text{x } 200$$

In the presence of lipase, the triglycerides present in the serum were converted successfully into hydrogen peroxide (H_2O_2) and fatty acids. The estimation was analogous to the cholesterol assessment procedure. The lipoproteins and sulfated α-cyclodextrin were the HDL substrate used for the high density lipoprotein (HDL). The HDL produced the unesterified cholesterol which afterwards converted to cholestenone and then ultimately to H_2O_2. To the reaction mixture, 5-aminophenazone was added directly. At 600 nm, the absorbance was recorded. The H_2O_2 formation was unswervingly relative to the plasma HDL concentration. Based on the Friedewald's formula, the very low density lipoprotein (VLDL) levels and the low density lipoprotein (LDL) levels were determined [18]:

$$\text{LDL (mg/dL)} = \text{TC} - \text{HDL} - (\text{TG}/5)$$

$$\text{VLDL (mg/dL)} = \text{TC} - \text{HDL} - \text{LDL}$$

4.1.9 ^{1}H-NMR based metabolomics spectroscopy

4.1.9.1 Sample preparation

All serum samples were thawed at room temperature, 250 µl of serum was taken and mixed with 250 µl of 0.9% saline sodium-phosphate buffer of strength 50 mM, pH 7.4 prepared in D_2O [9]. Further, to remove any precipitates, the samples were then centrifuged for 5 min duration at 10,000 rpm, before obtaining the NMR data. The supernatant content of 400 µL was employed in

the NMR tubes of dimension 5 mm for determining the data along with co-axial insert containing 0.1% external standard reference (sodium salt of 3-trimethylsilyl-(2,2,3,3-d4)-propionic acid, TSP which helps in the quantification of metabolites through NMR experiment. The sodium salt of trimethylsilylpropionic acid-d^4 (TSP) and deuterium oxide (D_2O) was employed as the co-solvent and also to offer a deuterium frequency lock or field. Sigma-Aldrich (RI, USA) supplied the main chemicals utilized for NMR experiments.

4.1.9.2 NMR measurements

NMR spectrometer system of Bruker Biospin Avance-III Make having 800 Mhz frequency was employed for recording the NMR spectra at a temperature of 298 K. The spectrometer runs at 800.21 MHz of proton frequency, operational with CryoProbe system, and 53 G/cm of maximum gradient-strength output. Topspin-2.1, a Bruker NMR data Processing Software was utilized for processing the raw data obtained from NMR analysis. The Carr–Purcell–Meiboom–Gill (CPMG) pulse sequence (cpmgpr1d, standard Bruker pulse program) was utilized for recording the diffusion edited (DE) ^{1}H NMR spectra as well as one-dimensional ^{1}H-NMR of each serum sample. The water peak was pre-saturated by irradiating the content continuously through the recycle delay process for the duration of 5 sec and the bipolar pulse pair longitudinal eddy current delay (BPP-LED) sequence was recorded. A total of 128 scans were performed for recording each CPMG spectrum which took 15 minutes approximately, individually. The broad signals obtained from cholesterols, triglycerides, phospholipids, proteins, etc. were removed by applying 60 ms of spin–spin relaxation time with 0.3 Hz as the line broadening factor (n = 300 and 2τ=200δs). For recording the NMR spectra under DE ^{1}H-NMR, the square gradients was set to 70% of the maximum gradient strength for the duration of 2 ms, which is followed by a 200 μs delay to prevent eddy current decay. For assuaging the signals obtained from the low molecular weight (LMW) compounds without distressing the signals obtained from lipid, 120 ms of diffusion time was utilized. After the suitable baseline correction and manual phase correction, Topspin-2.1 with standard Fourier Transformation (FT) was utilized for analysis of spectra. Before the application of FT, every FID was designated zero to 4096 data set points and the sine-bell apodisation function was taken into the application. After the application of FT, the chemical shift was internally referenced with the methyl peak of L-lactate (δ=1.33 ppm). The recorded NMR spectra were examined visually for their degree of satisfactoriness and further. All

procured spectra were examined visually for and were subject to multivariate statistical analysis to distinguish the customized metabolic prototypes.

4.1.9.3 Spectral assignment

For unmistakable allocation of a variety of peaks in the obtained ^{1}H-CPMG-NMR spectra, 2D NMR spectra were attained for the chosen samples such as ^{1}H-^{13}C heteronuclear single quantum correlation (HSQC) and ^{1}H-^{1}H total correlation spectroscopy (TOCSY). The desired chemical shifts were recognized and possibly allocated by evaluating them with the accessible chemical shifts with the assistance of software Chenomx 8.1 (Chenomx Inc., Canada). The residual peaks in the CPMG-^{1}H NMR spectra were designated employing the accessible literature reports and accessible databases [19-21].

4.1.9.4 Multivariate data analysis

By the application of Topspin 2.1, the baseline aberration and the phase aberration were corrected in the NMR spectra. The diffusion edited spectra (δ 0.5−5.6 ppm) and CPMG spectra (δ 0.5−8.5 ppm) were integrated into the integrated spectral content of 0.01 ppm strength by utilizing the AMIX package (Bruker) v.3.8.7, Bio Spin. For avoiding the interfering effect of water suppression, the distorted region in the spectra (δ 4.7–5.1) was eliminated both from the diffusion edited data and CPMG data. The data procured through AMIX after normalization process and mean centering process was carried out by splitting each and every data point present in the sample by their sum in order to recompense for the disparities in the metabolite concentrations of amongst every single serum samples. The data scaling was performed by employing the unit variance where indistinguishable mass was provided to every variables. The obtained data was further exported to the Microsoft Office Excel 2010 tool and multivariate analysis was then carried out through metabolomic data analyzing tool such as Unscrambler X Software v.10.3 (CAMO, Norway) and MetaboAnalyst. Both on diffusion edited (DE) datasets and Carr-Purcell-Meiboom-Gill (CMPG) datasets, the Principal component analysis was carried out in order to conclude the outliers. The supervised partial least squares discriminate analysis (PLS-DA) was performed to supplementary express the disparities amongst the dissimilar groups, which will aid in recognizing the various metabolites notably giving to the group demarcation. Model quality was assessed with R^2 indicating the validity of models against over-

fitting and Q^2 representing the predictive ability. The loading plots (for PLS-DA) serve as the identifier for the potential metabolites markers and the scores obtained for inconsistent significance on projections. The statistical implication of the produced metabolites was computed by t-test ($p < 0.05$).

4.1.9.5 Heat map analysis

Multivariate statistical analysis to visualize the alterations of remarkable metabolites in five groups, a heat map was created using the MetaboAnalyst v.3.0 (http://www.metaboanalyst.ca/).

4.1.9.6 Pathway analysis

The biochemical pathway was analyzed by utilizing the pathways library available in the metaboanalyst server for *Rattus norvegicus*. The altered metabolites in the obtained samples were identified through PLS-DA analysis with a good VIP scores and compared with CC. The pathway analysis module provided the information of affected metabolic pathways. The MetaboAnalyst software comprises of inbuilt functions of pathway topology analysis and enrichment analysis. The software do not recognizes lipid metabolites and membrane such as lipids, VLDL, LDL, HDL, OAG, NAG, etc., and are therefore were excluded from the analysis. The altered metabolites data were uploaded in Metabo Analyst and suitably analyzed by Over Representation analysis (ORA). In the *Rattus norvegicus* metabolic library, degree centrality algorithms and hypergeometric analysis were utilized for pathway improvement and pathway topology analysis. For every investigated pathway, an impact factor was generated by the pathway analysis module and pathway enrichment analysis produced statistically significant fit coefficient (p). Based on the *p*-values procured from pathway enrichment analysis (plotted in the Y-axis) and the color intensity and impact values intensity produced from pathway topology analysis (plotted in the X-axis), the impactful pathways (in the blue color) were determined by the common points (indicated by the size of circle) [23,24].

4.1.10 Statistical data analysis

The data were articulated as mean ± standard deviation. One-way analysis of variance (ANOVA) followed by Bonferroni's multiple comparison test was executed employing GraphPad Prism 5.0 software (San Diago, CA, USA). The considerable statistical disparities were scrutinized among the CC groups and test groups with ***$p<0.001$, **$p<0.01$ and*$p<0.05$.

4.2 Results.

4.2.1 Evaluation of the ratio of nitrite/nitrate and nitric oxide synthase (NOS) level

The protective efficiency of BNP was analyzed through various nitrative stress parameters including ratio of nitrite/nitrate ratio (Figure. 9A) and nitric oxide synthase (NOS) level (Figure. 9B) in the rat liver. Both nitrative stress parameters were up regulated in CC group as compared to NC group. However, after treatment with B and BNP, the levels of nitrite/nitrate ratio and nitric oxide synthase (NOS) were significantly down regulated as compared to the CC group.

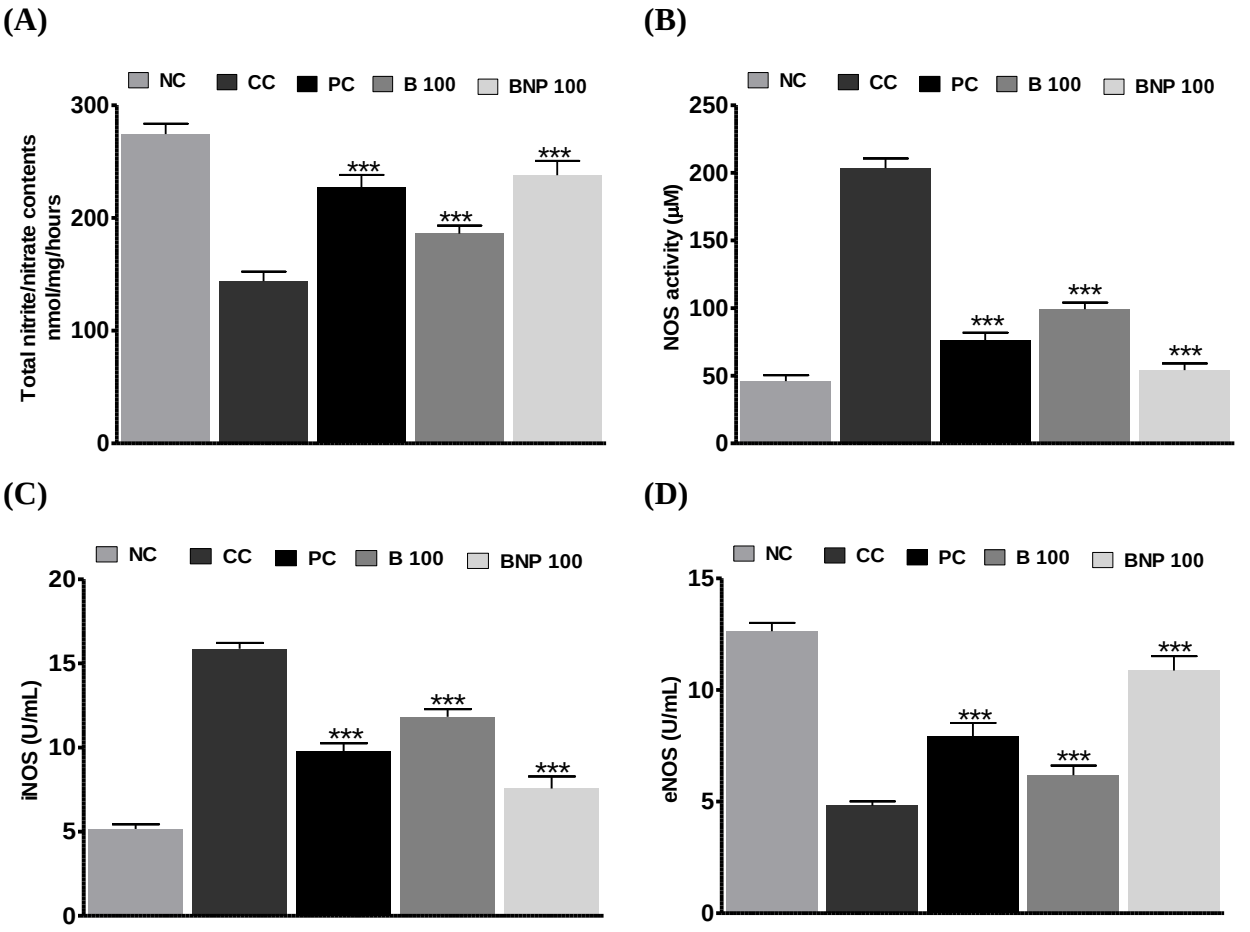

Figure 9 (A) Total nitrite/nitrate contents **(B)** Assay of nitric oxide synthase (NOS) activity, **(C)** iNOS **(D)** eNOS activities in the liver tissue after treatment with BNP and B.

Note: The data are signified as mean ± SD (n=8). Statistically considerable disparity were examined between test groups and carcinogen control groups [one way-ANOVA followed by Bonferroni multiple comparison test (***p<0.001, **p<0.01, *p<0.05)]. The studied groups are:

(CC: Carcinogen Control, NC: Normal Control, B100 (100 mg/kg), PC: Positive Control, and BNP (100 mg/kg).

4.2.2 Evaluation of e-NOS and i-NOS by ELISA

In order to explore the effects of BNP on cancer-associated NO based inflammatory event, we conducted enzyme linked immunosorbent assay (ELISA) of inflammatory isoform of NO (i-NOS and e-NOS) in hepatic tissue. The NDEA treated CC group triggered a robust induction i-NOS with a corresponding reduction in e-NOS in liver tissue (Figure. 9C and 9D), indicating the induction of pathogenic NOS during HCC condition. After oral administration of BNP and B, both e-NOS and i-NOS levels were significantly normalized in treatment group.

4.2.3 mRNA expression of the apoptotic markers during NDEA-induced HCC

The qRT-PCR analyses was carried out to assess the levels of gene expression of various NOS and biomarkers of mitochondrial apoptotic pathway. The NDEA treated CC group demonstrated a downstream regulation of BAX, e-NOS, BAD, Cyt C, Caspase-9, and Caspase-3 genes as compared to NC. However, B, BNP and 5-FU treatments significantly normalized ($p < 0.001$) the downstream expression of these genes. The efficacy of both B and BNP at a 100 mg/kg dose was found comparable to the marketed chemotherapeutics, 5-FU (Figure. 10 and 12). Alternatively, the differing drifts were perceived for i-NOS, Bcl-2, and Bcl-xl genes, where upstream regulations of these genes were significantly normalized ($p < 0.001$) following B, BNP and 5-FU treatments.

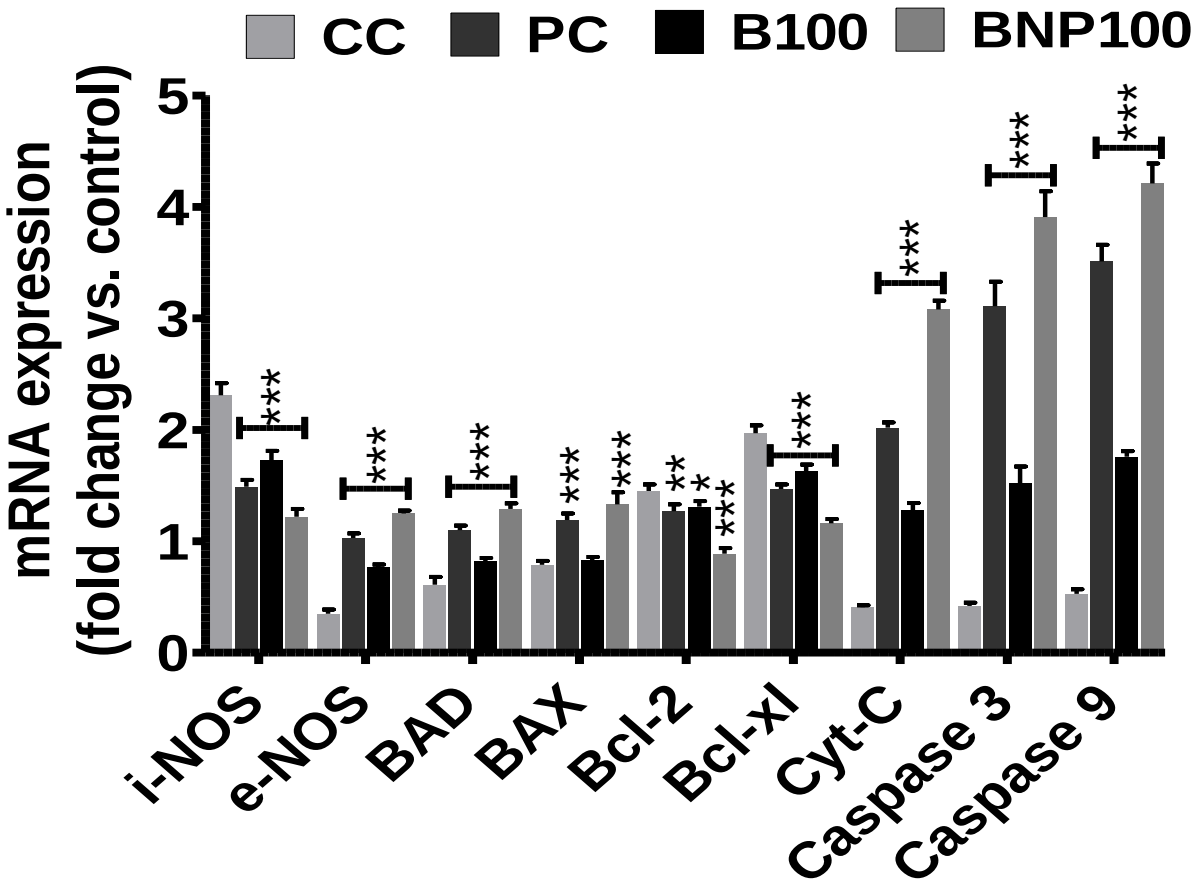

Figure 10 Gene expression levels of e-NOS, i-NOS, BAX, BAD, Bcl-xl, Bcl-2, Cyt-C, caspase-9 and caspase-3, and in liver tissue after B and BNP treatment.

Note: Data are represented as mean ± SD (n=8). Statistically considerable disparity were detected between the carcinogen control group and test group [one way-ANOVA followed by Bonferroni multiple comparison test (***p<0.001, **p<0.01, *p<0.05)]. The studied groups are: (CC: Carcinogen Control, NC: Normal Control, B100 (100 mg/kg), PC: Positive Control, and BNP (100 mg/kg).

4.2.4 Western blot analysis

The quantitative western blot analysis was further employed to measure the protein expression levels of BAD, Bcl-xl and Bcl-2. The levels of BAD protein was down regulated in CC with respect to NC, which were improved after B and BNP administration at higher dose (Figure. 11A, 11B and 12). An opposite trend was noted for Bcl-xl and Bcl-2 where these proteins were

up-regulated in CC and normalized after B and BNP treatment. The β-actin acted as housekeeping protein in these experiments.

(A)

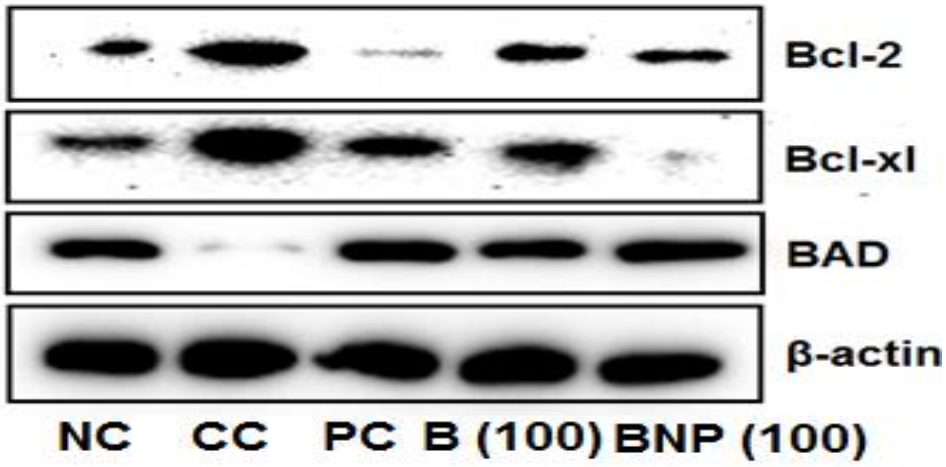

(B)

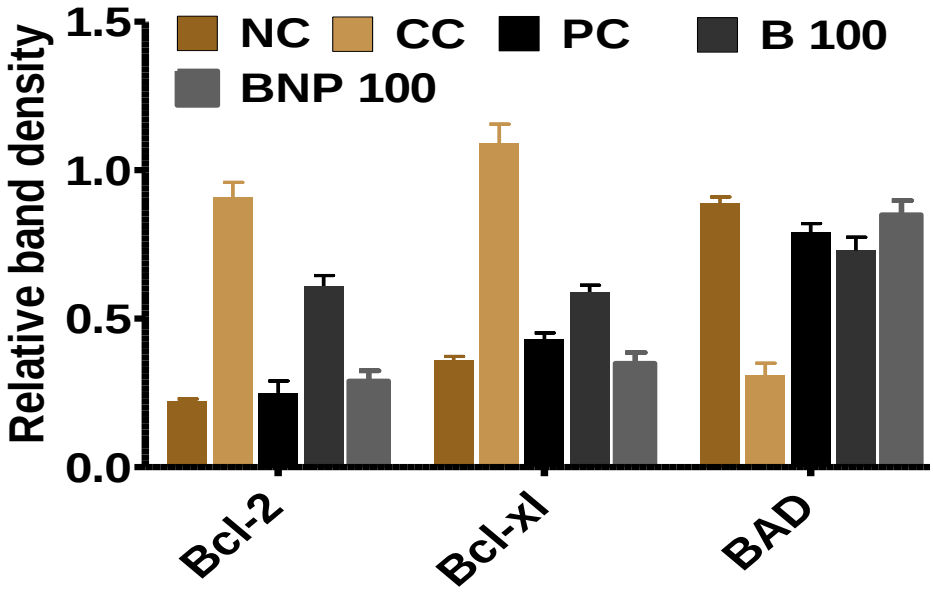

Figure 11 Protein expression levels of BAD, Bcl-xl, Bcl-2, and β-Actin in the liver tissue after treating with BNP and B (determined by quantitative western blot analysis). Data are represented as mean±SD (n=8). The studied groups are: (CC: Carcinogen Control, NC: Normal Control, B100 (100 mg/kg), PC: Positive Control, and BNP (100 mg/kg).

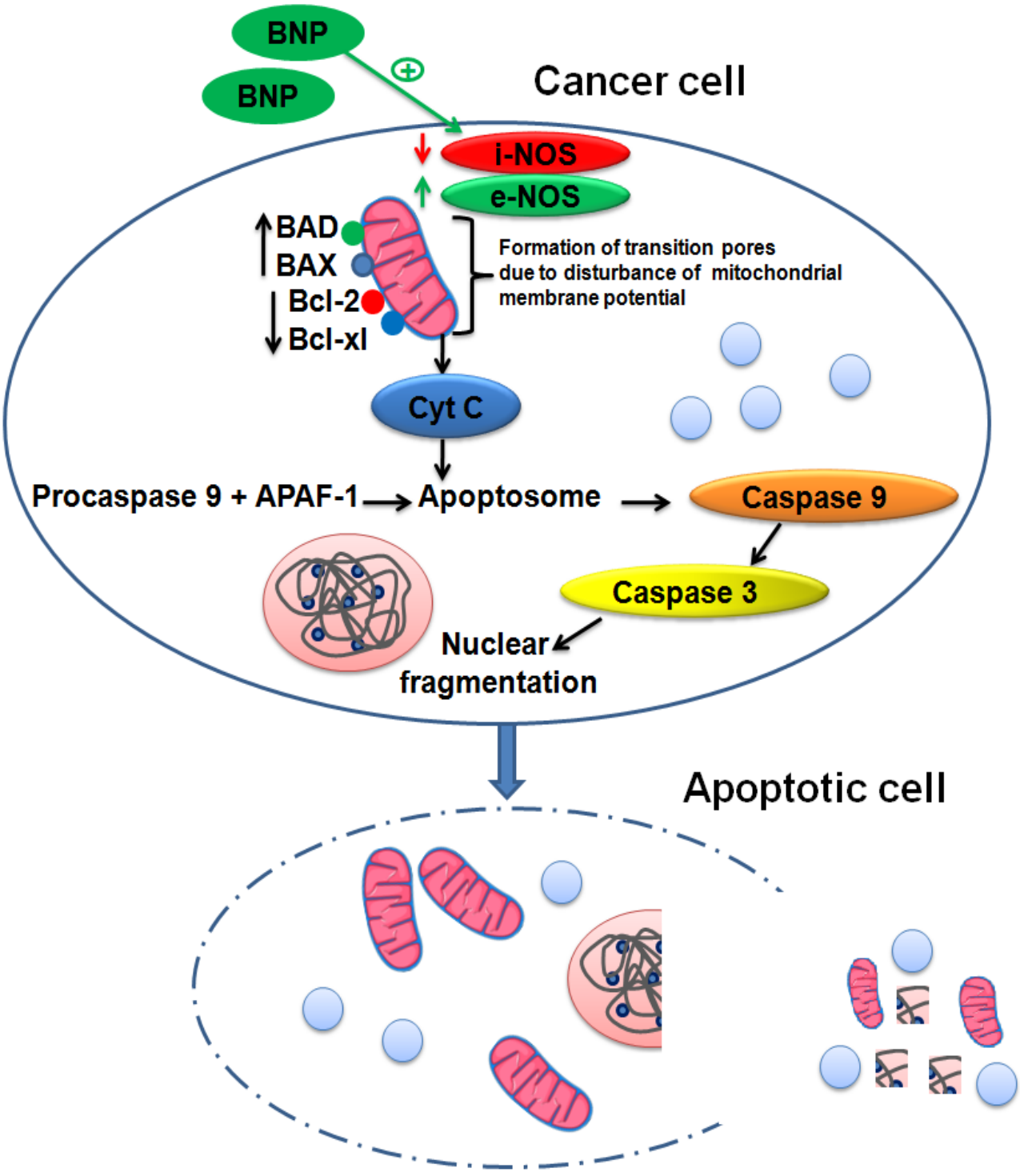

Figure 12 Conceivable mechanistic activities of BNP.

4.2.5 Mathematical modeling of mechanism of anticancer properties of BNP and B

We formulated the dynamics of plausible mechanisms of anticancer activity of BNP using a nonlinear mathematical model employing a system of ordinary differential equations. The individual steps of the core module (Figure. 13) were represented by a system of differential equations, each describing the dynamics of the per capita concentration of BAX+BAD, Bcl-2+Bcl-xl, cytochrome C, Caspase 3 and 9, Cancer cells over time respectively. In view of this, the following models were considered.

$$\frac{1}{x_1}\frac{dx_1}{dt} = k_1[eNOS] - k_2[iNOS]$$

$$\frac{1}{x_2}\frac{dx_2}{dt} = k_2[iNOS] - k_1[eNOS] \qquad \ldots(1)$$

$$\frac{1}{x_3}\frac{dx_3}{dt} = -k_3 x_2 + k_4 x_1$$

$$\frac{1}{x_4}\frac{dx_4}{dt} = k_5 x_3$$

$$\frac{1}{x_5}\frac{dx_5}{dt} = k_6 x_4$$

With initial conditions $x_i(0) > 0$, $i = 1,2,3,4,5.$

The [e-NOS] and [i-NOS] represent the concentration of induced e-NOS and i-NOS, respectively (obtained by quantitative western blot analysis) for different studied groups; x_1 refers to the concentration of BAX+BAD in cytoplasm, x_2 is the concentration of Bcl-2+Bcl-xl in cytoplasm, x_3 symbolize the cytoplasic cytochrome C concentration, x_4 designates the concentration of Caspase-9 and Caspase-3 in the cytoplasm and x_5 is the concentration of cancer cells in the body. The k_1, k_2, k_3, k_4 and k_5 are the positive rate constants.

To determine the quantitative behavior of the concentrations of BAX+BAD, Bcl-2+Bcl-xl, Caspase-9 and Caspase-3, Cancer cells, respectively with time, ODEs given by (equation 1) were

integrated by the Runge–Kutta method (4^{th} order) [17] employing the MATLAB software and the graphs were representation (Figure. 5 A, B, C, and D). The arithmetical simulation was carried out by means of the significance of dynamical parameters such as k_1, k_2, k_3, k_4, and k_5 from the previous literatures.

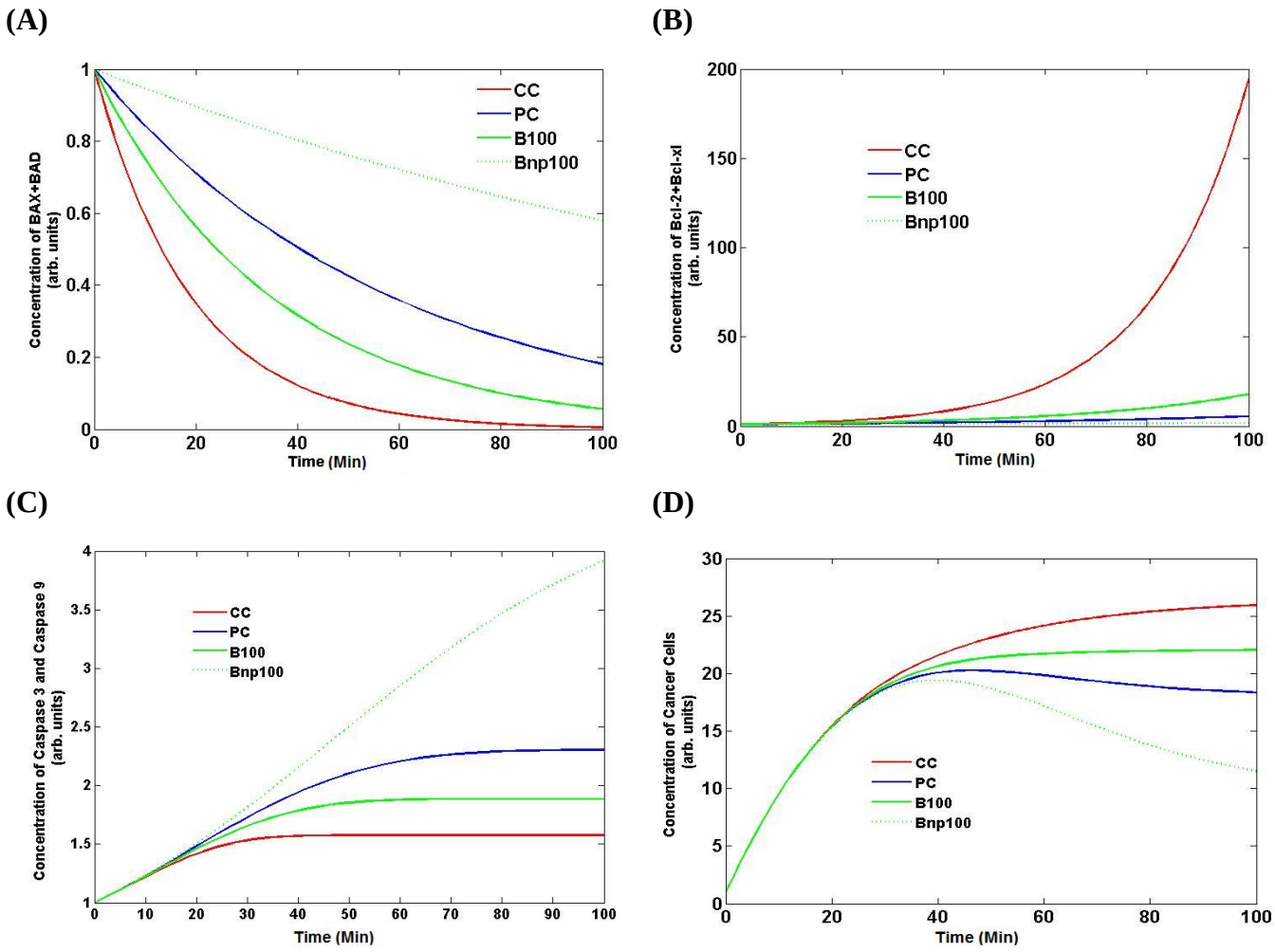

Figure 13 The graphs produced by the application of MATLAB software utilizing the derived arithmetical model depends on the strides entailed in the pathway. **(A)** Graph shows the quantitative behavior of BAX+BAD over a time course. **(B)** Graph shows the quantitative behavior of Bcl-2+Bcl-xl over a time course. **(C)** Graph shows the quantitative behavior of Caspase-9 and Caspase-3 over a time course. **(D)** Graph shows the concentration of cancerous cells over a time course.

It was observed from Figure 13A that the concentration of BAX+BAD in the cytoplasm increased in response to i-NOS and e-NOS stimulations. Furthermore, it was evidenced that the

increment was faster in NC and treatment groups (B and BNP) as compared to the CC group. Moreover, Figure 13B revealed the declining behavior of Bcl-2+Bcl-xl in cytoplasm, demonstrating that Bcl-2+Bcl-xl in cytoplasm declined due to the stimulation of iNOS and eNOS. The declination in the concentration of Bcl-2+Bcl-xl was found to be more pronounced in the normal and treatment groups as compared to the carcinogen control group. In addition, Figure 13C manifested the quantitative concentrations of Caspase-9 and Caspase-3 in reaction to the dual stimulation of e-NOS and i-NOS. The concentrations of Caspase-9 and Caspase-3 were observed to be quite superior for the treatment groups relative to the carcinogen control group. Figure 13D displayed the apoptosis of the cancer cells with time due to the stimulation of i-NOS and e-NOS. The apoptosis of the cancer cells was found to be maximum for BNP-treated group. This implied the efficacy of the BNP as compared to the marketed drug.

4.2.6 Evaluation of Lipid profile parameters

The TC, LDL, TG, HDL and VLDL are various parameters of the lipid profile, which were taken into consideration to measure the protective action of B and BNP. Except HDL, all other parameters were augmented in the CC group than NC. The TC, TG, VLDL and HDL were significantly normalized after oral administration of B and BNP. In contrast, the HDL level was spectacularly diminished in the CC (~ 24 mg/dL) as evaluated against NC (~ 55 mg/dL). The HDL concentration in serum turned to normal levels after the orally administered BNP and B at 100 mg/kg dose (Table 7).

Table 7 Lipid profiles in serum to evaluate the amiliorative effects after NDEA, BNP, and B administration, (CC: Carcinogen Control, NC: Normal Control, B100: Betulinic acid (100 mg/kg), PC: Positive Control, and BNP100: Betulinic acid nanoparticle (100 mg/kg).

Sr. No.	Parameters	NC	CC	PC	B100	BNP100
1.	**TC (mg/dL)**	138.15±4.02	186.23±6.37	143.15±5.34***	153.19±7.29***	141.28±4.85***
2.	**TG(mg/dL)**	72.79±3.89	167.29±6.72	86.46±6.19***	102.38±6.76***	75.39±4.41***
3.	**HDL(mg/dL)**	55.19±2.92	24.99±1.96	39.84±3.31***	33.52±3.79***	52.13±2.68***
4.	**LDL(mg/dL)**	68.40±3.29	127.78±6.61	86.01±4.43***	99.19±5.47***	74.07±4.43***
5.	**VLDL(mg/dL)**	14.55±1.14	33.45±1.94	17.29±2.21***	20.47±1.97***	15.07±2.28***

Note: Data represented here as mean±SD (n=8). Statistically significant differences were observed between CC and test groups [one way ANOVA followed by Bonferroni multiple comparison test (***p<0.001, **p<0.01 and *p<0.05)]

4.2.7 ^{1}H-NMR-based metabolomics to access the biochemical impact after BNP treatment

In an effort to gain a global picture of the univariate and chemometrics statistical analysis, we investigated the NDEA-induced metabolic alterations in HCC condition and the protective efficacy of BNP on it. The 1D ^{1}H-CPMG NMR spectra acquired from serum samples of various control and treated rats, exclusively with the allocated resonances are represented in Figure 14. The ^{1}H-NMR spectra of serum samples demonstrated signals, mainly from membrane metabolites (e.g. choline), lipids/lipoproteins (e.g. LDL, VLDL, PUFAs etc.), O-acetyl and N-acetyl glycoproteins (NAG, OAG), and amino acids (e.g. leucine, isoleucine, alanine, lysine, valine, glutamate, glutamine, histidine, tyrosine, and phenylalanine etc.). Other distinguished metabolites were, lactate, glucose, acetate, citrate, formate, creatine, biotin and trans-aconitate (Figure 15).

Further exploration of metabolic perturbations between control and carcinogenic rat, the ^{1}H-NMR dataset was subjected to statistical data modeling and analysis using multivariate analysis tools in MetaboAnalyst [25, 26]. Firstly, the Principal Component Analysis (PCA) was used to authenticate the analytical quality system performance and to investigate the possible outliers.

(A)

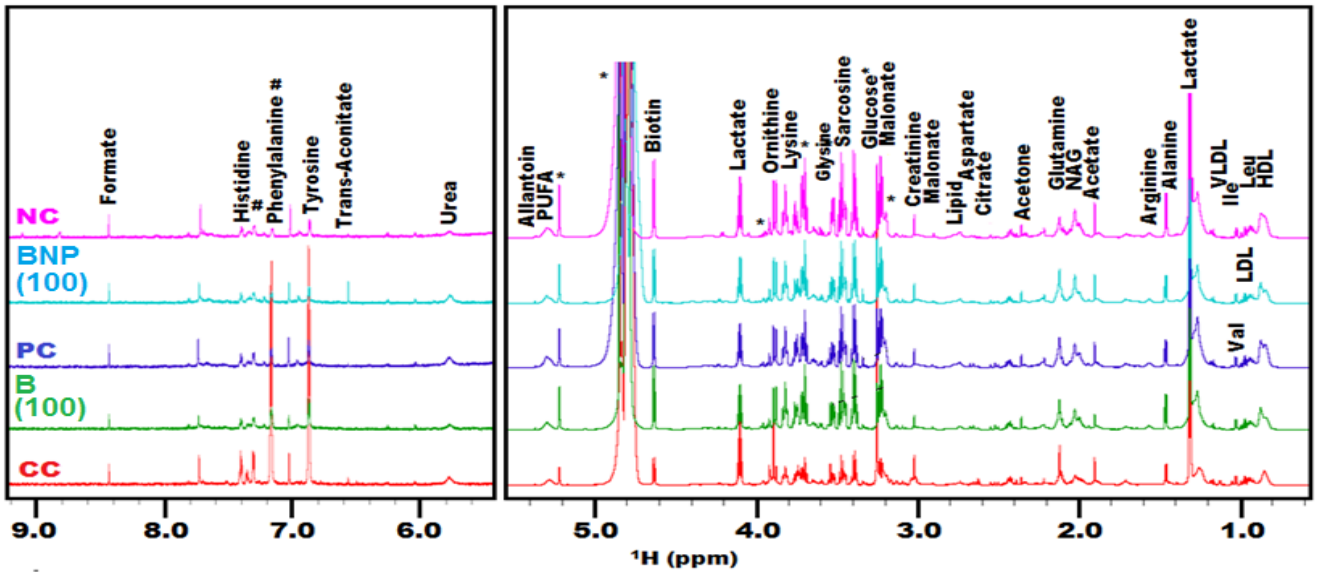

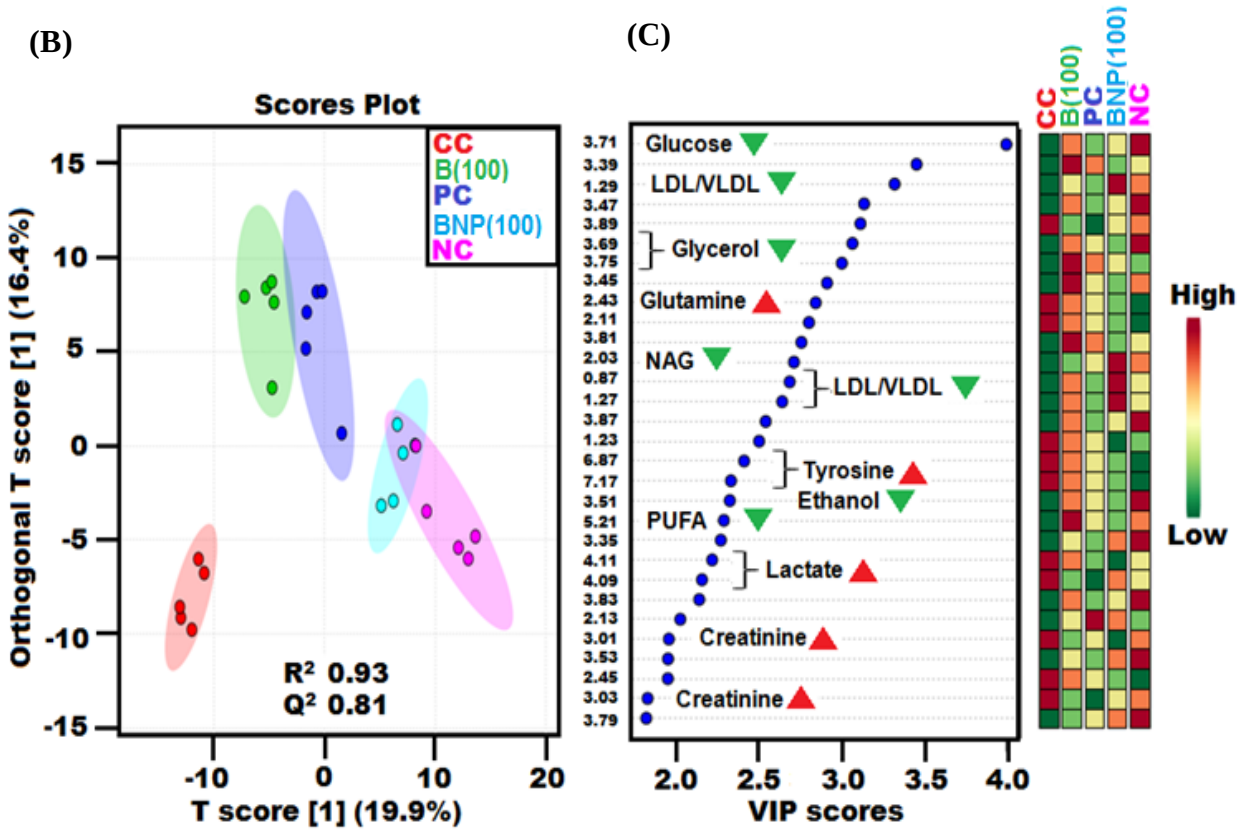

Figure 14 (A) The obtained stack plot representing 1D-^{1}H-CPMG-NMR spectra of serum sample of rat procured from various groups. Stack plot of representative 1D-^{1}H-CPMG-NMR spectra of the serum of rat acquired from diverse groups. Carcinogen control (CC), Betulinic acid (B 100), Positive control (PC), Betulinic acid nanoparticles (BNP 100) and Normal Control (NC) groups. **(B)** Pair-wise and Combined OPLS-DA analysis: The 2D OPLS-DA analysis of 1D-^{1}H-CPMG-NMR spectra score plot developed from the combined analysis encompassing all the groups: Carcinogen control (CC), Betulinic acid (B 100), Positive control (PC), Betulinic acid nanoparticles (BNP 100) and Normal Control (NC) groups. **(C)** The prospective discriminatory metabolite units recognized from the VIP scores obtained from PLS-DA modeling of entire data matrix and procured VIP scores for top 30 metabolite units are depicted in rising order of VIP score significance to emphasize their discriminatory prospective.

Further, the OPLS-DA model was used to achieve a summary of complete informational collection of samples and to discriminate the variables that are responsible of variations among the groups. The nature of OPLS-DA model was optimized with two factors i.e. Q^2 and R^2. The combined and pair wise analysis of PLS-DA data revealed $R^2 = 0.93$ and $Q^2 = 0.81$, representing a significant metabolic alteration between normal and NDEA treated carcinogenic groups (Figure 14B). The main metabolic dissimilarity between the CC groups and control groups along with their p-values, variable importance on projection (VIP) score, and chemical shifts (δ) are

listed in Table 8. There were significant increased levels of acetate, glutamine, tyrosine, LDL/VLDL, citrulline, choline, tryptophan, glycerol, creatinine, lactate, citrate and decreased levels of HDL, leucine isoleucine, arginine, glucose in NDEA treated group (Table 8). All these metabolites became regularized after treating BNP and B. The score plots obtained from 1D-^{1}H-CPMG-NMR spectra (Figure 14B) (from S-plots and OPLS-DA) demonstrated a reasonable separation among the groups on X-axis. The separation of different groups again analyzed in VIP score plots in Figure 14C and the combined correlations of VIP score analyses and 2D OPLS-DA analyses demonstrated noteworthy disparities in metabolic profiles amid a range of groups.

Table 8 Key observed metabolic differentiation between the NDEA induced carcinogenic rat serum and normal control. The chemical shift, AUC, VIP score, variation and p-values of the individual biomarkers are provided. p-values less than 0.05 were considered as significant. The metabolic differences between NDEA and NC, NDEA and PC, NDEA and B100, NDEA and BNP100 have also been presented.

PPM	Metabolite	Carcinogen Control (CC) Versus											
		Normal Control (NC)			Positive Control (PC)			B100			BNP100		
		VIP^{Coef}	AUC		VIP^{Coef}	AUC		VIP^{Coef}	AUC		VIP^{Coef}	AUC	
0.87	LDL/VLDL	1.8^{30}	0.8	↓	1.7^{38}	0.8	↓	2.0^{47}	0.8	↓*	2.7^{63}	1.0	↓*
0.85	HDL	2.9^{72}	1.0	↑*	2.7^{65}	0.9	↑*	3.0^{71}	0.9	↑*	3.5^{84}	1.0	↑*
0.91	Isoleucine	1.9^{32}	1.0	↑***	1.1^{25}	1.0	↑**	0.7^{17}	0.9	↑*	1.0^{22}	1.0	↑**
0.93	Leucine	1.3^{33}	1.0	↑*	1.2^{30}	1.0	↑*	0.8^{18}	1.0	↑*	1.0^{22}	1.0	↑*
1.05	Isobutyrate	1.1^{28}	1.0	↓*	1.0^{25}	1.0	↓*	1.2^{28}	1.0	↓*	1.1^{26}	1.0	↓*
1.13	Propylene glycerol	1.3^{33}	1.0	↓*	1.3^{33}	1.0	↓*	1.3^{30}	1.0	↓*	1.1^{27}	1.0	↓*
1.15	Propionate	0.2	0.6	↑	1.1^{26}	1.0	↑*	0.5^{12}	1.0	↑*	0.5^{09}	0.9	↑*
1.17	Ethanol	0.4	0.6	↓	1.2^{28}	0.8	↑*	0.3^{5}	0.6	↑*	0.3^{4}	0.8	↓
1.19	3 HB	0.7^{17}	0.8	↑*	1.4^{28}	1.0	↑*	0.6^{15}	0.8	↑	0.6^{13}	0.8	↑*
1.23	3 Aminoisobutyrate	2.6^{65}	1.0	↓**	2.6^{62}	1.0	↓**	2.6^{60}	1.0	↓**	2.9^{68}	1.0	↓***
1.27	LDL/VLDL	2.6^{61}	0.8	↑*	2.2^{52}	0.6	↑	2.7^{63}	0.8	↑	4.1^{100}	1.0	↑*
1.29	Lipid	2.9^{71}	0.8	↑*	1.6^{38}	0.6	↑	2.3^{52}	0.8	↑	3.8^{93}	1.0	↑***

1.43	Lysine	1.7^{27}	1.0	↓**	1.1^{27}	1.0	↓**	1.7^{31}	1.0	↓***	1.2^{29}	1.0	↓***
1.45	Alanine	1.5^{38}	1.0	↑*	1.3^{30}	1.0	↓*	0.4^{9}	0.6	↑	0.7^{17}	0.9	↓*
1.57	Citrulline	1.3^{33}	1.0	↑*	1.2^{30}	1.0	↑*	1.3^{31}	1.0	↑*	1.7^{41}	1.0	↑***
1.63	Arginine	0.85^{21}	1.0	↑**	1.1^{26}	1.0	↑***	0.8^{19}	1.0	↑*	1^{25}	1.0	↑**
1.77	Arginine	0.42^{10}	0.9	↑*	0.1^{2}	0.6	↓	0.3^{8}	0.9	↓*	0.1^{1}	0.6	↓
1.89	Acetate	1.6^{39}	1.0	↓*	1.3^{30}	0.9	↓*	1.6^{38}	1.0	↓*	0.5^{12}	0.7	↓
1.97	Proline	1.5^{36}	1.0	↓***	1.4^{33}	1.0	↓*	1.3^{31}	1.0	↓**	1.5^{37}	1.0	↓*
2.03	NAG	2.6^{66}	1.0	↑***	2.7^{64}	1.0	↑***	2.5^{60}	1.0	↑***	2.9^{71}	1.0	↑***
2.11	Methionine	2.6^{50}	0.9	↓*	0.6^{5}	0.6	↓	0.8^{9}	0.5	↓	0.6^{7}	0.6	↓
2.13	Glutamine	1.6^{40}	0.9	↑*	2.9^{71}	1.0	↑***	2.6^{62}	1.0	↑**	2.6^{63}	1.0	↑***
2.19	Glycoproline	0.8^{21}	1.0	↓*	0.6^{15}	1.0	↓*	0.8^{20}	1.0	↓*	0.7^{17}	1.0	↓*
2.21	Acetone		0.5		1.2^{30}	1.0	↑*	0.5^{9}	0.6	↑	0.9^{22}	1.0	↑*
2.23	LIPID	1.4^{35}	1.0	↑*	1.4^{34}	1.0	↑*	1.35^{31}	1.0	↑*	1.8^{44}	1.0	↑*
2.33	Glutamate	0.8^{21}	1.0	↓*	1.0^{23}	1.0	↓*	0.8^{19}	0.9	↓*	1.1^{27}	1.0	↓*
2.35	Pyruvate	0.3	0.8	↑	1.0^{24}	1.0	↑***	1^{24}	1.0	↑*	0.6^{14}	1.0	↑**
2.43	Glutamine	2^{50}	1.0	↓***	1.7^{40}	1.0	↓***	0.9^{19}	0.8	↓*	1.6^{40}	1.0	↓***
2.63	Citrate	1.1^{27}	1.0	↓*	1.0^{21}	0.8	↓*	0.9^{21}	0.8	↓*	1.0^{23}	1.0	↓*
2.71	Dimethylamine	1.0^{24}	1.0	↓***	1.0^{24}	1.0	↓***	1.0^{25}	1.0	↓**	1.1^{26}	1.0	↓***
2.79	Aspartate	0.7^{17}	1.0	↓*	0.7^{16}	1.0	↓*	0.8^{20}	1.0	↓*	0.8^{19}	1.0	↓*
2.91	Dimethylglycine	0.3^{8}	0.8	↓	0.6^{16}	1.0	↑*	0.6^{15}	1.0	↑*	0.5^{13}	1.0	↑*
3.01	Creatinine	3.5^{87}	0.8	↓*	3.9^{94}	1.0	↓*	3.9^{92}	1.0	↓*	3.6^{87}	1.0	↓*
3.03	Creatine Phosphate	1.9^{46}	1.0	↓**	2.0^{49}	1.0	↓*	2.0^{47}	1.0	↓*	1.9^{46}	1.0	↓*
3.15	Malonate	1.2^{30}	1.0	↓*	1.2^{28}	1.0	↓*	1.2^{28}	1.0	↓*	1.1^{27}	1.0	↓*
3.17	O-Acetylcarnitine	1.3^{31}	1.0	↓*	1.2^{27}	0.8	↓*	1.2^{27}	0.7	↓*	1.3^{31}	0.9	↓*
3.19	Choline	1.4^{32}	1.0	↑*	2.0^{48}	1.0	↑*	1.9^{44}	1.0	↑**	1.1^{25}	1.0	↑*
3.21	GPCho	2.3^{55}	1.0	↑*	2.2^{53}	0.8	↑*	2.9^{69}	1.0	↑***	1.6^{40}	1.0	↑***

3.27	Taurine/Betain	1.0^{22}	1.0	↓*	1.2^{28}	1.0	↓*	1.2^{27}	1.0	↓*	1.1^{27}	1.0	↓*
3.39	Glucose	3.8^{94}	1.0	↑*	4.1^{100}	1.0	↑*	4.2^{100}	1.0	↑*	3.4^{84}	1.0	↑*
3.55	Glycine	0.2^{4}	0.6	↓	1.8^{43}	1.0	↑*	1.5^{36}	1.0	↑*	1.3^{30}	0.8	↑*
3.71	Glucose	4^{100}	1.0	↑**	3.0^{72}	1.0	↑***	3.0^{72}	1.0	↑**	2.8^{69}	1.0	↑**
4.11	Lactate	2.3^{58}	1.0	↓*	2.5^{60}	1.0	↓*	2.2^{51}	0.8	↓	2.6^{62}	1.0	↓*
4.19	Threonine	1.2^{29}	1.0	↑*	1.0^{21}	1.0	↑*	0.7^{17}	1.0	↑*	1.0^{25}	1.0	↑*
4.27	Threonine	0.9^{23}	1.0	↑*	1.0^{26}	1.0	↑*	1.0^{23}	1.0	↑*	1^{25}	1.0	↑*
4.31	Cytidine	0.9^{22}	1.0	↑**	1.0^{26}	1.0	↑***	1.0^{23}	1.0	↑**	1^{25}	1.0	↑***
4.43	Carnosine	0.6^{13}	1.0	↑**	0.6^{15}	1.0	↑*	0.7^{16}	1.0	↑***	0.5^{12}	1.0	↑**
4.57	Glutathione	0.4^{8}	0.8	↑	0.7^{13}	0.9	↑*	0.7^{17}	1.0	↑***	0.4^{11}	0.9	↑*
5.27	Un	0.8^{20}	0.7	↓	1.1^{25}	0.8	↓*	1.3^{30}	0.9	↓*	1.5^{35}	1.0	↓**
5.31	PUFA	1.3^{33}	0.9	↑*	1.1^{25}	0.8	↑*	1.2^{27}	0.9	↑*	1.5^{38}	1.0	↑*
5.87	Cytidine	0.9^{4}	0.8	↓*	0.1^{2}	0.8	↓	0.2^{5}	0.9	↓**	0.2^{4}	0.9	↓*
6.57	Trans Aconitate	0.1^{2}	0.6	↓	0.2^{4}	0.6	↓**	0.4^{9}	0.8	↓***	0.1^{2}	0.9	↑*
6.87	Tyrosine	2.4^{60}	1.0	↓*	0.1^{3}	1.0	↑	2.5^{10}	1.0	↓	0.1^{2}	1.0	↑*
6.95	Anserine	0.3^{7}	1.0	↓*	2.5^{58}	1.0	↓*	0.3^{6}	1.0	↓**	0.2^{5}	1.0	↓*
7.01	Histidine	0.5^{11}	1.0	↑*	0.2^{4}	1.0	↓**	0.2^{6}	1.0	↑*	0.2^{4}	1.0	↓
7.31	Phenylalanine	1.1^{27}	1.0	↓***	0.3^{8}	1.0	↑**	1.1^{25}	1.0	↓**	1.1^{25}	1.0	↓*
8.43	Formate	0.1^{9}	0.8	↓	0.1^{1}	1.0	↑	0.1^{2}	1.0	↑	$0.1^{.2}$	1.0	↑

Note: Data represented here as mean±SD (n=8). Statistically considerable disparities were detected between the test groups and CC groups [one way ANOVA followed by Bonferroni multiple comparison test (***p<0.001, **p<0.01 and *p<0.05)]

The best 30 metabolite units were cautiously selected when the major verge of variable influence on projection (VIP) values attained from the OPLS-DA model was >1.0. For the meantime, the obtained *p*-values from the two-tailed Student's t-test on the normalized peak area were believed to be statistically considerable ($p< 0.05$). Log2 fold change (FC) was taken into the application to express how these predominantly differential metabolites diverse amongst all the studied groups. The results were believed statistically considerable when the p-value is <0.05. Some appropriate metabolic alterations are represented in the form of univariate box plots in the Figure 15.

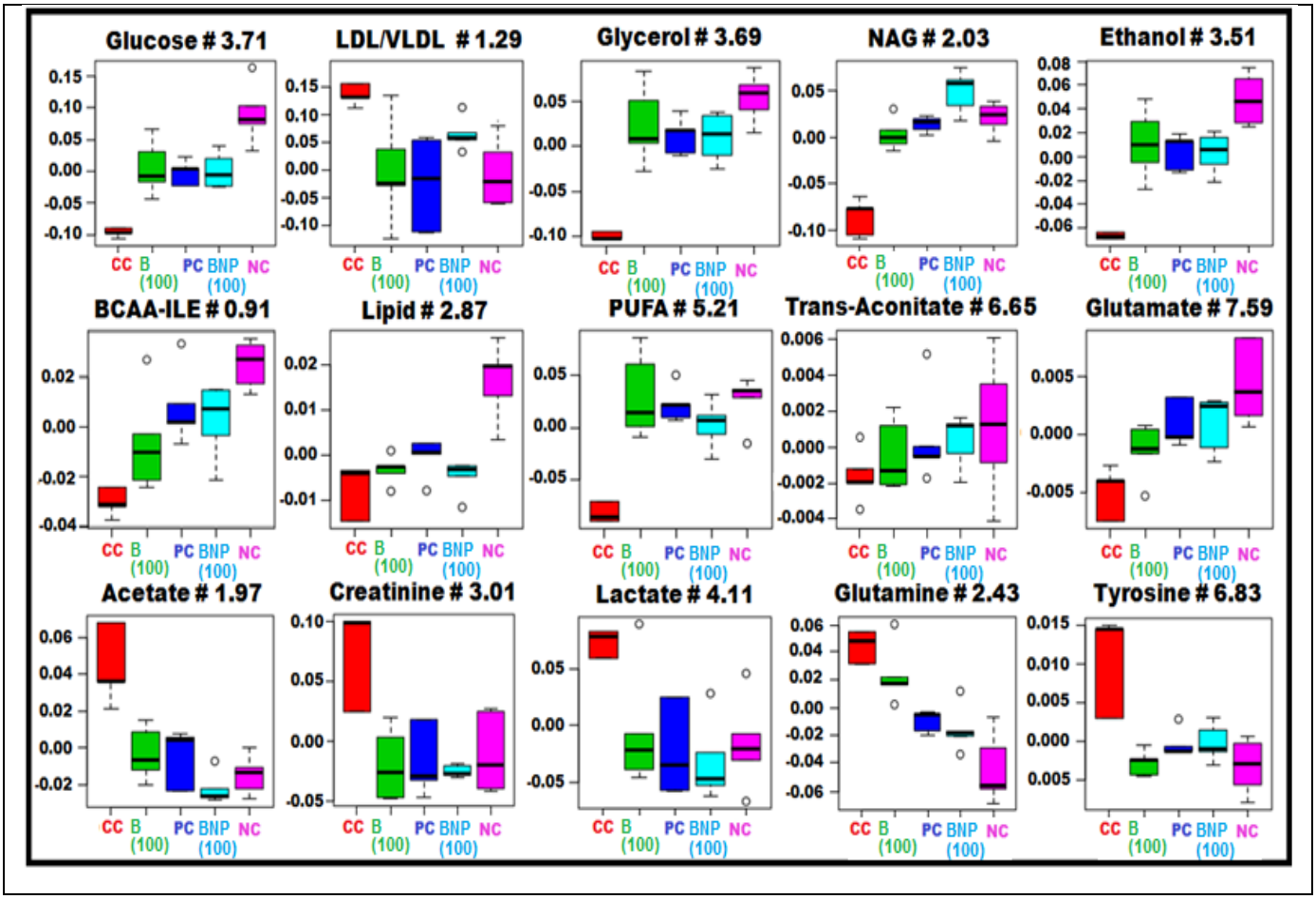

Figure 15 Metabolic outcomes of BNP and B treatment: The Box-cum-Whisker plots demonstrating the comparative distinction in the quantitative profiles of metabolites present in the serum with relevance to the hepatic cancer pathophysiology. In the box plots, the boxes signifies the interquartile assortment, the straight streaks within the box stand for the median, and the top boundaries and the bottom boundaries of boxes are designated as 75th and 25th percentiles, respectively. The upper whiskers and lower whiskers are in 95th and 5th percentiles. Where: Carcinogen control (CC), Betulinic acid (B 100), Betulinic acid nanoparticles (BNP 100), Positive control (PC) and Normal Control (NC) groups.

The heat mapping of each dataset revealed BNP treated group showed metabolomic profiles remarkably similar to control group (Figure 16A). A number of individual metabolites appropriate in the context of HCC significantly alternated in CC group that were reversed to varying degrees after B and BNP treatment. These single metabolites can then be integrated into a number of key pathways (Figure 16B and 16C). Major metabolic pathways changed by B and BNP treatment in our dataset included glycolysis, β-oxidation, lipolysis, ketogenesis, the Krebs cycle, and the urea cycle and methylamine metabolism.

(A)

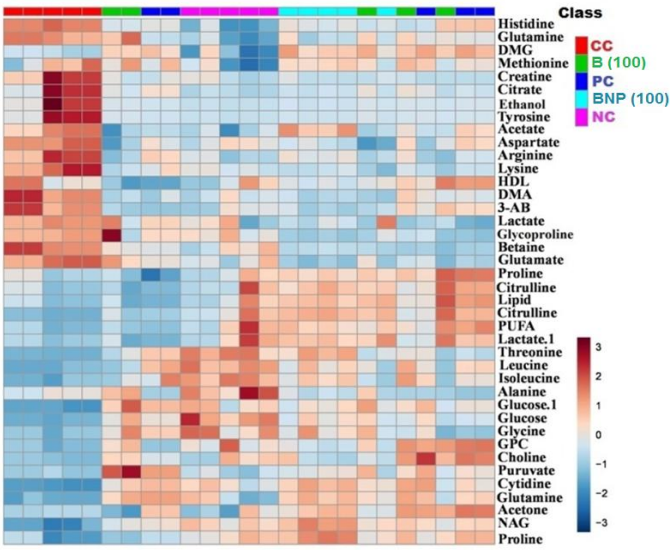

(B)

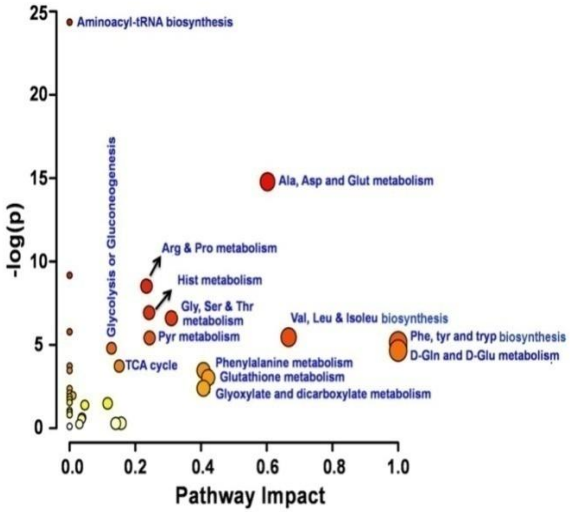

(C)

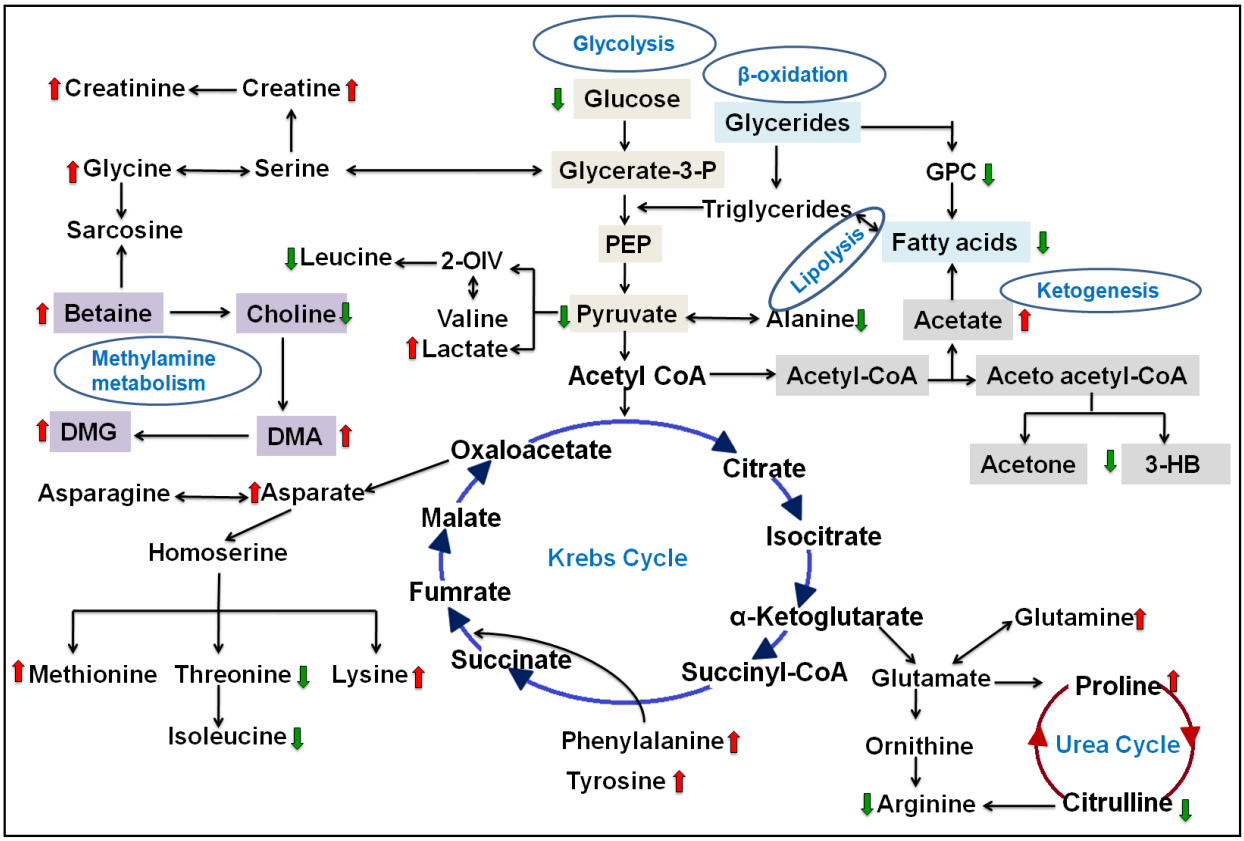

Fig 16 (A) Heatmap of significant metabolites represented their concentration changing pattern. **(B)** Showing the element supports pathway investigation of (incorporating pathway topological investigation and enrichment analysis) and revelation for one model organisms. Pathways impact

is shown the highly significant pathways of major metabolites. **(C)** Major metabolic pathways of the most relevant metabolites after B, Bnp treatments and CC group involved in glycolysis, β-oxidation, lipolysis, ketogenesis, the Krebs cycle, and the urea cycle and methylamine metabolism. It is shown i.e. red color: increase concentration profile of particular metabolites in CC group. Green color: decrease concentration profile of particular metabolites in CC group.

4.3 Discussion

B has strong pharmacological importance because of its greater cytotoxicity potential against various cancerous cells. The therapeutic window of B is considerably high due to less toxicity to normal cells [27,28,29]. The tumor inhibitory ability of B was identified in various cell line studies, where the normal cells are more resistant to B [27,28,29]. However, the most challenging sinario of its biomedical use is its low water solubility, which subsequently causes poor bioavailability [30,31]. In view of the above facts, our group developed PLGA-loaded nanoparticles (BNP) to improve its anticancer potentials [14]. In our previous studies, the anti-neoplastic abilities of BNP and B were measured both *in vivo* and *in vitro* models and it was found that BNP had more pharmacological responses than the pure B [14]. Herein, we explored the mechanism of anti-neoplastic properties of BNP and B at molecular levels and cellular levels.

5-fluorouracil (5-FU), the well known anti-metabolite drug is commonly utilized for treating the liver cancer as well as colorectal cancer. 5-FU exerts its anti-cancer activity through thymidylate synthase inhibition and integration of the metabolites into the DNA and the RNA. This mechanism often results in the resistance development to the drug, causing noteworthy restraints to its clinical applications [32]. Therefore, the recognition of novel curative armamentarium that will act through diverse mechanisms is essential in the present scenario. In the current study, we discovered the anti-cancer perspectives of BNP and B that might act by i-NOS activation and e-NOS mediated Bcl-2 family proteins→CytC→Caspase-3 and Caspase-9 signaling cascade.

In continuation with our previous work, we initially explored the mechanism of anti-HCC potential of BNP at molecular level. The results of the total nitrite/nitrate ratios and NOS activity after NDEA treatment revealed that the NO concentration was decreased in HCC rats, indicating liver injury. Interestingly, the concentration of NO was increased following treatment with 5-FU, B and BNP, demonstrating their protective action. NO plays both cytotoxicity actions and cytoprotective actions in the liver [33]. Significantly, NO produced by inducible form or inflammatory isoforms of the NOS (also referred to as i-NOS) resulting in a hepatic injury

during the hepatic carcinoma, whereas NO produced by endothelial form or constitutive isoforms of the NOS (also referred to as e-NOS) thereby offering the protection against these grievances [33]. In general, the higher NO levels induce apoptosis thus, our study is mainly based on differential expression of e-NOS and i-NOS in caspase mediated mitochondrial apoptosis. The obtained results point toward that the downstream expression of e-NOS and the upstream expression of i-NOS led to the incidence of HCC in CC group. However, treating with BNP and B normalized the expression levels of both the isoforms of NOS. The protective action was slightly higher for Bnp than parent B.

On the other hand, both e-NOS and i-NOS play an important role in cellular apoptosis [34,35]. The cellular apoptosis occurs in two ways i.e. extrinsic death receptor pathway and intrinsic mitochondrial pathway. Bcl-2 family regulates mitochondrial pathway where anti-apoptotic (Bcl-2 and Bcl-xl) and pro-apoptotic (BAX and BAD) proteins are released [34,35,36]. The results acquired from the qRT-PCR studies and western blot studies disclosed that increased expressions of Bcl-xl, Bcl-2, and decreased expressions of BAD, BAX in CC group restored to normal after B and BNP treatments. Cyt-c could release from the mitochondria with the activation of all these apoptogenic markers, which ultimately could attached with procaspase-9 and APAF1 to turn out apoptosome [34,35,36]. This complex formation takes place in presence of Caspase-9 and Caspase-3. We observed that both BNP and B restored the diminished levels of Caspase-9 and Caspase-3, and therefore, these might prove themselves as apoptotic activator. Considering altogether, both B and BNP causes induction of apoptosis through i-NOS and e-NOS induced activation of Bcl-2 family proteins → Cyt C → Caspase-3 and Caspase-9 signaling cascade. This action was more prominent for PLGA loaded nanoparticles of B i.e. BNP than the pure B.

To investigate efficacy of BNP due to the activation of e-NOS and i-NOS, we also applied a data based mathematical modeling approach in the present work. To achieve this, we translated the steps involved in stimulation of e-NOS and i-NOS pathway into a system of ordinary differential equations and put the quantitative values of qRT-PCR analysis into the formulated system through MATLAB software [16,17]. It was identified from mathematical modeling that the decrease in concentration of cancer cells is maximum for BNP than B. This implied that the enhanced activation of e-NOS and i-NOS by the BNP caused the apoptosis of cancer cells more

efficiently as compared to B and 5-FU. It was further observed from the graphs that stimulation of e-NOS and i-NOS resulted in elevation of BAX+BAD, declination of Bcl-2+Bcl-xl in the cytoplasm and increase in the concentrations of Caspase-9 and Caspase-3. Applying mathematical modeling, it had also been observed that the apoptosis of cancer cells was mediated by e-NOS and i-NOS stimulation in our experiment. Thus, the quantitative qRT-PCR and data-based mathematical modeling strongly supported the potential of BNP to induce apoptosis to the cancer cells mediated *via* stimulation of e-NOS and i-NOS.

In addition, it is obligatory to realize the metabolic discriminations during the carcinogenic condition and recovery after treatments with B and BNP. The tumor-induced hyperlipidemia leads to the progression of liver cirrhosis during the HCC development, which ultimately led to the liver damage [37]. Liver damage during carcinogenic condition was observed through increased TC, TG, LDL, VLDL and decreased HDL concentrations in CC rat sera as compared to the NC. The BNP and B treatments normalized these concentrations, which further accounted protective activities of B and BNP.

Finally, a ^{1}H-NMR-based serum metabolomic approach was employed to assess the capability of BNP and B to reinstate the metabolic perturbations related to NDEA-exposed HCC. The box-cum-whisker plots and OPLS-DA score plots employing the MetaboAnalyst [38] attained from 1D-^{1}H-CPMG-NMR spectral data of rat serum samples evidently expressed the noteworthy metabolic discriminations in the HCC conditions. The HCC condition was accentuated *via* decreased glucose and increased lactate levels, which further demonstrated cancerous condition [37]. We observed similar War-burg effects where superior quantity of glucose was consumed by cancerous tissue and formed lactate as by-product [39, 40]. The interesting observation documented in our study was to restore these two metabolic alterations i.e. reduced glucose and elevated lactate levels, a hallmark for tumor progression. Contrasting to it, tyrosine was up-regulated in the NDEA-induced rat that indicated higher rate of catabolism during the cancerous state [41,42]. Administration of BNP and B caused an extensive lowering in the tyrosine level, further supporting their hepatoprotective actions.

Tyrosine and glutamine are the important amino acids, which help for the catabolic reaction in humans during the carcinogenic conditions [43]. Administration of BNP and B caused a

noticeable decreased in the glutamine level. The protection against HCC condition was further noticed in NMR-based metabolomic studies. Box and whisker plot showed a lover amount of NAG and lipids in CC rat sera, indicating a higher cell membrane formation, as both are the imperative elements of the cell membrane [44,45]. Again, both these metabolites became normalized after treatments with 5-FU, B and BNP, demonstrating their protective ability against HCC. Furthermore, VLDL/LDL was observed to be augmented in CC rat as both metabolites are the precursor for the production of cholesterol and cholesterol is utilized by cell for cell membrane production [41,46,47,48]. B and BNP administration again normalized these metabolites concentration near to normal, which further demonstrated their anticancer properties. We perceived that the HCC rat sera had a lower amount of glycerol, demonstrating increased lipid metabolism in cancerous condition [49,50]. In addition, treatment with 5-FU, BNP and B regularized the glycerol serum levels, indicating their capability to augment the glycerol metabolism. B and Bnp treatment also normalized trans-aconitate, and formate in serum, the metabolic pathway was consequently established according to the VIP scores of the concerned metabolites. The metabolic perturbations showed a reduced tricarboxylic acid (TCA) cycle (glutamine) and elevated β-oxidation (lipoproteins and lipids) glycolysis or gluconeogenesis (glucose and lactate) during HCC condition which is well supported by earlier report [38,37,39,40,41,42,43,44,45,46.47,48,49,50]. The deregulated metabolites displayed the modified energy metabolism of the tumor cells and majority of the metabolic transformations were reorganized again to regular standard by 5-FU, BNP and B administration, advocated its potential concerning with balancing the metabolic irregularities pertaining HCC.

4.4 References:

1. Kumar A, Sunita P, Pattanayak SP. Silibinin inhibits the hepatocellular carcinoma in NDEA-induced rodent carcinogenesis model: An evaluation through biochemical and bio-structuralparameters. Journal of Cancer Science Therapy. 2015;7(10.4172):1948-5956.
2. Matsuzaki T, Murase N, Yagihashi A, Shinozuka H, Shimizu Y, Furuya T, Burrell N, Iwatsuki S, Starzl TE. Liver transplantation for diethylnitrosamine-induced hepatocellular carcinoma in rats. InTransplantation proceedings 1992;24(2):748.
3. Shiota G, Harada KI, Ishida M, Tomie Y, Okubo M, Katayama S, Ito H, Kawasaki H. Inhibition of hepatocellular carcinoma by glycyrrhizin in diethylnitrosamine-treated mice. Carcinogenesis. 1999;20(1):59-63.
4. Furuta K, Sato S, Miyake T, Okamoto E, Ishine J, Ishihara S, Amano Y, Adachi K, Kinoshita Y. Anti-tumor effects of cimetidine on hepatocellular carcinomas in diethylnitrosamine-treated rats. Oncology reports. 2008;19(2):361-8.
5. Motawi TK, Elgawad HM, Shahin NN. Gastroprotective effect of leptin in indomethacin-induced gastric injury. Journal of biomedical science. 2008;15(3):405-12.
6. Miranda KM, Espey MG, Wink DA. A rapid, simple spectrophotometric method for simultaneous detection of nitrate and nitrite. Nitric oxide. 2001;5(1):62-71.
7. Dolkart O, E A, AA W. Temporal determination of lung NO system and COX-2 upregulation following ischemia–reperfusion injury. Experimental lung research. 2014;40(1):22-9.
8. Kumar P, Agarwal A, Singh AK, Gautam AK, Chakraborti S, Kumar U, Kumar D, Bhattacharya B, Panda P, Saha B, Qidwai T. Antineoplastic properties of zafirlukast against hepatocellular carcinoma via activation of mitochondrial mediated apoptosis. Regulatory Toxicology and Pharmacology. 2019;109:104489.
9. Sahdev AK, Raj V, Singh AK, Rai A, Keshari AK, De A, Samanta A, Kumar U, Rawat A, Kumar D, Nath S. Ameliorative effects of pyrazinoic acid against oxidative and metabolic stress manifested in rats with dimethylhydrazine induced colonic carcinoma. Cancer biology & therapy. 2017;18(5):304-13.
10. Singh AK, Bhadauria AS, Kumar U, Raj V, Rai A, Kumar P, Keshari AK, Kumar D, Maity B, Nath S, Prakash A. Novel Indole-fused benzo-oxazepines (IFBOs) inhibit

invasion of hepatocellular carcinoma by targeting IL-6 mediated JAK2/STAT3 oncogenic signals. Scientific reports. 2018;8(1):1-3.

11. Anadol E, Yar AS, MENEVŞE S. The changes of Inducible Nitric Oxide Synthase, Endothelial Nitric Oxide Synthase and Cyclooxygenase-2 mRNA expressions in intrauterine tissues of pregnant rats. Ankara Üniversitesi Veteriner Fakültesi Dergisi. 2012;59(4):295-301.
12. Chandra D, Liu JW, Tang DG. Early mitochondrial activation and cytochrome c up-regulation during apoptosis. Journal of Biological Chemistry. 2002;277(52):50842-54.
13. Jafari Anarkooli I, Sankian M, Ahmadpour S, Varasteh AR, Haghir H. Evaluation of Bcl-2 family gene expression and Caspase-3 activity in hippocampus STZ-induced diabetic rats. Experimental diabetes research. 2008 Oct 12; 638467, 1–6.
14. Kumar P, Singh AK, Raj V, Rai A, Keshari AK, Kumar D, Maity B, Prakash A, Maiti S, Saha S. Poly (lactic-co-glycolic acid)-loaded nanoparticles of betulinic acid for improved treatment of hepatic cancer: characterization, in vitro and in vivo evaluations. International journal of nanomedicine. 2018;13:975.
15. Xu W, Guo G, Li J, Ding Z, Sheng J, Li J, Tan W. Activation of Bcl-2-caspase-9 apoptosis pathway in the testis of asthmatic mice. Plos one. 2016;11(3) e0149353.
16. Huber HJ, Duessmann H, Wenus J, Kilbride SM, Prehn JH. Mathematical modelling of the mitochondrial apoptosis pathway. Biochimica et Biophysica Acta (BBA)-Molecular Cell Research. 2011;1813(4):608-15.
17. Swameye I, Müller TG, Timmer J, Sandra O, Klingmüller U. Identification of nucleocytoplasmic cycling as a remote sensor in cellular signaling by databased modeling. Proceedings of the National Academy of Sciences. 2003;100(3):1028-33.
18. Singh AK, Raj V, Keshari AK, Rai A, Kumar P, Rawat A, Maity B, Kumar D, Prakash A, De A, Samanta A. Isolated mangiferin and naringenin exert antidiabetic effect via PPARγ/GLUT4 dual agonistic action with strong metabolic regulation. Chemico-biological interactions. 2018;280:33-44.
19. Wishart DS, Jewison T, Guo AC, Wilson M, Knox C, Liu Y, Djoumbou Y, Mandal R, Aziat F, Dong E, Bouatra S. HMDB 3.0—the human metabolome database in 2013. Nucleic acids research. 2012;41(D1):D801-7.

20. Nicholson JK, Foxall PJ, Spraul M, Farrant RD, Lindon JC. 750 MHz 1H and 1H-13C NMR spectroscopy of human blood plasma. Analytical chemistry. 1995;67(5):793-811.
21. Guleria A, Bajpai NK, Rawat A, Khetrapal CL, Prasad N, Kumar D. Metabolite characterisation in peritoneal dialysis effluent using high-resolution 1H and 1H–13C NMR spectroscopy. Magnetic Resonance in Chemistry. 2014;52(9):475-9.
22. MetaboAnalyst. www.metaboanalyst.ca/
23. Puig-Castellví F, Alfonso I, Piña B, Tauler R. 1 H NMR metabolomic study of auxotrophic starvation in yeast using Multivariate Curve Resolution-Alternating Least Squares for Pathway Analysis. Scientific reports. 2016;6:30982.
24. Quan-Jun Y, Jun B, Li-Li W, Yong-Long H, Bin L, Qi Y, Yan L, Cheng G, Gen-Jin Y. NMR-based metabolomics reveals distinct pathways mediated by curcumin in cachexia mice bearing CT26 tumor. RSC advances. 2015;5(16):11766-75.
25. Ulrich EL, Akutsu H, Doreleijers JF, Harano Y, Ioannidis YE, Lin J, Livny M, Mading S, Maziuk D, Miller Z, Nakatani E. BioMagResBank. Nucleic acids research. 2007;36(suppl_1):D402-8.
26. Xia J, Psychogios N, Young N, Wishart DS. MetaboAnalyst: a web server for metabolomic data analysis and interpretation. Nucleic acids research. 2009;37(suppl_2):W652-60.
27. Fulda S, Jeremias I, Steiner HH, Pietsch T, Debatin KM. Betulinic acid: A new cytotoxic agent against malignant brain-tumor cells. International journal of cancer. 1999;82(3):435-41.
28. Zuco V, Supino R, Righetti SC, Cleris L, Marchesi E, Gambacorti-Passerini C, Formelli F. Selective cytotoxicity of betulinic acid on tumor cell lines, but not on normal cells. Cancer letters. 2002;175(1):17-25.
29. Selzer E, Pimentel E, Wacheck V, Schlegel W, Pehamberger H, Jansen B, Kodym R. Effects of betulinic acid alone and in combination with irradiation in human melanoma cells. Journal of investigative dermatology. 2000;114(5):935-40
30. Jäger S, Laszczyk MN, Scheffler A. A preliminary pharmacokinetic study of betulin, the main pentacyclic triterpene from extract of outer bark of birch (Betulae alba cortex). Molecules. 2008;13(12):3224-35.

31. Drag-Zalesinska M, Kulbacka J, Saczko J, Wysocka T, Zabel M, Surowiak P, Drag M. Esters of betulin and betulinic acid with amino acids have improved water solubility and are selectively cytotoxic toward cancer cells. Bioorganic & medicinal chemistry letters. 2009;19(16):4814-7.
32. Longley DB, Harkin DP, Johnston PG. 5-fluorouracil: mechanisms of action and clinical strategies. Nature reviews cancer. 2003;3(5):330-8.
33. Clemens, M.G., 1999. Nitric oxide in liver injury. Hepatology, 30 (1), 1–5
34. Rang HP. Rang and Dale's Pharmacology 8th ed. E-book. Elsevier Health Sciences.
35. Brüne B, von Knethen A, Sandau KB. Nitric oxide and its role in apoptosis. European journal of pharmacology. 1998;351(3):261-72.
36. Snyder CM, Shroff EH, Liu J, Chandel NS. Nitric oxide induces cell death by regulating anti-apoptotic BCL-2 family members. PloS one. 2009;4(9).
37. Huang Q, Tan Y, Yin P, Ye G, Gao P, Lu X, Wang H, Xu G. Metabolic characterization of hepatocellular carcinoma using nontargeted tissue metabolomics. Cancer research. 2013;73(16):4992-5002.
38. Xia J, Sinelnikov IV, Han B, Wishart DS. MetaboAnalyst 3.0—making metabolomics more meaningful. Nucleic acids research. 2015;43(W1):W251-7.
39. Maurya V, Kumar P, Chakraborti S, Singh AK, Bhadauria AS, Kumar U, Kumar D, Pramanik A, Saha B, Gosipatala SB, Bhattachariya B. Zolmitriptan attenuates hepatocellular carcinoma via activation of caspase mediated apoptosis. Chemico-biological interactions. 2019;308:120-9.
40. Wang H, Wang L, Zhang H, Deng P, Chen J, Zhou B, Hu J, Zou J, Lu W, Xiang P, Wu T. ^{1}H NMR-based metabolic profiling of human rectal cancer tissue. Molecular cancer. 2013;12(1):121.
41. Liu Y, Hong Z, Tan G, Dong X, Yang G, Zhao L, Chen X, Zhu Z, Lou Z, Qian B, Zhang G. NMR and LC/MS-based global metabolomics to identify serum biomarkers differentiating hepatocellular carcinoma from liver cirrhosis. International journal of cancer. 2014;135(3):658-68.
42. Delage B, Fennell DA, Nicholson L, McNeish I, Lemoine NR, Crook T, Szlosarek PW. Arginine deprivation and argininosuccinate synthetase expression in the treatment of cancer. International journal of cancer. 2010;126(12):2762-72.

43. Fages A, Duarte-Salles T, Stepien M, Ferrari P, Fedirko V, Pontoizeau C, Trichopoulou A, Aleksandrova K, Tjønneland A, Olsen A, Clavel-Chapelon F. Metabolomic profiles of hepatocellular carcinoma in a European prospective cohort. BMC medicine. 2015;13(1):242.
44. Gao H, Lu Q, Liu X, Cong H, Zhao L, Wang H, Lin D. Application of 1H NMR-based metabonomics in the study of metabolic profiling of human hepatocellular carcinoma and liver cirrhosis. Cancer science. 2009;100(4):782-5.
45. Raouf AA, El-Sebaey HM, Abd El-Hamead AK, El-Fert AY, El-Gendy YE. Plasma free amino acid profile changes in hepatocellular carcinoma patients. Menoufia medical journal. 2016;29(4):895.
46. Katsuhiko Y, Chisato H. Clinical evaluation of serum levels of tryptophan in hepatobiliary disease. Clinica Chimica Acta. 1980;101(2-3):235-40.
47. Chen Y, Zhou J, Li J, Feng J, Chen Z, Wang X. Plasma metabolomic analysis of human hepatocellular carcinoma: diagnostic and therapeutic study. Oncotarget. 2016;7(30):47332.
48. Qin S, Bai Y, Lim HY, Thongprasert S, Chao Y, Fan J, Yang TS, Bhudhisawasdi V, Kang WK, Zhou Y, Lee JH. Randomized, multicenter, open-label study of oxaliplatin plus fluorouracil/leucovorin versus doxorubicin as palliative chemotherapy in patients with advanced hepatocellular carcinoma from Asia. J Clin Oncol. 2013;31(28):3501-8.
49. Rahman M, Hasan MR. Cancer metabolism and drug resistance. Metabolites. 2015;5(4):571-600.
50. Vander Heiden MG. Targeting cancer metabolism: a therapeutic window opens. Nature reviews Drug discovery. 2011;10(9):671-84.

Chapter 5

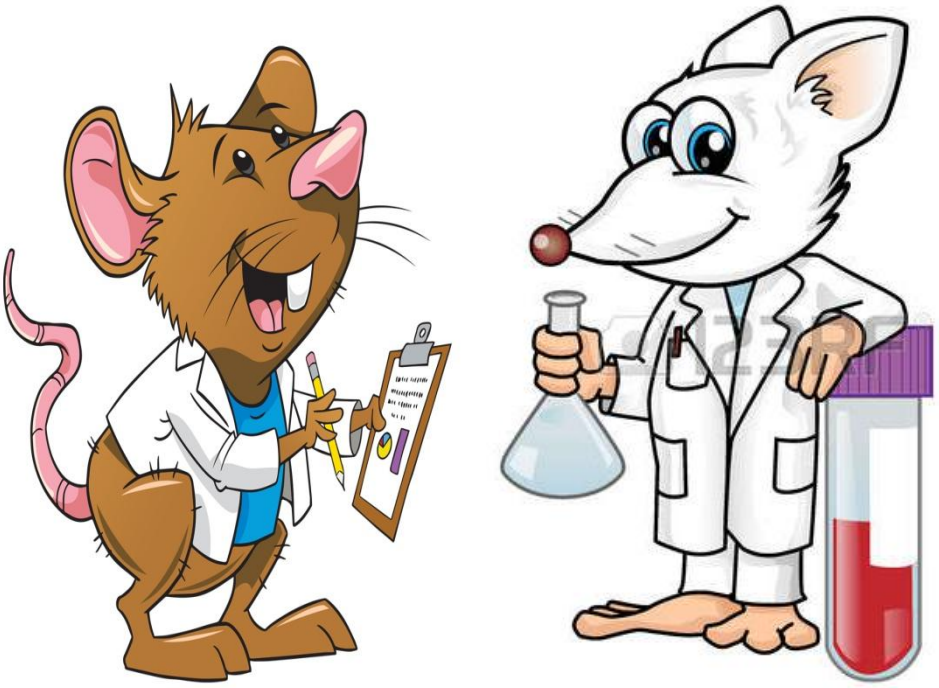

Summary and conclusion

5. Summary and conclusion.

Hepatocellular carcinoma, especially in the later stages, is a major problem in the clinic and *serious complication* of cirrhosis or other chronic liver disease. At present, the treatment strategies are limited and there is a clear need for new therapies. Only a few medications are available in the market for the treatment of HCC, possession of contraindication and side effects are the biggest unacceptability for the patient. Sorafenib is only FDA approved drug for the treatment of HCC with limited response rate due to local metastasis and chemotherapeutic resistance. Betulinic acid (B) is a naturally occurring product acquired from *Dillenia indica* stem bark, belonging to the family Dilleniaceae, having a pentacyclic triterpene nucleus with the broad range of pharmacological activities and biological activities like anticancer, antimalarial, anti-HIV, antibacterial, anti-inflammatory, anthelmintic, antinociceptive activities. The chief disadvantage associated with natural products is poor oral absorption, which may lead to lower effectiveness. Therefore, the foremost purpose of my research work is to isolate B, formulate nanoparticle of B (BNP) for treating HCC at molecular and cellular level.

Based upon the compatibility, desired biocompatible and biodegradable properties PLGA polymer was selected. The selected polymer was anticipated to possess capability of giving stable formulation, having high entrapment efficiency and drug loading. For polymeric nanoparticles, PLGA and PVA concentration was selected based on the particle size, %EE, drug loading and *in vitro* release.

Taking this scaffold as parent molecule B was isolated and formulated BNP by emulsifcation and the solvent evaporation technique with PLGA and different concentration of PVA. All batches of BNP subjected to zeta potential, particle size, PDI, entrapment efficiency, drug loading, *in vitro* drug release, SEM and FTIR analysis for optimization.

Once the formulation and characterization have been completed, optimized formulation BNP and B were subjected to *in vitro* screening on Hep-G2 cell line to investigate their anti-proliferative potential against HCC cells. Although the parent compound B represented the moderate cytotoxic potential (GI_{50} = 10 µg/mL) towards the Hep-G2 cell line, BNP exhibited high order of cytotoxicity (GI_{50} < 10µg/mL) against the Hep-G2 cell line. Again cellular uptake analysis was performed against Hep-G2 cells to reveal their cellular internalization potential. This action was

substantiated through confocal images where we established that BNP had good penetration power and entered inside the HepG2 cell to a greater extent than the parent compound B. Both these experiments suggested that BNP had more antineoplastic potential than the parent compound B.

On the basis of *in vitro* result, both BNP and B introduced for detailed *in vivo* pharmacological study. Prior to initiate this study, we performed *in vivo* pharmacokinetic studies for the estimation of drug concentration in the plasma as stated by the profile of BNP and B where experiment demonstrated that BNP had a higher volume of distribution in plasma than the parent compound B. This action may be due to the lower particle size of BNP, which was ultimately absorbed to a greater extent after the oral administration in the rats.

We, therefore, conducted *in vivo* anti-proliferative screening of both BNP and B in the NDEA-induced HCC model using male albino Wistar rats and provides few notable findings related to the mechanism underlying the BNP action. In our preliminary investigations, we assured for the induction of carcinogenic condition in NDEA-exposed rats by the reduced body weight of animals and higher incidence number of carcinogenic nodules in the liver tissue. The examined lessening in these alterations after BNP and B administration was principal proposition of its shielding effect against carcinogenic condition, which suggests the necessitation of additional biochemical and pathophysiological investigations. It has now been depicted that there is a decline in the action of anti-oxidants during the HCC conditions. The reduction in the enzymatic defense of SOD, CAT, and GSH and was profoundly observed after the NDEA treatment that unveils their increased utilization during excessive cellular proliferation. Further, the NDEA treatment increased the production of MDA and PC that validated the damage of the proteins and cellular lipids, respectively. It is notable that BNP and B administration reduced the levels of PC and MDA with restoration of enzymatic antioxidant defense of CAT, SOD and GSH, corroborated its tumor shielding capability with remarkable antioxidant effects.

Further, biliverdin and bilirubin are the catabolic by-products of RBCs, and the raised the levels of the following biomarkers which pointed toward hepatic damage. The elevation in these markers during the exposure to NDEA and their restoration after BNP and B administration also hold up the control of hepatic disease. Moreover, NDEA exposure elevated the levels of enzymes imperative for the liver function (AST, ALT and ALP) which reflect the advancement of

carcinogenesis condition. The observed efficacy of BNP to restore these enzyme levels indicated the ability of BNP to prevent hepatic damage. Similarly, the high concentration of LDH in the serum attained in the NDEA-exposed group could be accountable for NDEA-mediated damage to the liver due to incidence of pre-neoplastic lesions. Treatment with BNP led to the enhancement in LDH level which probably caused the attenuation in mitigation of pre-neoplastic lesions and hepatic damage and thereby potentiating its antitumor property.

Recent studies suggested that few pro-inflammatory cytokines and are engaged in the cancer progression inflammation pathogenesis. B usually brings to bear anticancer activity moreover by activating the apoptotic mitochondrial pathway or by inducing cellular stress, such as DNA damage and cytokine withdrawal. Therefore, we examined the modified stages of caspases and cytokines between diverse faction through the ELISA and investigated the consequences of BNP and B treatments over the carcinogen control group. In NDEA-exposed rats, the inflammatory cytokines were raised and were declined to a definite degree after BNP and B administrations. On the contrary, caspase-8 and caspase-3 were rapidly decline in the carcinogen control group and were notably raised again to the normal stages after BNP and B administrations. It was recognized that distinctive to the tested cytokines, the stages of caspase-8 and caspase-3 in the NDEA-exposed group were rapidly re-establish to the regular level after administration of BNP and B, and this effect was further distinct in the BNP-treated group as compared to the B-treated group. Further protective effect of BNP was evidenced through SEM analysis and histopathology. The microscopic image of histopathology showed irregular shaped cytoplasm and nuclei in the NDEA-treated rats that were most likely owing to unwarranted generation of free radical during the NDEA exposure. The potential reduction in denatured and ruptured cells (RC and dN) in BNP treated groups denoted the ameliorative perspectives of BNP against HCC. A similar trend was found in SEM analysis also.

Further, we investigated the mechanism of anti-HCC perspectives of BNP at molecular level. The levels of total nitrite/nitrate ratios, NOS, i-NOS are increased and e-NOS level decreased after NDEA treatment revealed that the NO concentration was decreased in HCC rats, representing liver injury. Interestingly, the concentration of NO was increased after BNP and B treatments, demonstrating their protective action, higher for BNP than parent B.

Further, gene expression analysis revealed that the BNP and B treatment provided a rapid reduction in i-NOS, Bcl-2, Bcl-xl and induction in e-NOS, Cyt-C, BAD, caspase-3, BAX, and caspase-9 mRNA expression which followed a trend similar to those measured in ELISA. Furthermore western blot study disclosed that increased expressions of Bcl-xl, Bcl-2, and decreased expressions of BAD in CC group re-established to the normal level after BNP and BP treatments Considering altogether, both BNP and B causes induction of apoptosis through e-NOS and i-NOS induced activation of Bcl-2 family proteins → Cyt C → Caspase-3 and Caspase-9 signaling cascade. This action was more prominent for BNP than the pure B.

Again we also applied a data based mathematical modeling approach in the present work. To accomplish the following, we deciphered the quantitative assessment of qRT-PCR analysis into the formulated method through the MATLAB software. It was recognized from the mathematical modeling that the decrease in concentration of cancer cells is maximum for BNP than B. It was further observed that stimulation of e-NOS and i-NOS resulted in elevation of BAX+BAD, declination of Bcl-2+Bcl-xl in the cytoplasm and increase in the concentrations of Caspase-9 and Caspase-3. Thus, the quantitative qRT-PCR and data-based mathematical modeling strongly supported the potential of BNP to induce apoptosis to the cancer cells mediated *via* stimulation of e-NOS and i-NOS.

In addition, the tumor-induced hyperlipidemia leads to the progression of liver cirrhosis during the HCC development, which ultimately led to the liver damage. Liver damage during carcinogenic condition was observed through increased TC, TG, LDL, VLDL and decreased HDL concentrations in CC rat sera as compared to the NC. The BNP and B treatments normalized these concentrations, which further accounted protective activities of BNP were more prominent than pure B.

We further implemented ^{1}H-NMR-based metabolomics to estimate whether BNP and B have the capability to reinstate the metabolic perturbations linked to NDEA-exposed HCC condition. The box-cum-whisker plots and OPLS-DA score plots by utilizing the MetaboAnalyst were achieved from the 1D-^{1}H-CPMG-NMR spectral results of the rat serum and clearly demonstrated significant metabolic modifications in the NDEA-exposed carcinogenic condition. Interestingly, a decreased glucose level and augmented lactate level were detected in the NDEA-exposed

group, which was well supported by earlier findings that demonstrate the carcinogenic condition. These findings completely prop up the Warburg effect and may be associated with a superior quantity of glucose utilization by the proliferating tissues pursued by the formation of the by-product, lactate. The noteworthy incidence witnessed in this investigation manifested the exceptional capability of BNP and B to reinstate two foremost metabolic perturbations, *i.e.*, elevated lactate levels and reduced glucose levels, a characteristic feature for the progression of tumor. Furthermore, VLDL/LDL was observed to be augmented in CC rat as both metabolites are the precursor for the production of cholesterol and cholesterol is utilized by cell for cell membrane production. B and BNP administration again normalized these metabolites concentration near to normal, which further demonstrated their anticancer properties. The metabolic perturbations showed a reduced tricarboxylic acid (TCA) cycle (glutamine) and elevated β-oxidation (lipoproteins and lipids) glycolysis or gluconeogenesis (glucose and lactate) during HCC condition.

In conclusion, developed PLGA based nanoformulation (BNP) demonstrated enhanced oral bioavailability, pharmacotherapeutic efficiency and anticancer effect. The current study substantiates the biochemical, pathophysiological and molecular link of BNP treatment and demonstrates the mechanism of anti-tumor response. Our obtained *in vivo* data confirms those of the earlier *in vitro* investigation. Although the molecular insights discovered for BNP action provides the caspase activation mediated mitochondrial apoptotic pathway. Moreover, using a metabolomics approach in an *in vivo* model, we discovered an advanced mechanistic understanding of BNP action at cellular level. Altogether, the results indicate that BNP has outstanding potential to obliterate HCC and could serve as prospective component for the growth of anti-HCC drugs.

International Journal of Nanomedicine

Dovepress
open access to scientific and medical research

Open Access Full Text Article

ORIGINAL RESEARCH

Poly(lactic-*co*-glycolic acid)-loaded nanoparticles of betulinic acid for improved treatment of hepatic cancer: characterization, in vitro and in vivo evaluations

This article was published in the following Dove Press journal:
International Journal of Nanomedicine

Pranesh Kumar[1]
Ashok K Singh[1]
Vinit Raj[1]
Amit Rai[1]
Amit K Keshari[1]
Dinesh Kumar[2]
Biswanath Maity[2]
Anand Prakash[3]
Sabyasachi Maiti[4]
Sudipta Saha[1]

[1]Department of Pharmaceutical Sciences, Babasaheb Bhimrao Ambedkar University, Vidya Vihar, Lucknow, Uttar Pradesh, India; [2]Centre of Biomedical Research, SGPGIMS Campus, Lucknow, Uttar Pradesh, India; [3]Department of Biotechnology, Babasaheb Bhimrao Ambedkar University, Vidya Vihar, Lucknow, Uttar Pradesh, India; [4]Department of Pharmacy, Indira Gandhi National Tribal University, Amarkantak, Anuppur, Madhya Pradesh, India

Correspondence: Sudipta Saha
Department of Pharmaceutical Sciences, Babasaheb Bhimrao Ambedkar University, Vidya Vihar, Raebareli Road, Lucknow 226025, Uttar Pradesh, India
Tel +91 80 9074 7008
Email sudiptapharm@gmail.com

Purpose: The application of betulinic acid (B), a potent antineoplastic agent, is limited due to poor bioavailability, short plasma half-life and inappropriate tissue distribution. Thus, we aimed to prepare novel 50:50 poly(lactic-*co*-glycolic acid) (PLGA)-loaded B nanoparticles (BNP) and to compare its anti-hepatocellular carcinoma (HCC) activity with parent B.

Methods: BNP were synthesized and characterized using different methods such as scanning electron microscopy (SEM), fourier-transform infrared (FTIR) spectrometry and particle size analyses. Particle size of BNP was optimized through the application of the stabilizer, polyvinyl alcohol (PVA). The anti-HCC response was evaluated through in vitro cell line study using Hep-G2 cells, confocal microscopy, in vivo oral pharmacokinetics and animal studies. Further, quantitative reverse transcription polymerase chain reaction (qRT-PCR) analysis was conducted to observe the changes in the expression of specific genes.

Results: Particle size of BNP was optimized through the application of the stabilizer, polyvinyl alcohol. Physicochemical characterization exhibited particle size of 257.1 nm with zeta potential –0.170 mV (optimized batch B, BNP). SEM and FTIR analyses of BNP showed that cylindrical particles of B converted to spherical particles in BNP and there were no interaction between B and used polymers. The release study of optimized BNP was highest (≥80%) than any other formulation. Later, in vitro cell culture analysis using Hep-G2 cells and confocal microscopy studies revealed that BNP had the highest inhibition and penetration properties than parent B. Oral pharmacokinetics studies using albino Wistar rats at single 100 mg dose again exhibited BNP had the higher 50% of plasma concentration ($t_{1/2}$), a higher maximum plasma concentration (C_{max}) and took longer to reach the maximum plasma concentration (T_{max}) than parent B. Next, our in vivo study using nitrosodiethyl amine (NDEA)-induced HCC model documented BNP decreased in number of nodules, restored body weight, oxidative stress parameters, liver marker enzymes and histological architecture than parent B. Lastly, qRT-PCR studies further demonstrated that anti-HCC properties of BNP may be due to over expression of antiapoptotic caspases i.e., caspase 3 and 8.

Conclusion: The prepared BNP showed a better therapeutic response against HCC and could be attributed as future candidate molecule for HCC treatment.

Keywords: betulinic acid, PLGA-loaded nanoparticles, HepG2 cells, hepatocellular carcinoma, caspase-3 and -8

Introduction

The development of drug delivery system of existing marketed drugs for better therapeutic index and reduced toxicological properties are the basic criteria of modern

submit your manuscript | www.dovepress.com
Dovepress
http://dx.doi.org/10.2147/IJN.S157391

Life Sciences 209 (2018) 24–33

Contents lists available at ScienceDirect

Life Sciences

journal homepage: www.elsevier.com/locate/lifescie

Review article

Betulinic acid as apoptosis activator: Molecular mechanisms, mathematical modeling and chemical modifications

Pranesh Kumar[a,1], Archana S. Bhadauria[b,1], Ashok K. Singh[a], Sudipta Saha[a,*]

[a] Department of Pharmaceutical Sciences, Babasaheb Bhimrao Ambedkar University, Vidya Vihar, Raebareli Road, Lucknow 226025, India
[b] Department of Mathematics and Statistics, Deen Dayal Upadhyaya Gorakhpur University, Gorakhpur 273009, India

ARTICLE INFO

Keywords:
Betulinic acid
Molecular mechanism
Apoptosis
Mathematical modeling
Chemical modifications and formulations

ABSTRACT

A natural product betulinic acid (BA) has gained a huge significance in the recent years for its strong cytotoxicity. Surprisingly, in spite of being an interesting cancer protecting agent on a variety of tumor cells, the normal cells and tissues are rarely affected by BA. Betulinic acid and analogues (BAs) generally exert through the mechanisms that provokes an event of direct cell death and bypass the resistance to normal chemotherapeutics. Among several cancer protecting natural products, BA is divulged as a potentially selective anti-melanoma agent and has been entered into phase II clinical trials against skin cancer. Although the major mechanism associated with its ability to induce direct cell death is mitochondrial apoptosis, there are several other mechanisms explored recently. Importantly, mathematical modeling of apoptosis has been an important tool to explore the precise mechanism involved in mitochondrial apoptosis. Thus, this review is an endeavor to sum up the molecular mechanisms underlying the action of BA and future directions to apply mathematical modeling technique to better understand the precise mechanism of BA-induced apoptosis. The last section of the review encompasses the plausible structural modifications and formulations to enhance the therapeutic efficacy of BA.

1. Introduction

3β-Hydroxy-lup-20(29)-en-28-oic acid (betulinic acid, BA, Fig. 1) is chemically a lupan-skeleton pentacyclic triterpene and has a remarkable place in natural anticancer medicine [1]. The pentacyclic triterpene nucleus of BA is comprised of six isoprene units that possess different biological activities including antitumor activity [2,3]. The antitumor activity of BA has been well documented due to its ability to trigger apoptosis in variety of tumor cell types. Apoptosis is a process of programmed cell death that occurs due to several biochemical events followed by characteristic changes in cell morphology and death. Cancer cells have a strong ability to impair the mitochondrial pathway of apoptosis [4]. Besides cellular bioenergetics, mitochondria play an imperative role in the persistent regulation of apoptosis. In particular, BA and analogues (BAs) have been known to exhibit potential antitumor action via provoking the mitochondrial pathway of apoptosis [5].

Several authors have reported their views over the mechanisms underlying the antitumor action of BAs. For example, the downstream regulation of Bcl-2 family proteins (Bcl-2 and Bcl-xl) [6], cytosolic caspase activation and nuclear fragmentation [7], inhibition of pro-apoptotic p38, MAPK and SAP/JNK kinases [8], and decreased expression of pro-apoptotic proteins and vascular endothelial growth factor (VEGF) [9].

Despite the availability of plethora of literatures signifying the awesome function of BA in cancer drug discovery, none of the previous artwork emphasized its mechanistic action in correlation with mathematical modeling of apoptosis to the best of our knowledge. This article is consequently devoted to review the explored molecular mechanisms of BA action and to direct the future needs in search of precise mechanism of BA action using mathematical modeling. Other important aspects in the study of BA cytotoxicity are its chemical modifications and various formulations, summarized in last section of the review.

2. Molecular mechanism of BA

2.1. General mechanism for anticancer activity of BA

Although the exact mechanism underlying BA-induced cytotoxicity is broadly unexplored to date, several studies have offered considerable insights into BA-induced cell death through a number of apoptotic mechanisms. Apoptosis occurs due to several biochemical events leads

* Corresponding author.
E-mail address: sudiptapharm@gmail.com (S. Saha).
[1] These are the main authors who contributed equally.

https://doi.org/10.1016/j.lfs.2018.07.056
Received 11 May 2018; Received in revised form 16 July 2018; Accepted 30 July 2018
Available online 01 August 2018

ARCHIVES OF PHYSIOLOGY AND BIOCHEMISTRY
https://doi.org/10.1080/13813455.2020.1733024

Taylor & Francis
Taylor & Francis Group

ORIGINAL ARTICLE

Mechanistic exploration of the activities of poly(lactic-*co*-glycolic acid)-loaded nanoparticles of betulinic acid against hepatocellular carcinoma at cellular and molecular levels

Pranesh Kumar[a], Anurag Kumar Gautam[a], Umesh Kumar[b], Archana S. Bhadauria[c], Ashok K. Singh[a], Dinesh Kumar[b], Tarun Mahata[b], Biswanath Maity[b], Hriday Bera[d] and Sudipta Saha[a]

[a]Department of Pharmaceutical Sciences, Babasaheb Bhimrao Ambedkar University, Lucknow, Uttar Pradesh, India; [b]Department of Molecular Diagnostics and Phenome Research, Centre of Biomedical Research, SGPGIMS Campus, Lucknow, Uttar Pradesh, India; [c]Department of Mathematics and Statistics, Deen Dayal, Upadhyaya Gorakhpur University, Gorakhpur, Haryana, India; [d]Department of Pharmaceutics, Shenyang Pharmaceutical University, Shenyang, Liaoning, China

ABSTRACT

The effectiveness of betulinic acid (B) and PLGA loaded nanoparticles of B (Bnp) against hepatocellular carcinoma (HCC) was established and reported earlier. In continuation of our previous report, the present study described the molecular mechanisms of their antineoplastic responses. In this context, the antineoplastic properties of both B and Bnp were evaluated on DEN-induced HCC rat model. The quantitative real-time polymerase chain reaction and western blot analyses revealed that HCC was developed through lower expressions of e-NOS, BAX, BAD, Cyt C and higher expressions of i-NOS, Bcl-xl, Bcl-2. B and Bnp normalised the expressions of these apoptogenic markers. Particularly, both activated i-NOS and e-NOS mediated Bcl-2 family proteins→CytC→Caspase 3 and 9 signalling cascades. The ^{1}H-NMR-based metabolomics study also demonstrated that the perturbed metabolites in DEN-induced rat serum restored to the normal level following both treatments. Moreover, the antineoplastic potential of Bnp was found to be comparable with the marketed product, 5-flurouracil.

ARTICLE HISTORY
Received 15 November 2019
Revised 23 January 2020
Accepted 17 February 2020
Published online 5 March 2020

KEYWORDS
PLGA nanoparticles; betulinic acid; hepatocellular carcinoma; Bcl-2; Bcl-xl and BAX proteins; ^{1}H-NMR-based metabolomics

Introduction

Now-a-days, hepatocellular carcinoma (HCC) is the second leading cause of death in the developing countries and sixth common cause of death in the developed countries (Torre *et al.* 2015). Unfortunately, the treatment of HCC is still remained unsatisfactory due to the unexplored cellular mechanisms of HCC development into cellular levels (http://seer.cancer.gov/faststats). Various synthetic chemotherapeutic agents have showed promising effects on HCC, but, these could develop chemoresistance to patients following a long-term treatment (Newman *et al.* 2003). Sorafenib, a leading drug molecule used for HCC treatment (Bruix and Sherman 2011), often produces disease related metastasis and resistance (Wilhelm *et al.* 2006). In addition, it display significant adverse effects and its cost of treatment is extremely high (Kondo *et al.* 2017). To overcome these shortfalls, the natural products could be the alternative choice for hepatic cancer treatment (Cragg *et al.* 1997).Therefore, there is an urgent need to discover newer plant-derived anticancer agents for effective treatment of HCC cancer.

Cancer chemotherapy is the most challenging scenario in modern drug development where low toxicity with improved pharmacological responses and lower side effects are always a priority (Davaran *et al.* 2006). Betulinic acid (B, Figure 1) is a naturally occurring pentacyclic triterpenoid and it demonstrates diverse pharmacological responses such as anti-malarial, antiviral, anti-inflammartory and anti-carcinogenic properties (Armstrong and Doll 1975, Fujioka *et al.* 1994, Mayaux *et al.* 1994). The anticancer property of B is mainly due to the activation of mitochondrial Bcl-2 pathways where caspase enzymes, various pro-apoptotic (BAX and BAD) and anti-apoptotic (Bcl-2 and Bcl-xl) proteins are involved (Armstrong and Doll 1975, Fujioka *et al.* 1994, Mayaux *et al.* 1994, Wick *et al.* 1999, Fulda 2008, Adamson *et al.* 2009).

The major drawback associated with natural products is poor oral absorption and limited bioavailability, which might lead to its lower therapeutic effectiveness. B is the similar class of natural product which has poor oral absorption and bioavailability (Xu *et al.* 2012). Recent investigations suggested that these problems might be overcomed via its delivery through nanoformulations (Roy *et al.* 2010, Xie *et al.* 2011, El-Say 2016). Inspired by the previous literatures, our group recently developed poly(lactic-*co*-glycolic acid) PLGA nanoparticles containing B (i.e. Bnp) to improve its oral bioavailability and anti-HCC potential (Kumar *et al.* 2018). However, the mechanism of antineoplastic potentials of both

CONTACT Sudipta Saha sudiptapharm@gmail.com Department of Pharmaceutical Sciences, BabasahebBhimraoAmbedkar University, VidyaVihar, Rai Bareli Road, Lucknow, Uttar Pradesh, 226025, India

Supplemental data for this article can be accessed here.

विद्ययामृतमश्नुते

S. D. College of Pharmacy & Vocational Studies

(Approved By AICTE, PCI, New Delhi & Affiliated to U.P. Technical University, Lucknow)

Bhopa Road
Muzaffarnagar 251 001 (U.P.)

Office : 0131 2604546
Fax : 0131 2604546
E-mail : sdcop@rediffmail.com
Web : sdcopmzn.com

Ref. No. : SDCOP&VS/AH/CPCSEA/01/0027 Dated 06/05/2014

INSTITUTIONAL ANIMAL ETHICAL COMMITTEE (IAEC)

REG. No. 876/ac/05/CPCSEA Dated 13/09/2004 UNDER THE RULE 13 OF THE "BREEDING OF AND EXPERIMENTS ON ANIMALS (CONTROL AND SUPERVISION) RULE 1998"

DATE: 06/05/2014

Approval No.: SDCOP&VS/AH/CPCSEA/01/0027

CERTIFICATE

This is to certify that Mr./Ms./Mrs. **Sudipta Saha/ Pranesh Kumar** student of M.Pharm / Ph.D. are permitted to carry out experiments for dissertation / thesis work entitled **"In vitro Hepatoprotective and Anticancer Activity and in vivo pharmacokinetics studies of Betulinic acid Nanoparticles"** as per the details mentioned and after the observing the usual formalities laid down by IAEC as per the provisions made by CPCSEA.

MEMBER SECRETARY

CHAIRMAN

Plagiarism report of the thesis

URKUND

Urkund Analysis Result

Analysed Document: revised thesis for plagrism_pranesh.psit@gmail.com.docx (D89797612)
Submitted: 12/17/2020 7:46:00 AM
Submitted By: gbl.bbau@gmail.com
Significance: 1 %

Sources included in the report:

Ashok Kumar Singh.doc (D34438935)
https://www.dovepress.com/polylactic-co-glycolic-acid-loaded-nanoparticles--of-betulinic-acid-fo-peer-reviewed-fulltext-article-IJN

Instances where selected sources appear:

2

List of Publications

Publication related to Ph.D. thesis work:

1. **Pranesh Kumar**, Ashok K Singh, Vinit Raj, Amit Rai, Amit K Keshari, Dinesh Kumar, Biswanath Maity, Anand Prakash, Sabyasachi Maiti, Sudipta Saha: *Poly(Lactic-co-glycolic acid)-loaded nanoparticles of betulinic acid for improved treatment of hepatic cancer: Characterization, in vitro and in vivo evaluations*. International Journal of Nanomedicine 02/2018; Volume 13. DOI:10.2147/IJN.S157391. **(IF- 5.115)**
2. **Pranesh Kumar,** Archana Singh Bhadauria, Ashok K Singh, Sudipta Saha: *Betulinic acid as apoptosis activator: Molecular mechanisms, mathematical modeling and chemical modifications.* Life sciences. DOI:10.1016/j.lfs.2018.07.056 **(IF- 3.647)**
3. **Pranesh Kumar,** Anurag Kumar Gautam, Umesh Kumar, Archana S. Bhadauria, Ashok K. Singh, Dinesh Kumar, Tarun Mahata, Biswanath Maity, Hriday Bera, Sudipta Saha: *Mechanistic exploration of the activities of poly(lactic-co-glycolic acid)-loaded nanoparticles of betulinic acid against hepatocellular carcinoma at cellular and molecular levels*. Archives of physiology and biochemistry.05/2020; DOI:10.1080/13813455.2020.1733024. **(IF-2.575)**

Other Publications:

4. Raquibun Nisha, **Pranesh Kumar**, Umesh Kumar, Nidhi Mishra, Priyanka Maurya, Samipta Singh, Priya Singh, Anupam Guleria, Sudipta Saha, Shubhini A Saraf: *Fabrication of Imatinib mesylate loaded lactoferrin modified PEGylated liquid crystalline nanoparticles for mitochondrial-dependent apoptosis in hepatocellular carcinoma*. Molecular Pharmaceutics, 2020, (**Impact factor- 4.321)**.
5. Raquibun Nisha, **Pranesh Kumar**, Anurag Kumar Gautam, Hriday Bera, Bolay Bhattacharya, Poonam Parashar, Shubhini A Saraf, Sudipta Saha*: Assessments of in vitro and in vivo antineoplastic potentials of β-sitosterol-loaded PEGylated niosomes against hepatocellular carcinoma*. Journal of Liposome Research, 2020, (**Impact factor- 2.45)**.
6. Madhuri Basak, Tarun Mahata, Sreemoyee Chakraborti, **Pranesh Kumar**, Bolay Bhattacharya, Sandip Bandyopadhaya, Madhusudan Das, Adele Stewart, Biswanath Maity, Sudipta Saha: *Malabaricone C attenuates NSAID-induced gastric ulceration*

by reducing oxidative/nitrative stress and inflammation and promoting angiogenic auto-healing. Antioxidants and Redox Signaling 12/2019. DOI:10.1089/ars.2019.7781. **IF- 7.04**

7. Poonam Parashar, Ifrah Mazhar, Jovita Kanoujia, Abhishek Yadav, **Pranesh Kumar**, Shubhini A Saraf, Sudipta Saha: *Appraisal of Antigout Potential of Colchicine Loaded Chitosan Nanoparticle Gel in Uric Acid Induced Gout Animal Model.* Archives of Physiology and Biochemistry 12/2019; DOI:10.1080/13813455.2019.1702702. **IF- 2.575**
8. **Pranesh Kumar**, Aakriti Agarwal, Ashok K Singh, Anurag Kumar Gautam, Sreemoyee Chakraborti, Umesh Kumar, Dinesh Kumar, Bolay Bhattacharya, Parthasarathi Panda, Biswajit Saha, Tabish Qidwai, Biswanath Maity, Sudipta Saha: *Antineoplastic properties of zafirlukast against hepatocellular carcinoma via activation of mitochondrial mediated apoptosis*. Regulatory Toxicology and Pharmacology 10/2019;, DOI:10.1016/j.yrtph.2019.104489 **IF - 2.652**
9. Vimal Maurya, **Pranesh Kumar**, Sreemoyee Chakraborti, Ashok K Singh, Archana Singh Bhadauria, Umesh Kumar, Dinesh Kumar, Gosipatala Sunil Babu, Bolay Bhattacharya, Biswanath Maity, Sudipta Saha*: Zolmitriptan attenuates hepatocellular carcinoma via activation of caspase mediated apoptosis*. Chemico-Biological Interactions 06/2019; 308:120-129., DOI:10.1016/j.cbi.2019.05.033 **IF - 3.723**
10. Ashok K Singh, Archana Singh Bhadauria, Umesh Kumar, Vinit Raj, Amit Rai, **Pranesh Kumar**, Amit K Keshari, Dinesh Kumar, Biswanath Maity, Sneha Nath, Anand Prakash, Sudipta Saha: *Novel Indole-fused benzo-oxazepines (IFBOs) inhibit invasion of hepatocellular carcinoma by targeting IL-6 mediated JAK2/STAT3 oncogenic signals*. Scientific Reports 04/2018. **IF- 3.998**
11. Vinit Raj, Archana S Bhadauria, Ashok K Singh, Umesh Kumar, Amit Rai, Amit K Keshari, **Pranesh Kumar**, Dinesh Kumar, Biswanath Maity, Sneha Nath, Anand Prakash, Kausar M Ansari, Jawahar L Jat, Sudipta Saha: *Novel 1,3,4-thiadiazoles inhibit colorectal cancer via blockade of IL-6/COX-2 mediated JAK2/STAT3 signals as evidenced through data-based mathematical modeling*. Cytokine 03/2018;, DOI:10.1016/j.cyto.2018.03.026 **IF- 2.952**
12. Priyanka Mishra, Vinit Raj, Archana Singh Bhadauria, Ashok K. Singh, Amit Rai, **Pranesh Kumar**, Amit K. Keshari, Arnab De, Amalesh Samanta, Umesh Kumar, Dinesh Kumar, Biswanath Maity, Sneha Nath, Anand Prakash, Kausar M Ansari, Sudipta Saha: *6,7-dimethoxy-1,2,3,4-tetrahydro-isoquinoline-3-carboxylic acid*

attenuates colon carcinogenesis via blockade of IL-6 mediated signals. Biomedicine & Pharmacotherapy 02/2018; 100:282-295., DOI:10.1016/j.biopha.2018.02.009. **IF- 4.545**

13. Amit Rai, Umesh Kumar, Vinit Raj, Ashok K. Singh, **Pranesh Kumar**, Amit K. Keshari, Dinesh Kumar, Biswanath Maity, Arnab De, Amalesh Samanta, Sneha Nath, Anand Prakash, Sunil Babu Gosipatala, Gyan Chand, Sudipta Saha: *Novel 1,4-benzothazines obliterate COX-2 mediated JAK-2/STAT-3 signals with potential regulation of oxidative and metabolic stress during colorectal cancer*. Pharmacological Research 12/2017;, DOI:10.1016/j.phrs.2017.12.010 **IF- 5.893**

14. Ashok K Singh, Vinit Raj, Amit K Keshari, Amit Rai, **Pranesh Kumar**, Atul Rawat, Biswanath Maity, Dinesh Kumar, Anand Prakash, Arnab De, Amalesh Samanta, Bolay Bhattacharya, Sudipta Saha: *Isolated mangiferin and naringenin exert antidiabetic effect via PPARγ/GLUT4 dual agonistic action with strong metabolic regulation*. Chemico-biological interactions 12/2017; 280., DOI:10.1016/j.cbi.2017.12.007 **IF- 3.723**

15. Chandra Bhusan Tripathi, Neha Gupta, **Pranesh Kumar**, Ashok Kumar Singh, Vinit Ra, Poonam Parasar, Mahendra Singh, Jovita Kanoujia, Malti Arya, Sanyog Jain, Shubhini A Saraf, Sudipta Saha: *ω-3 Fatty Acid Synergized Novel Nanoemulsifying System for Rosuvastatin Delivery: In Vitro and In Vivo Evaluation*. AAPS PharmSciTech 11/2017; 19(3)., DOI:10.1208/s12249-017-0933-8 **IF- 2.401**

16. Ashok K. Singh, Vinit Raj, Amit Rai, Amit K. Keshari, **Pranesh Kumar**, Sudipta Saha: *Determination of 5H-Benzo[2,3][1,4]oxazepino[5,6-b]indoles in rat plasma by Reversed-Phase High-Performance Liquid Chromatographic-Ultraviolet Method: Application to pharmacokinetic studies*. Asian Journal of Pharmaceutical and Clinical Research 11/2017;10(12):425-430.,DOI:10.22159/ajpcr.2017.v10i12.22565 **IF- 0.655**

17. Amit K Keshari, Ashok K Singh, Umesh Kumar, Vinit Raj, Amit Rai, **Pranesh Kumar**, Dinesh Kumar, Biswanath Maity, Sneha Nath, Anand Prakash, Sudipta Saha: *5H-benzo[h]thiazolo[2,3-b]quinazolines ameliorate NDEA-induced hepatocellular carcinogenesis in rats through IL-6 down-regulation along with oxidative and metabolic stress reduction*. Drug Design, Development and Therapy 08/2017; Volume 11., DOI:10.2147/DDDT.S143075 **IF- 3.216**

18. Shalini Chauhan, Pranesh Kumar, Ashok K Singh, Vinit Raj, Amit Rai, Amit K Keshari, Anand Prakash, Sudipta Saha: *Protective Effect of Naringin against Pylorus Ligation-induced Esophagitis in Male Wistar Rats*. Indian Journal of Pharmaceutical

Sciences 04/2017; 79(2):250-256., DOI:10.4172/pharmaceutical-sciences.1000223 **IF- 0.73**

19. **Pranesh Kumar**, Ashok K Singh, Vinit Raj, Amit Rai, Siddhartha Maity, Atul Rawat, Umesh Kumar, Dinesh Kumar, Anand Prakash, Anupam Guleria, Sudipta Saha: *6,7-dimethoxy-1,2,3,4-tetrahydro-isoquinoline-3-carboxylic acid attenuates hepatocellular carcinoma in rats with NMR based metabolic perturbations*. Future science OA, 04/2017; 3(3)., DOI:10.4155/fsoa-2017-0008
20. Amit K. Keshari, Ghanendra Kumar, Priya S. Kushwaha, Monika Bhardwaj, **Pranesh Kumar**, Atul Rawat, Dinesh Kumar, Anand Prakash, Balaram Ghosh, Sudipta Saha: *Isolated flavonoids from Ficus racemosa stem bark possess antidiabetic, hypolipidemic and protective effects in albino Wistar rats*. Journal of ethnopharmacology 02/2016; 181., DOI:10.1016/j.jep.2016.02.004 **IF- 3.69**
21. **Pranesh Kumar**, Atul Rawat, Amit K Keshari, Ashok K Singh, Siddhartha Maity, Arnab De, Amalesh Samanta, Sudipta Saha: *Antiproliferative effect of isolated isoquinoline alkaloid from Mucuna pruriens seeds in hepatic carcinoma cells*. Natural Product Research 03/2015;30(4):1-4.,DOI:10.1080/14786419.2015.1020489. **IF- 1.99**

Patent:

22. Ashok K Singh, Sudipta Saha, Vinit Raj, Amit Rai, Amit K Keshari, **Pranesh Kumar**: *5H-benzo[2,3][1,4]thiazepino[5,6-b]indoles for the treatment of liver cancer*. Ref. No: Application Number 201711026168, Year: 07/2017

Book chapter:

23. Ashok K Singh, Archana Singh Bhadauria, **Pranesh Kumar**, Sudipta Saha, "*Bioactive and drug delivery potentials of polysaccharides and their derivatives*" Polysaccharide Carriers for Drug Delivery, Elsevier.

Presentations, Conference and Workshop Attended:

1. Attended Flow Cytometry Workshop on Basics of Flow Cytometry and its application in Biomedical Sciences, Lucknow, 5-7 March, 2020 organized by BBAU Lucknow.
2. Attended and presented poster in "World Immunology Day" organized by BBAU Lucknow in 2019.

3. Attended 11th NIPER (R) Symposium on "Natural products based theraputics in drug developmet" organized by NIPER, Raebarelly in 2019.
4. Attended and presented poster in two days National conference on "**Tourists and green space: Healthier life style approaches from nature"** organized by BBAU Lucknow in 2017.
5. Four days "**International Conference on updates in cancer prevention and research"** organized by BBAU Lucknow in 2017.
6. Two days International Pharmaceutical Conference 2015 on **"Nanoformulations and Translational Research: Small Getting Bigger"** organized by BBAU Lucknow.

Brief Curriculum Vitae

Pranesh Kumar
Contact No. +91-8542929351
Email ID. pranesh.psit@gmail.com

Educational details

Degree	University/Institute	Discipline	Division
Ph.D.	BBAU, A Central University, Lucknow	Pharmaceutical sciences	Pre-Ph.D. Submitted
M.Pharm.	BBAU, A Central University, Lucknow	Pharmacology	First Division
B.Pharm.	PSIT, Kanpur	Pharmacy	First Division

Achievements

- DST INSPIRE Fellowship JRF (2017) & SRF (2018).
- DST Project Fellow, JRF (2016)
- Double Gold medalist of M.Pharm (Pharmacology) session 2013-2015.
- GPAT Qualified in 2013, 2014 & 2015.

Research publications

	Publications on Ph.D. Thesis	Other Publications
Number of Papers in journals	**03**	**18**
Number of Patents	**-**	**01**
Number of Book chapters	**-**	**01**

Conferences and workshops:

Number of Training and workshops	**01**
Number of International Seminars/Conferences	**02**
Number of National Seminars/Conferences	**03**

Research expertise

Anti-Cancer, Nanoformulations, Isolation of natural products, Spectroscopic Analysis, Anti-diabetic, Drug Design and Discovery, *In silico* Drug Design, *In vitro* and *In vivo* pharmacological screening of novel molecules, Pharmacological Screening at molecular levels, NMR based metabolomics.

Personal details

Nationality	Indian	**Permanent Address**	Village and Post- Shikargarh, Dist- Maharajganj, UP- 273309
Language Known	Hindi, English		
Gender	Male		